CURRENT BALANCING CIRCUIT DESIGN FOR PARALLEL LED STRINGS IN DUAL-TRANSFORMER LLC RESONANT TOPOLOGY

A Thesis

by

Melisa Ersoy

Submitted to the
Graduate School of Sciences and Engineering
In Partial Fulfillment of the Requirements for
the Degree of

Master's Degree

in the
Department of Electrical and Electronics Engineering

Özyeğin University
November 2022

CURRENT BALANCING CIRCUIT DESIGN FOR PARALLEL LED STRINGS IN DUAL-TRANSFORMER LLC RESONANT TOPOLOGY

Approved by:

Asst. Prof. Gokturk Poyrazoglu, Advisor
Department of Electrical and Electronics Engineering
Ozyegin University

Asst. Prof. Dr. Ahmet Tekin
Department of Electrical Engineering
Istanbul Technical University

Prof. Dr. Duygun Erol Barkana
Department of Electrical and Electronics Engineering
Yeditepe University

Date Approved: 21 November 2022

To my lovely family.

ABSTRACT

New display technologies require small form factor designs with more backlight power. When multiple transformers drive parallel-connected LED strings, the difference in transformer leakage inductance and LED string voltage creates a backlight current imbalance. This current imbalance causes the following problems,

- The low-voltage string draws more current.
- High current causes hot spots on the backlight and a shorter lifespan.

This issue is seen as an unevenly distributed backlight on the customer side. In this study, a cost-efficient balancing circuit for eight parallel-connected LED strings is simulated and developed utilizing two transformers in the half-bridge LLC resonant topology while providing the power in a comparatively slim design.

The current imbalance for the 145W backlight power was 57.58% when there was an 8% change in leakage inductance between the transformers and a 10% change in LED string voltages. When the back cover was removed, the difference in temperature between the LED strings was recorded at room temperature as 31.8°C. The current imbalance between the LED strings is decreased to 9.99% when the current balancing components are connected to the circuit. When there is no difference between the LED string voltages, the maximum current imbalance is 2.59%. The cost of the proposed method is almost three times less than the conventional method, and for the same backlight power, it is 5.6% more efficient.

ÖZETÇE

Yeni ekran teknolojileri, daha fazla arka ışık gücüne sahip ve küçük form faktörlü tasarımlar gerektirmektedir. Paralel bağlı LED dizileri birden fazla transformatör tarafından sürüldüğünde, transformatörler arasındaki kaçak endüktans ve LED dizileri arasındaki tolerans kaynaklı voltaj farkı, arka ışıkta diziler arasında akım dengesizliği yaratır. Bu akım dengesizliği aşağıdaki sorunlara neden olur.

- Düşük voltajlı LED dizisi daha fazla akım çeker.
- Yüksek akım arka aydınlatma üzerinde sıcak noktalar oluşturur ve ürünün ömrü kısalır.

Bu sorun, son kullanıcı düzeyinde arka ışıkta parlaklık farkı (dalgalanma) olarak kendini göstermektedir.

Bu çalışmada, LLC yarım köprü rezonans topolojisinde iki transformatör kullanılarak sekiz paralel bağlı LED dizisi uygun maliyetli bir akım dengeleme devresi ile simüle edilmiş ve %0.9288 verimde çalışan nispeten ince bir tasarımda gerçeklenmiştir.

145W arka ışık gücü için, trafo kaçak endüktansında %8 ve LED dizi voltajları arasında tolerans kaynaklı %10 fark olduğunda LED dizilerinde ölçülen akım sapması %57.58 idi. Bu durumda LED dizileri arasındaki sıcaklık farkı, TV arka kapağı açıkken oda sıcaklığında 31.8℃ olarak ölçülmüştür. Akım dengeleme devresi ile LED akımları farkı %9.99'a düşürülmüştür. Dizi gerilimleri aynı olduğunda akımdaki maksimum sapma %2,59 olarak ölçülmektedir. Sunulan method aynı arka ışık gücü için klasik arka ışık aydınlatma yöntemine göre maliyet olarak yaklaşık üç kat daha avantajlıdır ve %5,6 daha verimlidir.

ACKNOWLEDGEMENTS

I would like to express my deep gratitude to my advisor Asst. Prof. Gokturk Poyrazoglu for his guidance and support during this thesis study. I have been extremely lucky to have an advisor who cared so much about my work.

I am grateful to my managers, Osman Oral Kıvrak and Cengiz Tarhan. Their theoretical and practical knowledge guided me through this work. Also, I would like to thank my colleagues in Vestel TV Power Electronics R&D Group for their valuable support.

Most importantly, I would like to thank especially my family for their continuous support, encouragement, and patience. I couldn't achieve this without you.

TABLE OF CONTENTS

LIST OF TABLES

LIST OF FIGURES

CHAPTER I

INTRODUCTION

The TVs in our houses and smart screens that we are used to seeing almost everywhere have become brighter and more colorful, yet, each new model has a slim and half-back cover. To keep up with this trend, more power should be transmitted with a smaller form factor on the power board of the television. Since it directly impacts the product lifespan, the temperature of the electronic components inside the back cover must be maintained while transmitting the power demand.

1.1 Motivation

In the backlight block of televisions, cascaded DC-DC converters are generally used. This leads to a decrease in efficiency and an increase in the area of the backlight block on the PSU. There is not enough space for using this method in slim designs. Instead of using cascaded DC-DC converters, in this study, the backlight is driven directly from the transformer using dual transformer LLC resonant topology.

Diodes have a forward voltage that changes with temperature and current. The forward voltage is affected by the chemical nature of the junctions, from the manufacturing process or changes in the semiconductor wafer. The tolerance range in the forward voltage varies across manufacturers and even between lots made by the same manufacturer. When multiple transformers drive parallel-connected LED strings, the difference in transformer leakage inductance and LED string voltage creates a backlight current imbalance problem. This current imbalance results in drawing more current from the low-voltage string and causing hot spots on the backlight and a shorter lifespan. The two-stage current balancing circuit minimizes this imbalance.

In this study, a PSU with 145W backlight power is designed, simulated and implemented in dual transformer LLC half-bridge resonance topology for eight parallel connected LED strings. Design achievements are,

- minimum current imbalance, better reliability performance
- better efficiency
- slim form factor
- cost-effective design

1.2 Backlight Driving Methods

As seen in Fig. 1, the forward voltage value was recorded between 2.45V and 3.08V when the same current was supplied through two separate diodes, as mentioned in [2]. When the number of LEDs in parallel connected LED strings increases or if the forward voltage tolerance is large, these differences cause current mismatch and reliability problems.

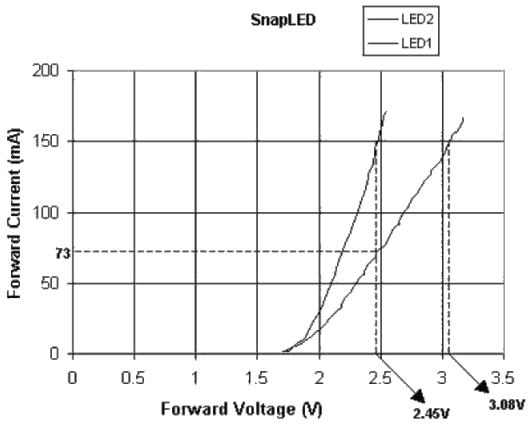

Figure 1 Forward voltage variation between LEDs in [2]

The problem of the current imbalance in parallel connected strings was also a design problem when the backlight was created with cold cathode fluorescent lamp

(CCFL) tubes. In order to obtain sufficient luminous flux in the backlight, a separate transformer was used for each parallel connected string in cases where all strings could not be connected in series and the voltage was high. However, current mismatch and hot spots on the back cover come about in circumstances, as in [16], when the voltage of the LED string increases or decreases due to tolerances or due to an error. In these cases, the change in voltage and the imbalance in current are directly proportional to each other. The LED string current mismatch is seen on the customer side as an unevenly distributed backlight.

In the method proposed in [3], the error rates of the current imbalance were compared by changing the value of the leakage inductance and resonance capacity of the transformer by 10%, providing a 7% fluctuation in the string voltages. In result of the cases, DC blocking capacitor is used in front of the strings in full bridge LLC topology to eliminate the imbalance in the current, the voltage change that may occur in the strings will not provide a current imbalance between the strings as seen in Fig. 2.

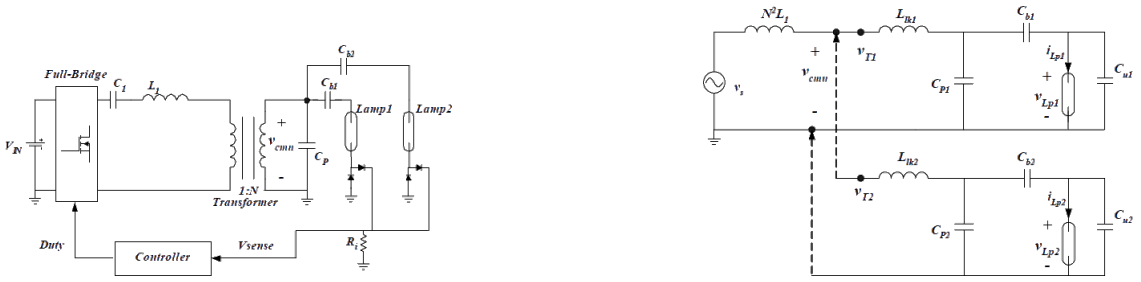

(a) Proposed circuit diagram

(b) Equivalent circuit

Figure 2 Parallel connected CCFL circuit in [3]

An additional DC-DC converter, usually a buck or boost converter, is used at the output of the main SMPS block to create the backlight in televisions as shown in Fig. 3. On the other hand, using a DC-DC converter for each string or string group will increase the number of controllers, and semiconductors in the system. The cost

will be increased. The efficiency will be equal to the product of the efficiencies of the cascade-connected systems, it will decrease and the loss will cause an increase in ambient temperature, which will cause reliability issues. On the other hand, the converter block to be added will occupy an extra space, it is an unfavorable decision in terms of designs with the small form factor [4].

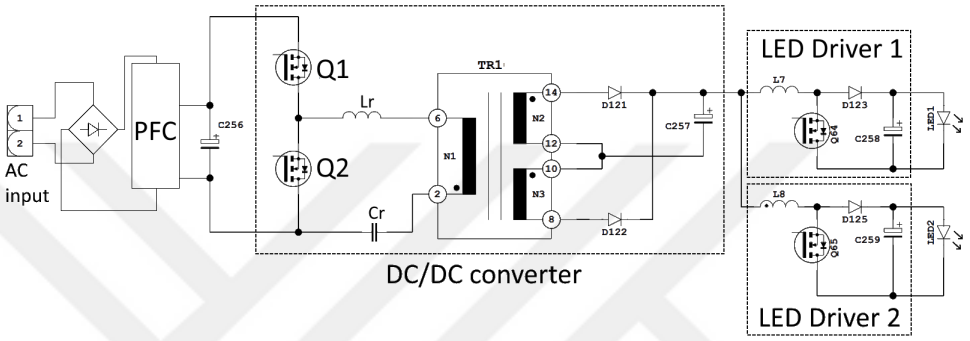

Figure 3 Conventional circuit diagram

In Fig. 4a, a single-stage led driver was presented for 6 parallel strings for 46" LCD TV with 120W backlight by using three transformers. A DC blocking capacity is used as used in CCFL tubes. The current balancing is examined under different dim conditions. As a result of the study, 1.5W less power consumption was measured between the conventional system and the proposed system. Component-based calculation of the power consumption is given in Fig. 4b. The biggest difference comes from the second stage MOSFET and diode.In addition, with this balancing in the current, system reliability has increased [4].

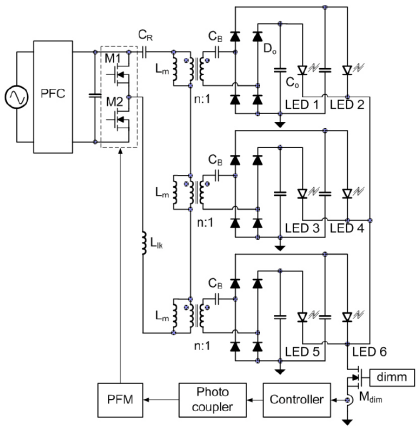

(a) Proposed circuit diagram

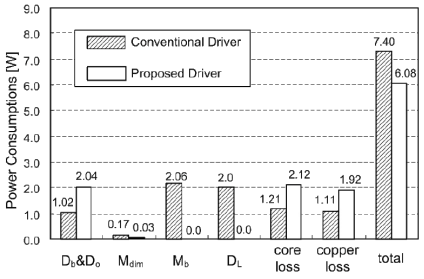

(b) Power loss comparison between drivers

Figure 4 Proposed circuit diagram and loss comparison in [4]

In [5], current balancing in parallel connected strings in AC LEDs was provided in LCC resonant topology with series capacitance connected to strings as in Fig. 5. The method is, to keep the equivalent resistance value of the capacitance connected in series to the strings larger than the load differences that will occur between the strings. The method is the same as [3] and [4]. But the difference in this study is, the limitations of the method were modeled by examining the tolerance change in the LED voltages and the capacity value to be used for balancing. All five strings were canceled in order and the gain graph of the converter and the operating frequency of the system were simulated. The system keeps the current in balance in case of possible LED errors.

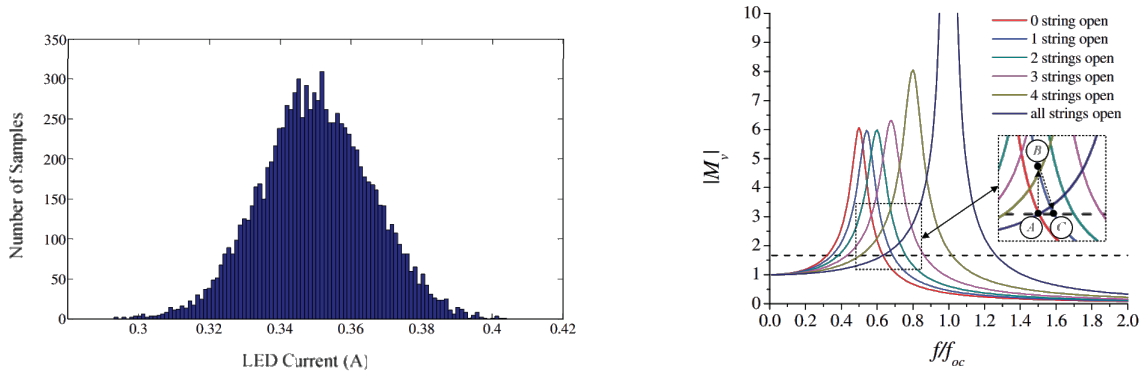

(a) Led equivalent resistance and balancing capacitor value change histogram based on manufacturing

(b) Gain curve change

Figure 5 Capacitive current balancing analysis in [5]

To improve reliability in a standard backlight converter, the current imbalance between strings was minimized using the current mirror circuit and opamps, as stated in [17] and in [18]. The currents in the channel returns are sensed through the resistor and are equalized independently from the string voltage. For eight strings, when 20mA is drawn per string 0.1% error is measured when the difference between the forward voltages of the LEDs is 1.1V. On the other hand, due to the significant losses on transistors, this approach is not applicable to high-power circuits.

As given in [6], a current balancing transformer was used in an 80W LED lighting product to minimize the current mismatch between four parallel LED strings. The distinction in this approach is that instead of an additional coil, the current balancing transformer is wounded on the transformer's outer legs, as shown in Fig. 6. When the output power was 60W, the maximum efficiency was measured as 96.5% and the maximum current mismatch between the LED currents was recorded as 4.34%.

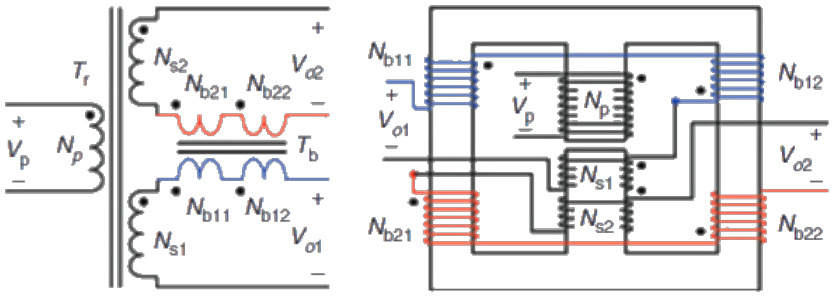

Figure 6 Integrated current balancing transformer in [6]

In the proposed circuit, 8 parallel LED strings are driven in dual transformer LLC resonance topology. Each transformer has two output windings, one winding feeds two parallel strings. Current balancing between these parallel strings is done in two stages. In the first step, inside the transformer, current balancing is done with one current transformer and two DC-blocking capacitors. In the second step, current balancing between the transformers is done with a current transformer added to the ground returns of the transformers.

CHAPTER II

LITERATURE REVIEW

Since the proposed method is a backlight driving technique with LLC resonance topology from the transformer instead of using an additional DC-DC converter to the SMPS output, which is the conventional method, in this section, backlight and display technologies, isolated DC-DC converter topologies, switching techniques, and resonant circuits (series resonance, parallel resonance and series-parallel resonance) are reviewed.

2.1 Backlight and Display Technologies

The first studies on television began in the 1920s. In 1925, Charles Jenkins sent a still image over radio waves in the USA [19]. In 1926, the first public television appearance was demonstrated in the United Kingdom by John Logie Baird with 12.5 frames per second [20]. The first fully electronic TV set patent was received by Philo Farnsworth of the USA in 1927 [21]. In the 1940s, color television studies gained momentum. In the 1950s, the first color television went on sale in the United States [22].

The display technologies that we use starting from the first televisions are examined in two groups in Fig. 7. These are the conventional displays we used to use and the new technology slim displays. Cathode ray tube displays (CRT) and projection TVs are examples of conventional screens. Slim displays, on the other hand, are classified into two types, non-emissive, which needs backlighting to create images, and emissive, which does not need backlighting to create images. Self-illuminating displays include plasma displays and organic light-emitting diode (OLED) displays. Quantum dot (Qdot) displays and liquid crystal displays (LCD) are examples of non-emissive technologies.

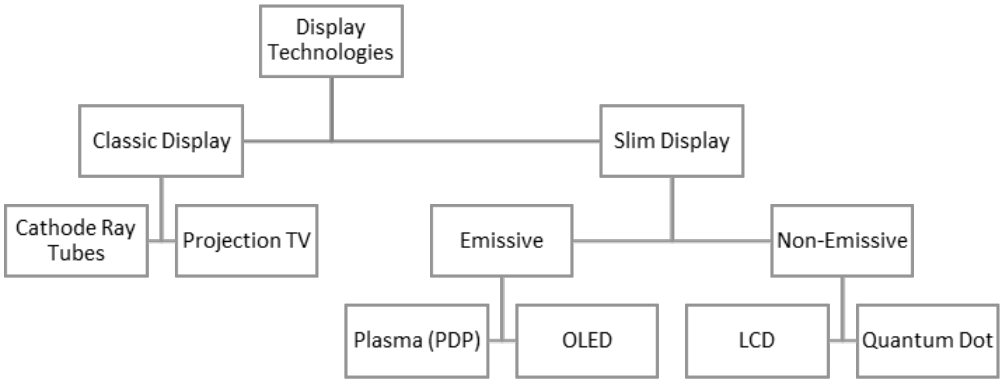

Figure 7 Display technologies

Fig. 8 includes the types and historical development of backlight technologies. Backlight technologies have been created with cathode tubes in the past. Today, mostly LEDs are used. LED backlight instead of a cathode backlight gives a couple of advantages such as lower power consumption and thinner form factors. LED backlight can be categorized into two groups according to the position of the LEDs on the panel. If the placement of the LEDs is horizontal or on the sides, it is called edge LED (ELED). Homogeneous distribution of light in ELED is provided by reflectors. If the LEDs are positioned sequentially behind the panel, it is called a direct led (DLED). While the advantage of DLEDs is cost, the disadvantage is that it creates thermal stress for the power card or motherboard positioned behind the television.

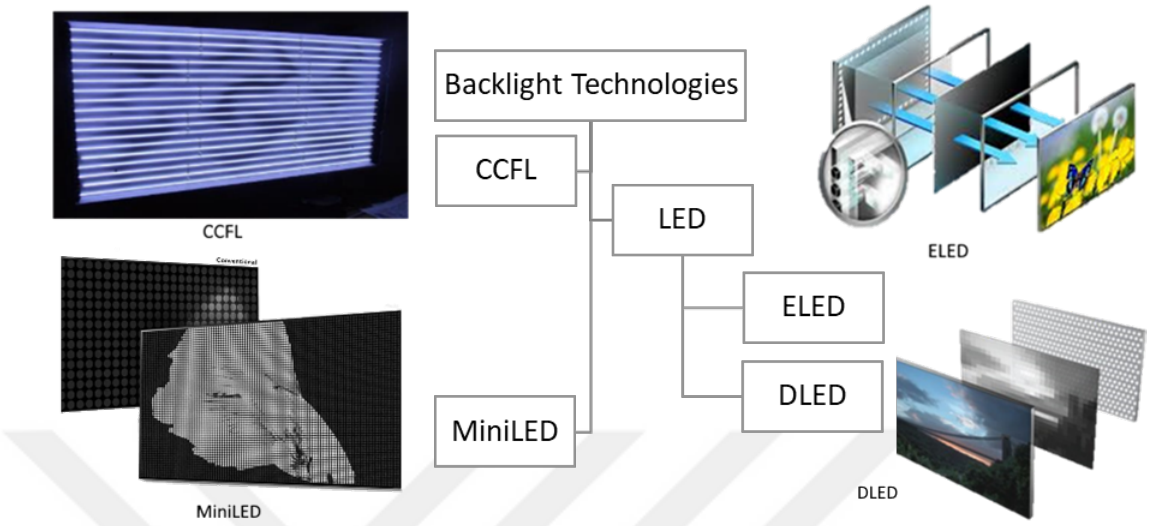

Figure 8 Backlight technologies

CRT TVs have an electron gun on the back. The flyback transformer generates a high voltage at the anode to attract electrons to the front of the screen and coats the inner surface of the tube with a phosphor. When the electron sent from the gun hits the phosphor, it emits light through fluorescence. Two deflection yokes are used to control the beam. The magnetic field directs the electron beam both horizontally and vertically. An image can be created by controlling the intensity of the beam [23]. CRT TVs have fast response times however, they consume more power than LCDs and geometrical errors occur at edges. Also, LCDs are brighter and have a better resolution than CRT displays.

Projection TVs are grouped as self-luminous if they are CRT and backlit if they are LED. The working logic of CRT projections is similar to that of CRT TV, light is directed with the help of mirrors, but the image is created at a distant point with the help of the lens. In digital light processing (DLP) LED projections, approximately two million mirrors in micro sizes are tilted with the help of chips to create a pixel-like image. A spinning color wheel is added to create a colorful image [24]. The disadvantage of the Projection TV is that the contrast ratio is low. The contrast

ratio is the ratio between the brightness of the brightest white and the brightness of the darkest black a TV can produce.

LCD screens need a backlight to create the image. As seen in Fig. 9, when light leaves the backlight it travels along different planes including the horizontal and vertical planes the first polarizer only allows light traveling along the horizontal plane to pass through it. Then it passes on to the color filters with another polarizer that only allows light to pass along the vertical axis. Liquid crystals typically orient themselves in random directions until the horizontally etched glass in the rear and the vertically etched glass in the front force by passing electricity through the electrodes to twist into a predictable pattern as light passes through [25].

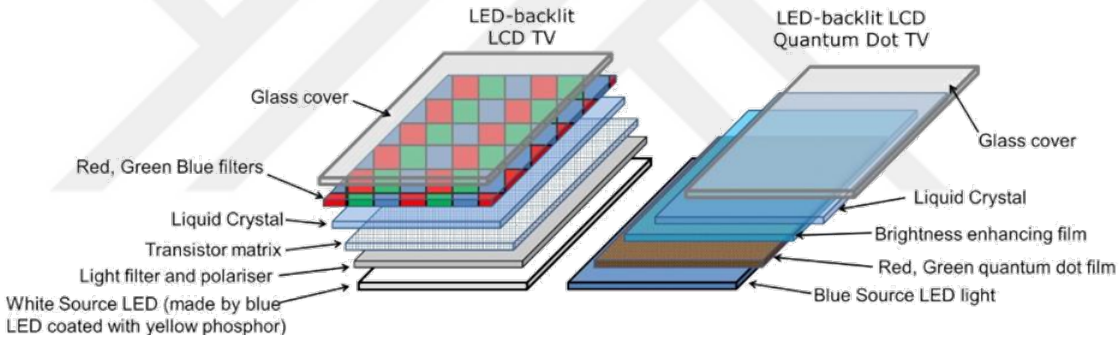

Figure 9 LED backlight and QDot backlight

One of the drawbacks of LCD is that it can never produce true blacks because the screen would have to become completely opaque. However, the advantages of LCDs are that it's relatively inexpensive these days and unlike traditional CRT tube TVs, they are extremely thin.

Each pixel that makes up the OLED screen emits its own light. In this way, there is no need for backlighting as seen in Fig. 10. It allows for thinner designs. It also supports transparent and foldable screen technology and the moving picture response time is 1.5 times faster than the LED LCD screen. It is a technology that addresses the contrast ratio, more efficient than conventional LCD-TFT (thin-film transistor)

displays. The drawback is the potential of display burn-in, which is usually caused by when light is not the output of the transitions between energy levels. One example is Auger recombination [26]. Also, the ghost image may occur on OLED displays as a result of the image remaining on the screen for a long time.

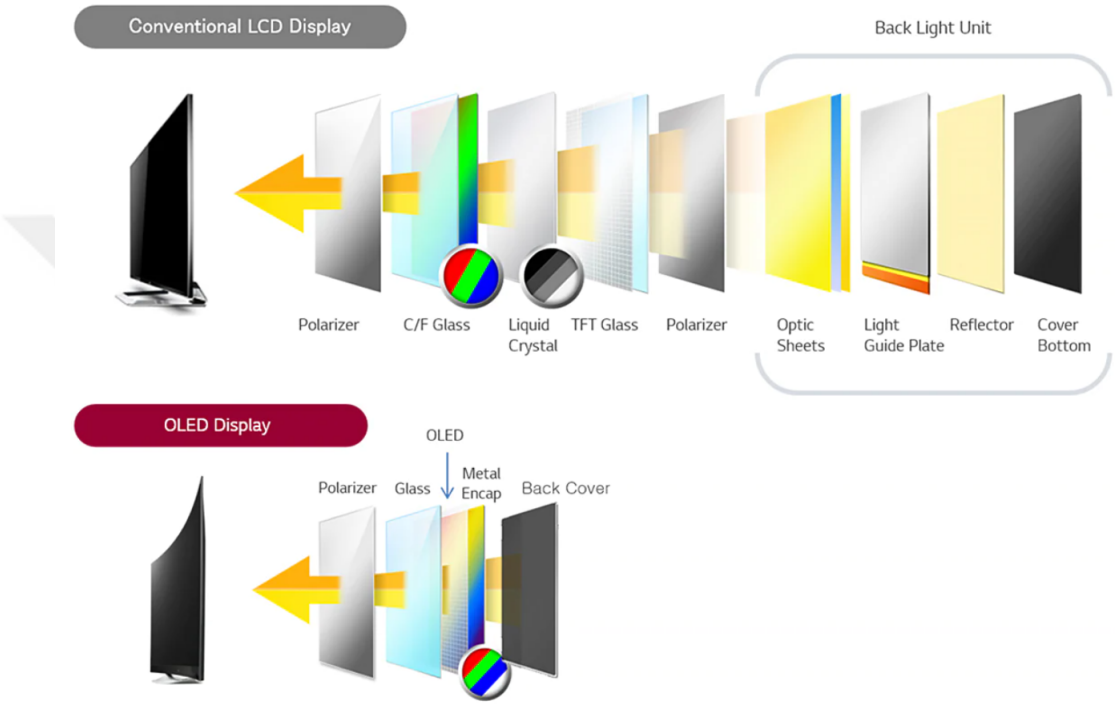

Figure 10 LED LCD and OLED

QDot LCDs start with a blue backlight layer as shown in Fig. 9. An extra layer of film is placed between the glass and the LED backlight. This layer contains red and green nano-sized particles ranging in size from one to four nanometers. When the blue backlight passes through red and green nanoparticles, it creates a purer white color than the LED backlight. Because every color filter on an LCD display blocks other colors to render the image, this is a less efficient way. By converting the color of the light using particles brighter and more vivid color options are offered on QDOT screens, with increased color gamut. In terms of image quality, Qdot displays are 1.26 times more efficient than OLED displays [27]. The disadvantages are slow response time and poorer viewing angles than OLED displays.

In MiniLed technology, backlighting can be controlled locally by using many small LEDs. The backlight is divided into more than a thousand zones and the control of the zones can be done on the motherboard using SPI communication. Using zone control, the contrast ratio is increased compared to conventional TFT screens, and deeper blacks are obtained by local dimming. It is more efficient than LCD displays, power consumption is decreased by 50%. However, smaller die brings cost in terms of manufacturability, specifically in lithography and die placement steps [28]. The advantage over OLED display is image quality can be achieved without the risk of led burn-in.

2.2 Isolated DC-DC Converters

During the design phase, the topology is determined in the first place by considering the output power level, cost, form factor, isolation requirement, efficiency, and other standard requirements of the product group, such as power factor, current harmonics etc. The topologies that can be selected considering the output power level are marked in table 1.

Flyback converters are the most preferred topology because the number of semiconductors used in DC-DC converter topologies where we will transfer power in isolation is low. However, its efficiency is low as it stores energy in a period while the MOSFET is in transmission and transfers this energy to the secondary when the MOSFET is in the cutoff. Therefore, it is preferred for low power transfers at low current [29].

The two switch flyback topology, on the other hand, is preferred to increase the efficiency in the topology and reduce the thermal stress on the semiconductor elements by storing the energy originating from the leakage inductance on the primary side with diodes. However, the topology cost is higher than the single switch flyback

structure. 78.2% efficiency was achieved in the single switch flyback structure operating in 30W continuous conduction mode, 75.87% with the single switch flyback with RCD clamping circuit, and 83.35% with the 2-switch flyback topology [30].

In the forward converter topology, unlike the flyback topology, there is an instantaneous energy flow to the secondary, therefore there are two diodes. A reset is performed with a third winding so that the energy to be induced in the primary due to the forward windings does not cause core saturation. When the two-switch and RCD snubber forward converters are compared, lower voltage stress was measured on semiconductor elements in the two-switch forward converter, also the transient response time at the output is lower. When the efficiency of the two topologies is compared, at the 280V input, the efficiency was 87% in the two-switch forward converter, while it remained at 83% in the RCD clamp forward converter[31].

LLC is favored where flyback and forward converters are inadequate because of topology efficiency, component temperatures, or power losses in high-power applications. Leakage inductance, one of the transformer parameters, is a parameter that is generally desired to be low in DC-DC converters. It causes MOSFET current peaks to be extremely high, hence losses. On the other hand, in LLC half-bridge topology, the transformer uses a series resonance capacitance to turn the leakage inductance into a resonance point, thus ZVS is obtained. Resonant converters are not cost-efficient at low output power levels due to the number of elements they contain but soft switching advantages can be used in this topology. Since losses will be less with this technique, it allows for the operation of high switching frequencies at high power, lowering the size of the filter components. This topology provides high power density at low dimensions. In the 56V, 350W LLC HB converter topology, the system efficiency is 85%-95% in the 10%-100% load range. With the compensation circuit added to the primary side, the efficiency was measured in the range of 88%-95% [32].

Table 1 SMPS topology selection [1]

Topology	0-100W Iout< $10A$	0-100W Iout> $10A$	100-400W	400-1200W
Single-switch flyback	✓	-	-	-
2-switch flyback	✓	-	-	-
Single-switch forward	✓	-	-	-
2-switch forward	✓	✓	✓	-
LLC Half Bridge	-	✓	✓	✓

2.3 Switching Techniques

A general TV power board block diagram is given in Fig. 11. Generally, a TV power board rectifies the 220V AC input to the DC output voltage in the rectifier block, then boosted to 400V with a higher power factor value in the PFC block. The output of the PFC has a DC to DC converter block that powers the motherboard. A backlight block, which is also added to the output of this block, meets the power requirement of the backlight. In the block diagram, switching is done in the PFC, SMPS, and backlight blocks. In these blocks when the switching element is switched on and off under voltage and/or current, sudden changes in voltage and current cause losses.

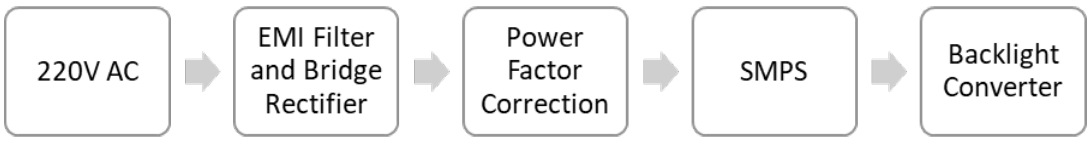

Figure 11 TV power board block diagram

In the 1kW DC to DC converter design in Fig. 12, the largest part of the losses is given as secondary conduction losses. However, it is given that the switching and conduction losses in the primary block should be considered [7].

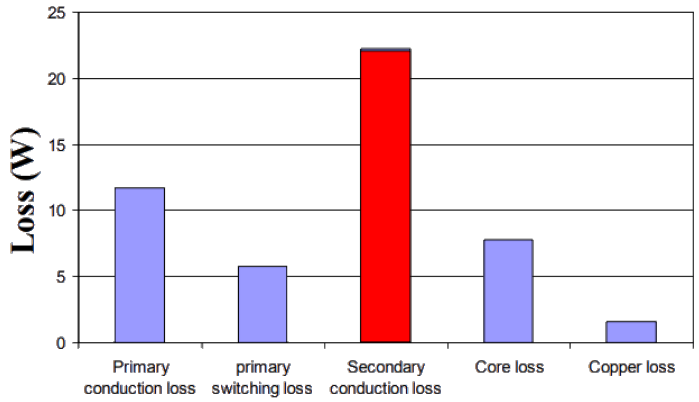

Figure 12 DC to DC converter loss analysis in [7]

Conduction losses and switching losses are seen when MOSFETs are switched on and off [33]. In SMPS circuits, it is preferred to reduce the power consumed on semiconductor elements, MOSFETs, to obtain higher efficiencies when the driver power increases. To decrease conduction losses, MOSFETs with lower on-resistance are used. On the other hand, the switching losses depend on the switching frequency and the internal capacities of the MOSFET.

Fig. 13 shows internal capacitances between the MOSFET ports, which we call parasitic capacitance, are formed during the production of the MOSFET. MOSFETs cause the switching losses at every switching cycle due to these internal capacitances between terminals.

In equations (1), (2) and (3), C_{iss} is the input capacity, C_{oss} is the output capacity, and C_{rss} is the feedback capacity and is equal to the capacity between the MOSFET's gate to drain electrode. The capacity most affected by the drain source voltage change is the feedback capacity and one of the biggest factors causing loss during switching is the C_{gd}. The reason for the losses is the delay in the current depending on the capacitance value.

$$C_{iss} = C_{gs} + C_{gd} \tag{1}$$

$$C_{oss} = C_{ds} + C_{gd} \tag{2}$$

$$C_{rss} = C_{gd} \tag{3}$$

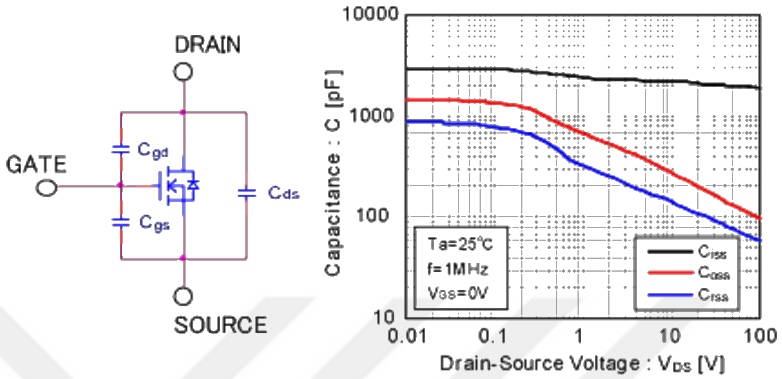

Figure 13 MOSFET capacitance and V_{ds} dependence [8]

In Fig. 14, the transition moment of the voltage and current between the drain and source ports at the turn on and turn off of the MOSFET is given.

There is a delay time for the capacitors in drain and gate electrodes until the drain-source voltage reaches a constant level. At this time, the current passing through the MOSFET does not change and this effect is called the Miller plateau [9]. In all these transition moments, switching losses are proportional to the length of this period. This is why semiconductor manufacturers try to keep the internal capacities as minimum as possible so that these transition moments within the MOSFET is short.

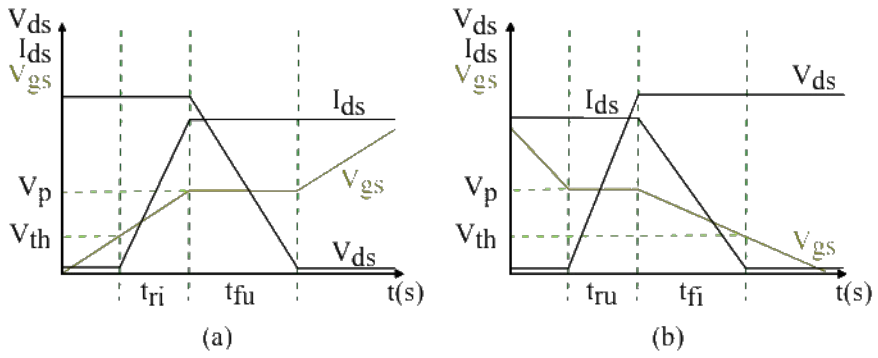

Figure 14 t_{on} and t_{off} characteristics of the MOSFET [9]

Depending on the topology, several switching approaches can be applied to decrease switching losses on MOSFETs while not limiting the converter's frequency. MOSFETs can be switched by soft switching or hard switching. In topologies where high efficiency is aimed, soft switching is favorable because the loss on semiconductors will be less. Hard switching can be used in low-power and low-loss applications.

2.3.1 Hard Switching

As seen in Fig. 15, it is the situation where both the current and voltage have a certain value in the opening and closing states. For this reason, maximum loss occurs on the switching elements, and the temperature increases. In applications that require high frequency, the loss increases in direct proportion to the frequency [34]. Efficiency is not the only drawback of this switching technique. High di/dt and dv/dt values due to steep variations create high EMI. The advantage of this switching technique is that the design time is short and the design is easy. It is preferred in low-power applications.

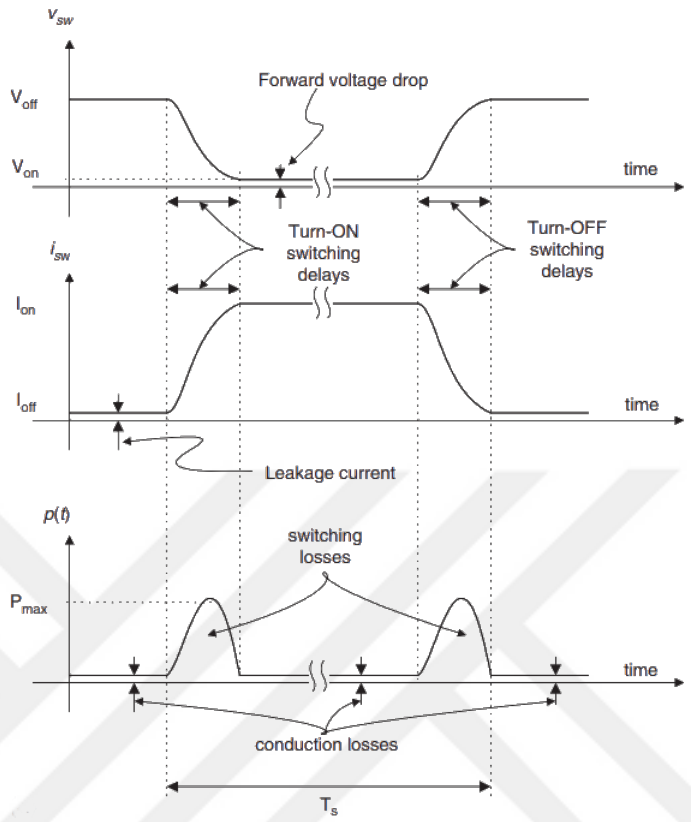

Figure 15 Hard switching characteristics of the MOSFET [10]

One of the ways to reduce losses is to use snubber circuits. Snubber circuits reduce the switching losses and stress on the element by preventing high voltage and current jumps on the semiconductor elements at the time of switching. Snubber circuits are built with resistors, diodes and capacitors. For example, during the turn off, the MOSFET current minimizes the voltage between the drain and source terminals until it reaches zero [33]. Minimizing the losses also reduces the thermal stress that will occur in hard switching circuits.However, the turn off snubber circuit causes a loss on the resistor at turn on [35].

2.3.2 Soft Switching

In this switching method, voltage and current expect each other to be zero (Zero voltage switching, Zero current switching). With this method, the switching losses

that prevent us from operating at high frequencies are minimized. Soft switching technique gives us the chance to maximize efficiency with much less switching losses at much higher frequency and provides EMI improvement.

The waveforms at the time of switching for ZVS and ZCT techniques are given in Fig. 16. In the zero voltage switching method as shown in Fig. 16a, when the internal diode of the MOSFET is in conduction, that is, the voltage between the drain and source terminals is zero, and the MOSFET is turned on. In addition, ZVS can be obtained by slowing down the change in voltage with a capacitance connected in parallel to the drain and source ports of the MOSFET, but the parallel connected capacitance will cause an additional loss at turn on. In the ZCS technique as shown in Fig. 16b, the switching is done when the current is zero, the delay in the current can be obtained with an inductor connected in series [11].

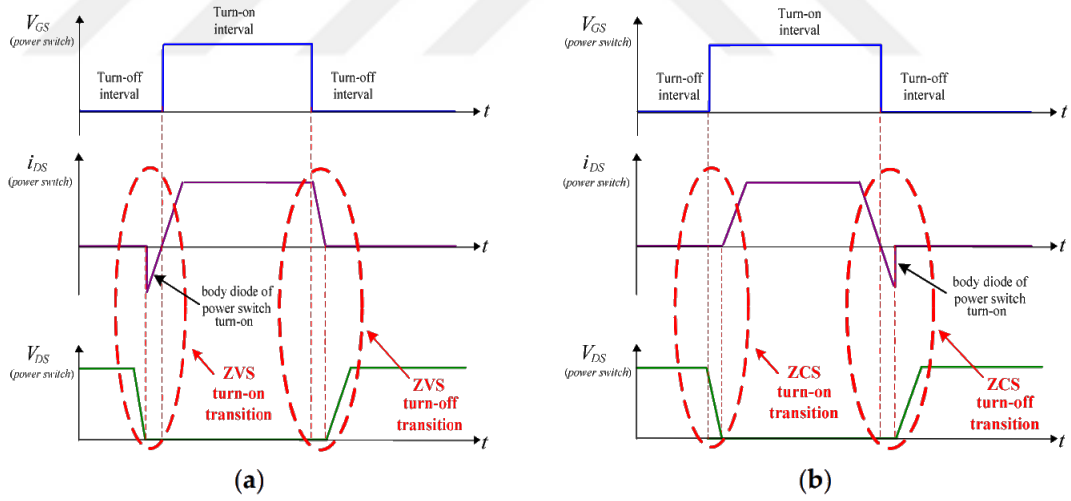

Figure 16 (a) ZVS turn-on and turn-off transitions; (b) ZCS turn-on and turn-off transitions [11]

When comparing the switching losses on the MOSFET in Fig. 17a that the snubber technique we use to limit the sudden voltage and current changes on the element is more efficient than the hard switching technique. However, the minimum losses in the system are obtained with the soft-switching technique [10].

Fig. 17b represents an analysis of the PFC circuit for variable powers. While obtaining a maximum efficiency of 91% with hard switching, this value has been increased to 98% with soft switching technique.

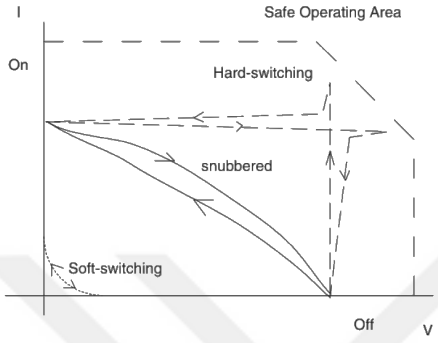

(a) Snubber effect[10]

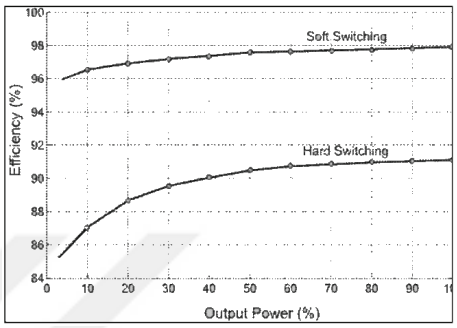

(b) PFC efficiency comparison [36]

Figure 17 Switching techniques comparison

2.4 Resonant Converters

In tank circuits, resonance is the point where the magnetic energy stored on the coil turns into electrical energy above the capacity, and the energy transfer, that is, the oscillation, continues forever in the ideal environment. However, due to the energy transferred to the load on the circuit, the oscillation period depends on the value of the coil and the capacitance.

If a square wave is applied to the input of the resonant converter block, the LC circuit, as shown in Fig. 18, behaves like a band-pass filter and only sinusoidal current is allowed. In this way, high current harmonics are filtered by the resonant tank, and only the sinusoidal component (fundamental component) is obtained at the output of the tank circuit [37]. In parallel resonant circuits, the value of inductive reactance at the resonance point is equal to the value of capacitive reactance and is in the opposite direction, and therefore the current in the circuit is minimum. However, in series resonant circuits, the value of inductive reactance is equal to the value of

capacitive reactance, and therefore the current in the circuit is maximum.

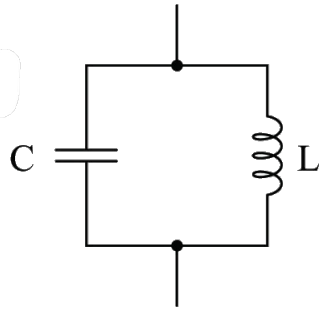

Figure 18 Tank circuit

Pan detection circuits, which only look at how many periods the oscillation continues, are used in induction cookers and wireless energy transfer in electric vehicles to increase efficiency [38] [39]. Resonant circuits can be grouped as series resonance, parallel resonance, and series-parallel resonance (LCC and LLC) circuits.

2.4.1 Series resonant circuit

In the resonant circuit as shown in Fig. 19a, the resonance capacitance (C_r) and the resonance inductance (L_r) are connected in series to the midpoint of the switching elements. In this topology, the secondary current is continuous as the transformer current, that is, the resonance current, will be as much as the transformer ratio. The disadvantage of series resonant circuits is the maximum gain here is one and the problem of the unregulated output voltage at no-load, as the slope is very steep at the point where the gain is one in Fig. 19b. A very small change in frequency will cause spikes in output voltage. In addition, another disadvantage brought by the topology is that the current ripple value in the output capacitor is very high, so the series resonant converter is preferred in applications that require low output current [12].

The biggest advantage of the series resonance circuit is its suitability for the full-bridge topology, which is more preferred in high voltage applications, its resonance

capacity functions as DC blocking. Another advantage is the steep slope of the gain graph, although it is a disadvantage in no-load, since the current passing through the primary decreases at low output loads, it significantly reduces the transmission loss of the MOSFETs, which contributes greatly to the efficiency, and its superiority over the parallel resonance topology comes from this [12].

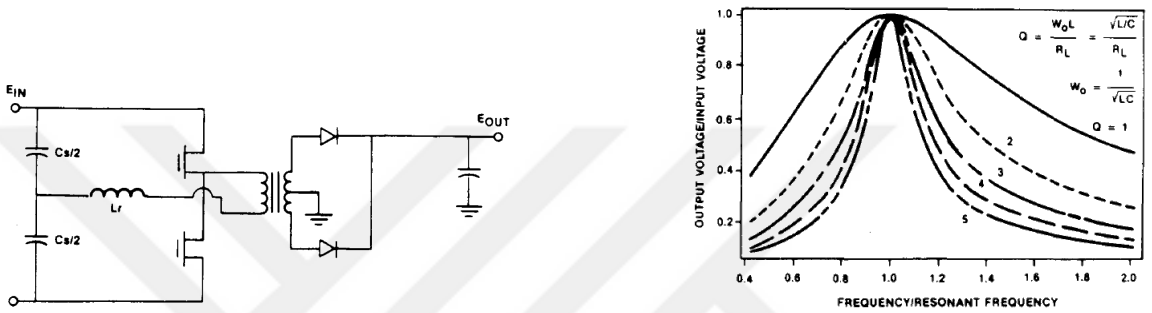

(a) Circuit diagram (b) Gain graph

Figure 19 Series resonant circuit [12]

2.4.2 Parallel resonant circuit

In the parallel resonance circuit as shown in Fig. 20b, unlike the previous topology, the resonant capacity is placed parallel to the primary winding of the transformer. Due to this placement, the reflection of the capacitance current passes through the diodes in the secondary rectification circuit. In order to reduce the ripple value of the current passing through the load, a coil is placed at the output [12].

Parallel resonant circuits provide output voltage control by operating above the resonant frequency, unlike series resonant circuits, as seen in the gain graph given in Fig. 20b. However, the disadvantage of this topology is the working condition at light load, although it increases the switching frequency to provide output voltage regulation, the power consumed on the primary side does not decrease according to the load. For this reason, light load efficiency in parallel resonance circuits is less than in series resonance. This topology is more efficient when the input voltage range

is narrow, the output current is high, and the load is near the designed power. By operating above the resonant frequency, ZVS is achieved and operating below it, ZCS is achieved, thereby minimizing switching losses [12].

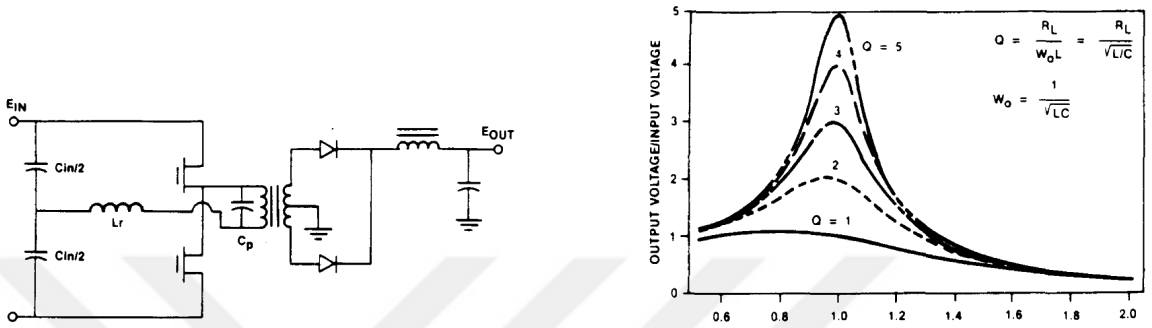

(a) Circuit diagram (b) Gain graph

Figure 20 Parallel resonant circuit [12]

2.4.3 Series parallel resonant circuit

The fact that the output voltage cannot be regulated at no load in the series resonance circuit and the maximum gain is limited to one limits the application areas of this topology. In a parallel resonance circuit, the problem is that the current circulating in the primary of the transformer independent of the load causes low efficiency. The series-parallel resonant circuit combines the advantages of these two topologies, so the application area is wider.

If the elements forming the resonance points consist of two inductors and one capacitor, it is called LLC, if two capacitors consist of one inductor, it is called LCC. Considering the circuit structure of LCC in Fig. 21a, it looks identical to the parallel resonant circuit. However, while the capacitance at the input does not participate in the resonance in the parallel resonance circuit, here this capacitance named as the series resonant capacitance creates a separate resonance point together with the resonant inductor.

Fig. 21b shows how much the voltage gain will be affected when the converter's

working frequency changes. This value varies depending on the resonant capacity, inductor, and load. When the gain graph of the LCC circuit is examined, the frequency response depending on the load is similar to the series resonance circuit at high Q values, while it is like a parallel resonance circuit at low Q values [12].

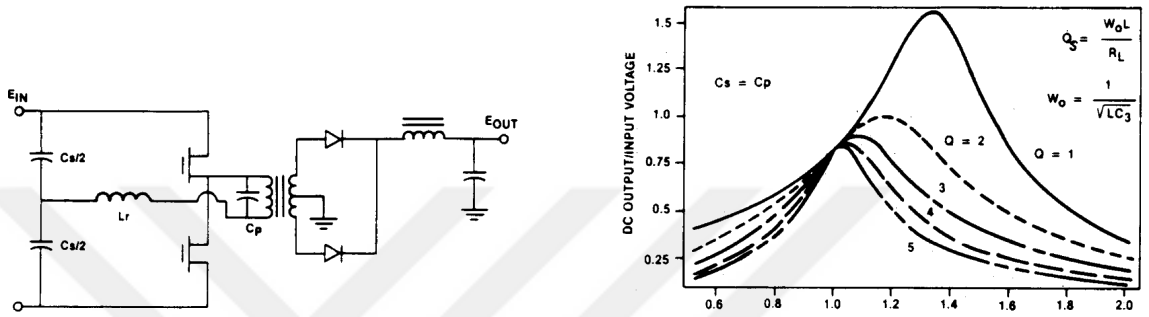

(a) Circuit diagram (b) Gain graph

Figure 21 LCC resonant circuit [12]

When the LLC converter circuit diagram is examined in Fig. 22a, it is seen that this converter actually resembles the series resonant circuit. The difference between them is that the leakage inductance, which is not in the series resonance circuit and can be obtained by using the air gap of the transformer, creates a second resonance point here and changes the characteristics of the gain graph, as shown in Fig. 22b. The leakage inductance of the transformer and the total inductance on the primary side forms two separate resonance points with the resonance capacitor. Considering the circuit diagram difference between LLC and LCC topologies, it is seen that a coil is not needed to correct the current at the output in the LLC topology on the secondary side [13].

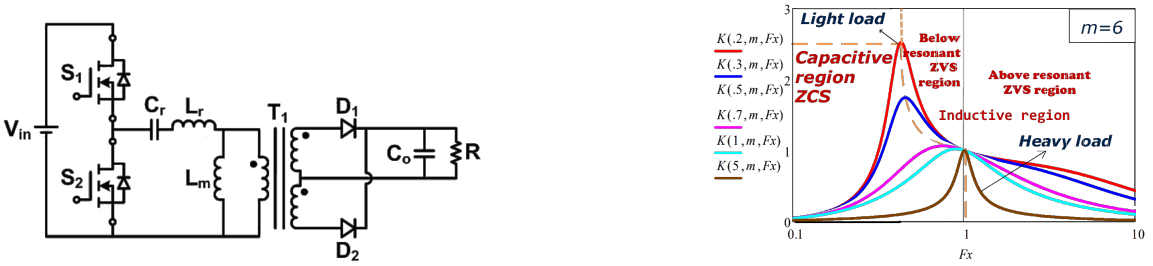

(a) Circuit diagram (b) Gain graph

Figure 22 LLC resonant circuit [12]

When LLC and LCC topologies are compared in terms of performance, LLC is more complex due to the adjustment process of the transformer's leakage inductance. Hovewer, LLC converter works under variable output load much more reliable than LCC. It has been observed that the switching frequency does not change much and the circuit works almost independently of the load in LLC, and in the LCC converter, the change in switching frequency is quite high under variable output load. The frequency span of converters is given in Fig. 23a and Fig. 23b.

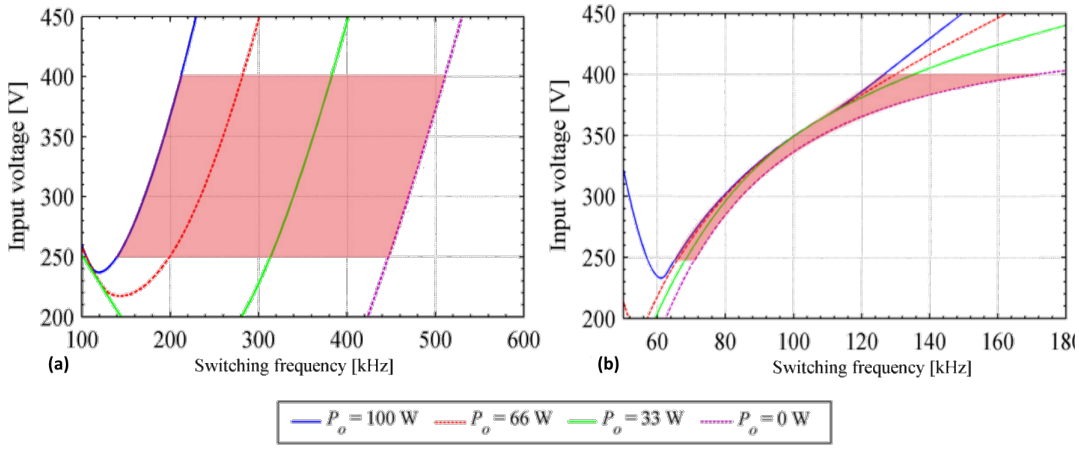

Figure 23 Variation of switching frequency according to input voltage (a) LCC converter (b) LLC converter [13]

Also, as stated in [13], when the additional variable input voltage is added to the variable output power, as shown in Fig. 24, the LLC converter has 93% efficiency

even under 20% load and the efficiency almost does not change when the input voltage is 300V and 380V, while the efficiency in the LCC converter circuit is almost 85% at 40% load. Also, the efficiency decreases further to 73% at minimum load when the input voltage drops from 380V to 300V. The reason for this is that the current circulating in the primary is high in the case where the capacitance is parallel to the load, as examined in the parallel resonance converter.

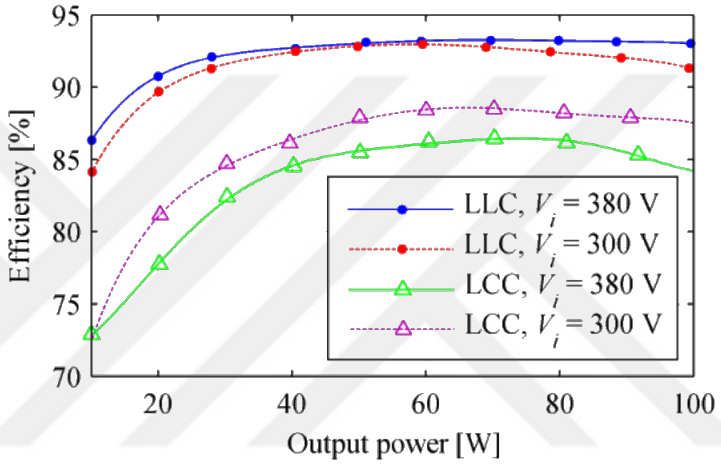

Figure 24 Variation of efficiency according to input voltage in [13]

CHAPTER III

POWER SUPPLY UNIT DESIGN

In this chapter, from the AC input to the rectifier block feeding the LEDs, the EMI filter block in the AC-DC converter, inrush current limiting circuit, PFC circuit, backlight driving circuit, and secondary rectification block will be explained.

In the backlight driving circuit section, the problem definition will be given by comparing conventional backlight driving topology with the proposed backlight driving topology. Also LLC resonant circuit structure, LLC operating regions and timing diagram, resonant converter operating modes depending on the frequency, LLC equivalent circuit parameters will be explained and in the design part, backlight transformer calculations, controller review, and proposed current balancing circuit will be explained.

3.1 AC to DC Block

In this part of the thesis, the AC to DC block analysis will be made. The input block with circuit elements as shown in Fig. 25 consists of filtering elements, an inrush current limiter, a rectifier, and a power factor corrector (PFC). Filter elements are used to suppress electromagnetic noises caused by high-frequency switching of power semiconductor materials (MOSFET, IGBT, etc.) in switching power supplies. Circuit elements for limiting the inrush current when charging the high-value capacitor at the initial state of energizing the power supply are used in this block after the EMI filter. 90V-270V AC voltage is passed through the filter block and rectified in the full-bridge rectifier at the input. Also, DC to DC boost converter circuit elements is used to increase the power factor. The obtained DC voltage output of the rectifier block is passed through the PFC block and a DC voltage of 390V is obtained. Bulk capacitors

are used for the backlight block supply and the motherboard block supply.

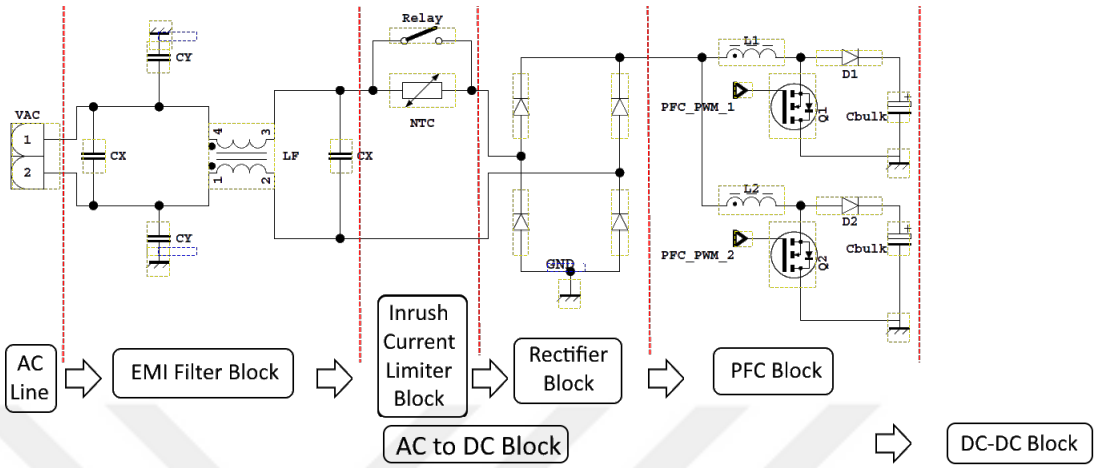

Figure 25 AC to DC block

3.1.1 Electromagnetic Interference Filter

As a result of high-voltage and high-current semiconductor materials that provide power transmission to the output, two types of noise sources occur on them as a result of switching at high frequencies.

The first of these noise sources is the conducted noise measured from the mains input of the device, usually measured up to a frequency of 30 MHz. This is because conduction path interference noise signals in conductors lose their effect after 30 MHz. The other source of noise is the radiated noise measured by the antenna specified in the standards covering the product, it covers after 30 MHz.

Noise types emitted from switch mode power supplies are divided into two, differential mode and common mode, as shown in Fig. 26.

In differential mode noise type, the noise goes from the source, denoted as reference point 1, to the load, denoted as reference point 2, over one of the paths (line or neutral) and returns over the other path. There is a potential difference between these reference points and this potential difference cause electromagnetic radiation. The strength of the radiation is directly proportional to the square of the frequency,

the propagation path length, and the distance between the paths. In conducted emission (CE) tests, differential mode noise is more dominant in the 150kHz-2 MHz frequency region.

In the common mode noise type, the noise moves from the source to the load in the direction of the load over all the conductors of the transmission line and turns over the ground line, completing the circuit. The electromagnetic radiation caused by common-mode currents is directly proportional to the frequency and the length of the propagation path. While the capacitors (C_x) connected between the phase-neutral in the circuit diagram in Fig. 25 suppresses the differential mode noise, the common mode coil (LF) and the capacitors (C_y) connected between the phase-ground and neutral-ground suppress the common-mode noise. In order to suppress all these noises, the C-L-C-L-C structure is used in the filter block.

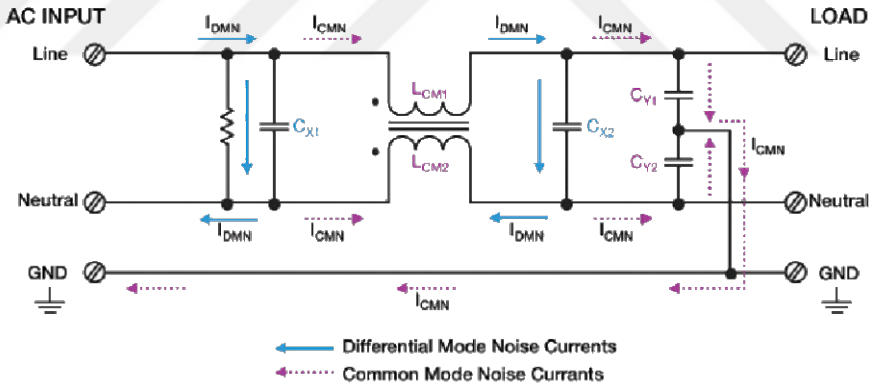

Figure 26 Differential mode noise and common mode noise

3.1.2 Inrush Current Limiter

The energy stored in the AC to DC block of the power supply is stored on the high-value capacitor as shown as C_{bulk} in Fig. 25. However, when the power supply unit (PSU) is energized for the first time since the capacitor's initial voltage value is zero, a high current is drawn from the ac supply for a short time, this current is called inrush current. It is seen that this current also passes over the full-bridge rectifier diodes

when the phase line in Fig. 25 is followed. If the maximum inrush current is more than the instantaneous maximum current carrying capacity of the diodes, then diodes will fail. Therefore, the current at the input is limited by the NTC. However, since this resistor will cause unnecessary efficiency loss when it is in continuous conduction in the system after the voltage on the capacitor reaches the DC mains voltage value, the relay connected to the NTC is switched on and the NTC is deactivated. This also reduces the inrush currents on the system during short-term power cuts.

3.1.3 Power Factor Corrector Circuit

In this block, the rectified input voltage in the AC-DC block is fixed to a constant DC voltage using a step-up DC/DC converter. In addition, the main task of this block is to correct the power factor, the waveform of the current drawn by the load is approximated to the waveform of the input voltage. The angle difference between the phases is minimized. The reason for the phase difference is the output filter capacitor located at the output of the AC-DC block and used to obtain a smooth DC voltage, causes the currents drawn from the network to be intermittent. So the current has many harmonic components.

In the power factor corrector (PFC) block, the boost converter topology is preferred because the current on the coil is continuous when the MOSFET is on and off. In this way, the rectifier output voltage can be easily followed. The working mode can be selected as continuous conduction mode, transition mode, or discontinuous conduction mode depending on the design requirement. As a structure, interleaved PFC or totem pole PFC structure can be preferred. In the Interleaved PFC structure, there are two PFC blocks working synchronously with each other. In this way, the heat performance of the PFC block is improved, the component sizes are reduced and the RMS current on the output capacitances is reduced. However, the number of components and the area used in the layout increase. This structure was preferred

to maintain temperature performance in a slim design.

In this design, interleaved boost converter working in transition mode is used in the PFC block, and Onsemi's NCP1631 IC is used. The circuit diagram is given in Fig. 27. PFC block boost 90-270V input to 390V output with 10% ripple. The inductances of the PFC transformers used are equal and 180uH. The total value of the output capacitances is 329uF. The hold-up time is calculated as 60ms.

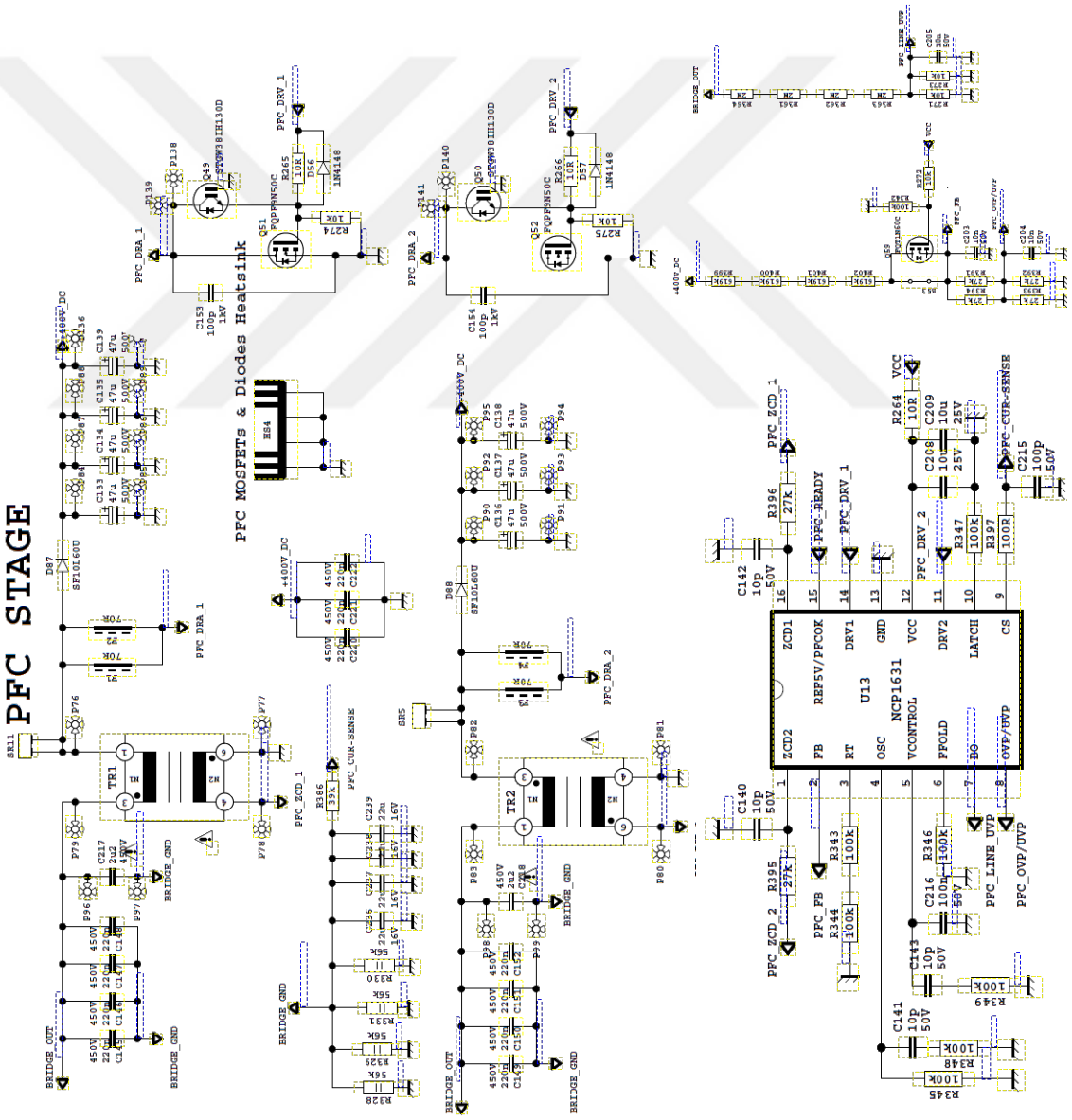

Figure 27 PFC circuit diagram

3.2 Backlight Block

In the backlight driving circuit section, the problem definition will be given by comparing conventional backlight driving topology with the proposed backlight driving topology. Also, LLC resonant circuit structure, LLC operating regions and timing diagram, resonant converter operating modes depending on the frequency, LLC equivalent circuit parameters will be explained and in the design part, backlight transformer calculations, controller review, and proposed current balancing circuit will be explained.

3.2.1 Standard Backlight Circuit

In the backlight block of televisions, cascaded DC-DC converters are generally used in the SMPS block. In this application, the SMPS transformer output is set to the input voltage of the DC-DC converter used to step up to the panel voltage. In the circuit diagram, two boost converter blocks are used, which are fed from the same 24V input, work in parallel with each other and increase the output to the panel voltage. Although this level changes depending on the optical design, since the backlight voltage will be at 150V in this application, the main transformer's 24V output should be taken and using a center tap transformer the voltage should be increased to 150V. One of the boost converter blocks can be seen in Fig. 28.

However, since using boost converters in parallel with each other will increase the number of semiconductors in the system, the total reliability will decrease and the cost of the board will increase. The cost comparison of the system with the proposed method will be given in the next chapter. In addition, when more than one boost converter block is used, the area occupied by the backlight block on the power board will increase. Apart from space and cost, another disadvantage is the variation in system efficiency. As stated in the literature review, when we cascade the DC-DC converters, the total efficiency of the system will be equal to the product of the LLC

and boost converter block's efficiencies, so the system efficiency will decrease and the loss will cause an increase in ambient temperature.

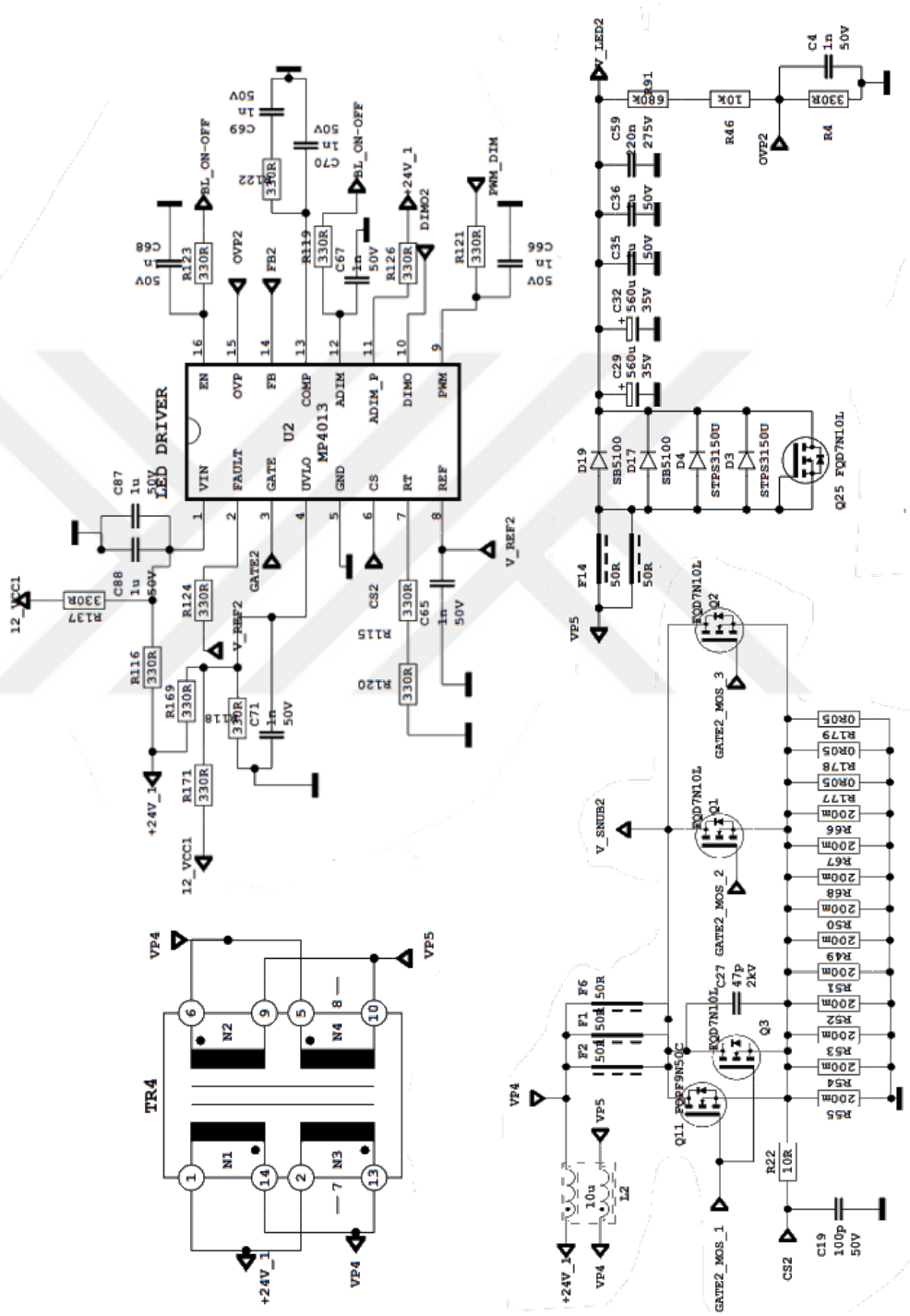

Figure 28 Conventional backlight block circuit diagram

The proposed method for transferring 145W backlight power on the closed back-cover in relatively slim designs is as follows.

3.2.2 LLC Resonant Topology

In the proposed circuit, which circuit diagram is given in Fig. 29, the two-transformer LLC half-bridge topology with the primary of the transformers connected in series is used in the backlight block. The LLC circuit is located at the end of the power factor corrector block. LLC is favored where flyback and forward converters are inadequate because of topology efficiency, component temperatures, or power losses in high-power applications.

In the next subsections, LLC operating regions and timing diagram, resonant converter operating modes depending on the frequency, and LLC equivalent circuit parameters will be explained to be used in the design parameters calculation part.

Resonant circuits are divided into three main parts. The first section contains MOSFETs that switch the PFC output voltage to create a square wave and their gate driver circuit called the switching block. The second part is the resonance block, which contains the transformer and resonance capacitance, which passes only the first harmonic of the square wave and that is the only harmonic that transfers power. The third is the rectification block, which contains diodes or MOSFETs that convert the voltage obtained in the secondary of the transformer to a DC voltage.

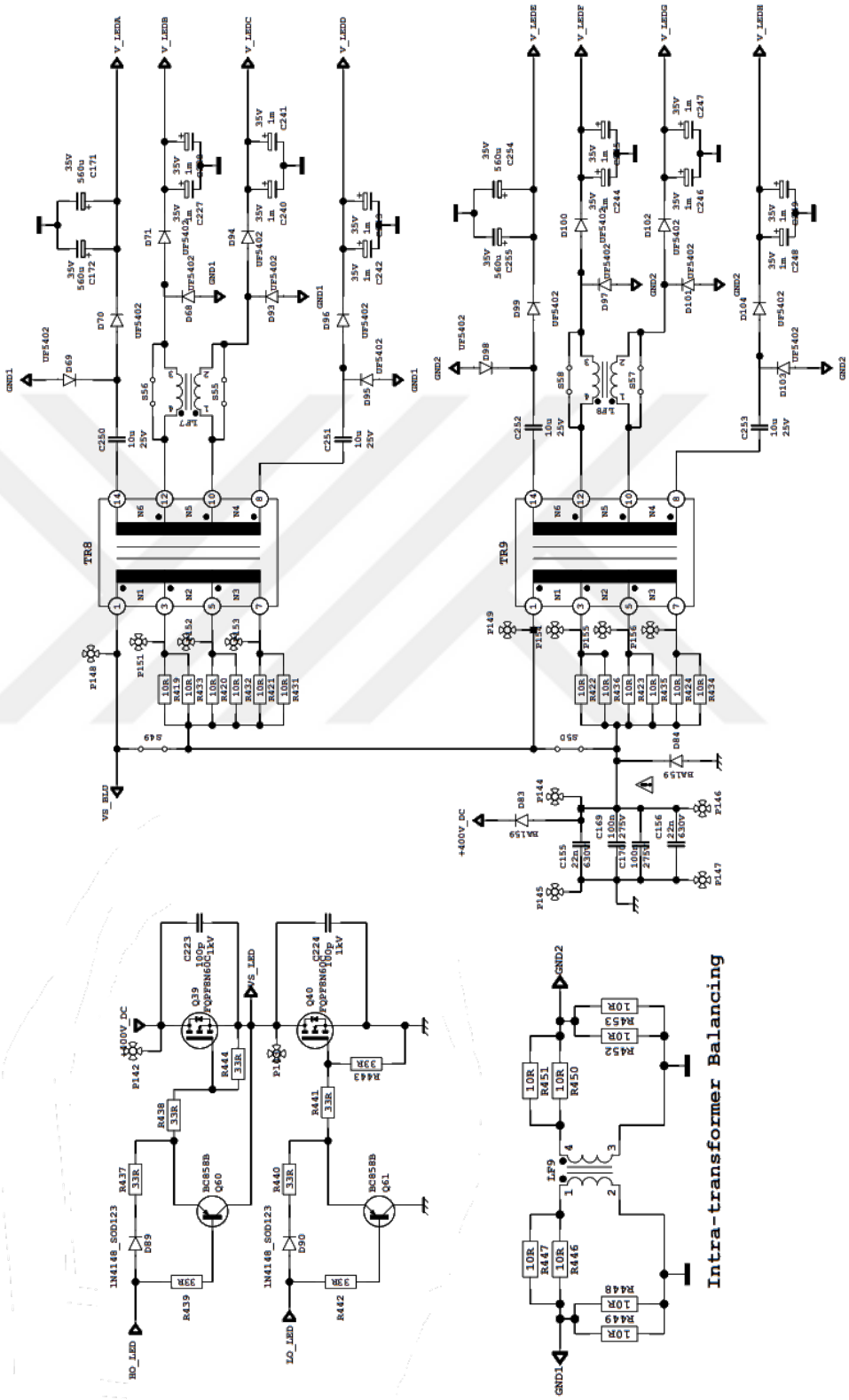

Figure 29 Proposed circuit diagram

In Fig. 30, a simplified LLC circuit is given using a single transformer. The operating modes of the circuit will be explained through this figure.

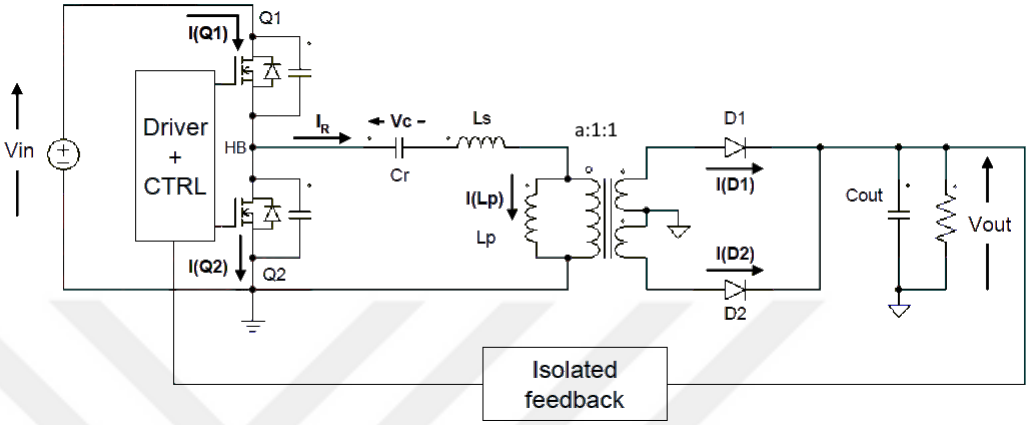

Figure 30 Simplified LLC circuit [14]

3.2.2.1 LLC Operating Regions

LLC converter has three main operating regions, ZCS region, above ZVS and below ZVS regions, seen in Fig. 31. If the converter is intended to operate in the ZCS region, it is actually expected to operate in the region below the maximum gain on the gain graph. Resonant current leads the resonant voltage in this region. Since the gain curve will turn negative in this region, the feedback block must be changed accordingly. Another disadvantage of switching in the capacitive region is on the body diodes, the diode with current flowing through it enters reverse recovery and causes emission. Above and below ZVS regions are referred to as inductive regions. Since the resonant current in this region follows the resonant voltage behind, the semiconductors are switched while the MOSFET body diode is conducting, and ZVS is provided. The region above the max gain is the inductive region. The work on the above and below resonance points will be explained in detail in the next chapter.

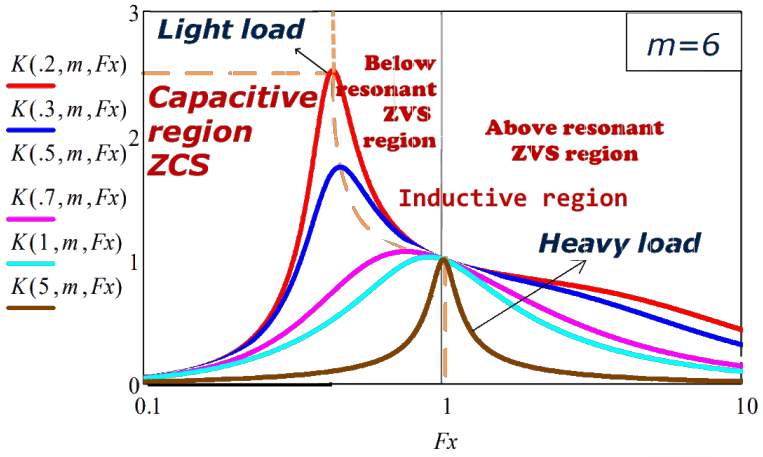

Figure 31 LLC operation regions [12]

3.2.2.2 LLC Circuit Switching Period

In the $t_0 - t_1$ time interval in Fig. 32, Q_2 is turned off, while Q_1 is turned on. At t=t_0, the resonant circuit current is in the positive half cycle, and Q_1 works in the first region on the I-V curve. D_2 is reversed biased, its reverse voltage is -2Vout, and D_1 is forward biased. The magnetic inductance denoted by L_p is short-circuited, in this case, it does not participate in resonance. The value of the voltage across the winding is -nVout. The frequency of the sinusoidal current flowing over the resonant tank is w_o. The stored energy on C_r and L_s is used to power the load. At t_1, Q_1 is turned off, the current on the magnetic inductance becomes equal to the current flowing through the leakage inductance, and in this case, the current on the secondary diode is zero.

In the $t_1 - t_2$ time interval in Fig. 32, both MOSFETs are turned off. The energy consumed in this cycle is the energy stored on the magnetic inductance. Until the voltage accumulated on the output capacity of the second MOSFET reaches the zero volts, the current passing through the leakage inductance and magnetic inductance charges the output capacity of the first MOSFET, while it discharges the output capacity of the second MOSFET. As the energy flows towards the ground, the body

diode of the Q_2 MOSFET turns on. No energy is transferred to the secondary during this time interval. At t_2, the Q_2 MOSFET starts conducting.

Allowing time between switching two MOSFETs is left on the order of nanoseconds by the controller as a safety requirement to avoid the situation where 400V is pulled to ground with a very low $R_{ds(on)}$ value. In addition, this time is required to provide ZVS.

In the t_2-t_3 range in Fig. 32, Q_1 is off, while the body diode of Q_2 is in conduction. Q_2 MOSFET turns on with ZVS and works in the third region on the I-V curve. At this region, voltage is positive while current flows from source to drain terminal. On the secondary side, D_1 is reversed biased, its reverse voltage is -2Vout. D_2 is forward-biased. The magnetic inductance denoted by L_p is short-circuited, in this case, it does not participate in resonance. The value of the voltage across the winding is -nVout. The frequency of the sinusoidal current flowing over the resonant tank is w_o. The energy stored on C_r and L_s is used to power the load until the resonant current becomes zero.

In the $t_3 - t_4$ time interval in Fig. 32, Q_1 is turned off, while Q_2 is turned on. At t=t_3, the resonant circuit current turns negative. D_1 is reversed biased, its reverse voltage is -2Vout and D_2 is forward biased. The magnetic inductance denoted by L_p is short-circuited, in this case, it does not participate in resonance. The value of the voltage across the winding is -nVout. The frequency of the sinusoidal current flowing over the resonant tank is w_o. The stored energy on Cr and L_s is used to power the load. At t_4, Q_2 is turned off, the current on the magnetic inductance becomes equal to the current flowing through the leakage inductance, and in this case, the current on the secondary diode is zero.

In the $t_4 - t_5$ time interval in Fig. 32, both MOSFETs are turned off. Until the voltage accumulated on the output capacity of the second MOSFET reaches the level of V_{in}, the current passing through the leakage inductance and magnetic inductance

charges the output capacity of the second MOSFET, while it discharges the output capacity of the first MOSFET. As the energy flows towards V_{in}, the body diode of the Q_1 MOSFET turns on. No energy is transferred to the secondary during this time interval. At t_5, the Q_1 MOSFET starts conducting.

In the t_5-t_6 range in Fig. 32, Q_2 is off, while the body diode of Q_1 is in conduction. Q_1 MOSFET turns on with ZVS, Q_1 works in the third region on the I-V curve. At this region, voltage is positive while current flows from source to drain terminal. On the secondary side, D_2 is reversed biased, its reverse voltage is -2Vout. D_1 is forward-biased. The magnetic inductance denoted by L_p is short-circuited, in this case, it does not participate in resonance. The value of the voltage across the winding is -nVout. The frequency of the sinusoidal current flowing over the resonant tank is w_o. The energy stored on C_r and L_s is used to power the load until the resonant current becomes zero.

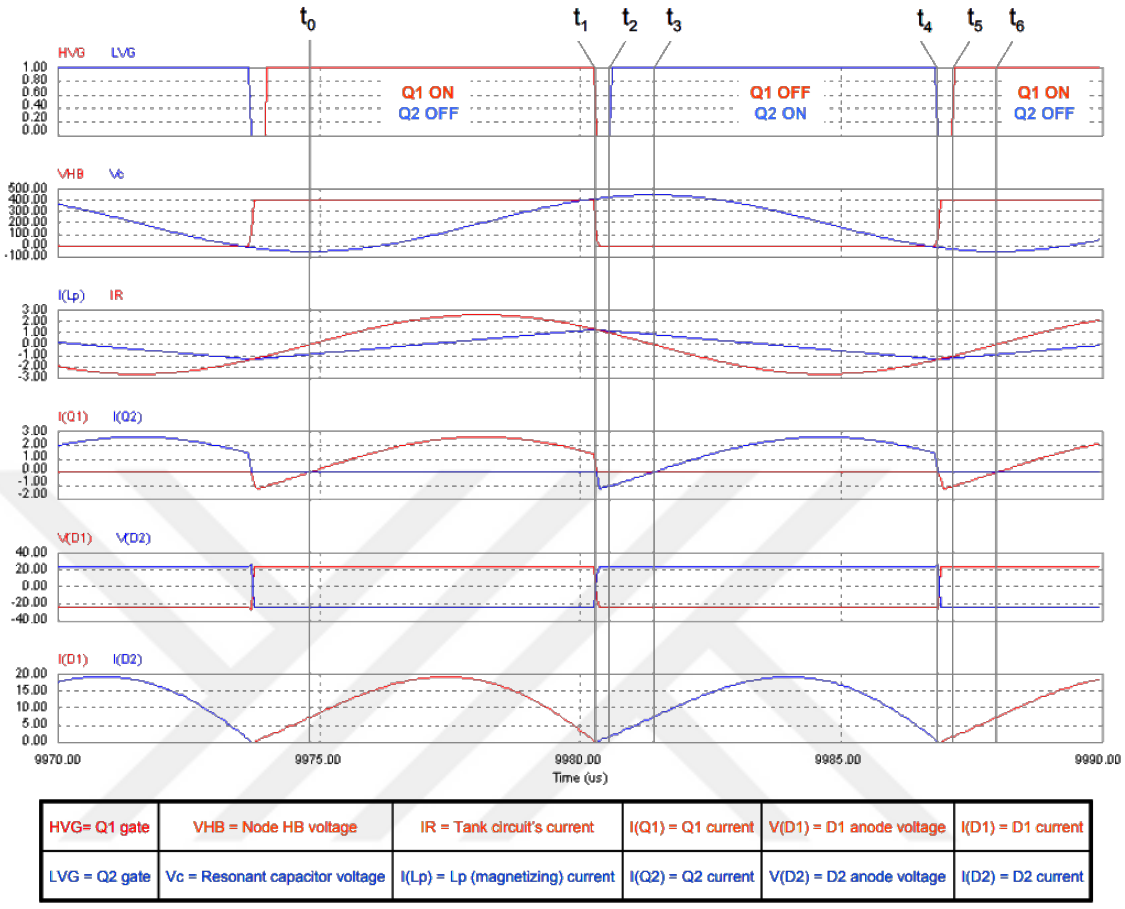

Figure 32 LLC circuit waveforms at $f = f_0$ [14]

3.2.2.3 LLC Circuit Modes of Operation

In each switching period, resonant tank transfers full power to the load when the switching frequency is the resonant frequency. As explained above with the timing diagram, at the end of each half-period, when the current passing through the series resonance inductance reaches the current passing over the transformer magnetic inductance, the energy transfer to the transformer secondary stops. The gain of the resonant tank is one when the switching frequency is the resonant frequency. The simplified waveform where the operating frequency is the resonant frequency is given in Fig. 33.

In each switching period, when the switching frequency is above the resonant frequency, the next semiconductor is switched before the half-cycles are completed. For this reason, the losses at the turn-off on LLC MOSFETs are high, but the conduction losses are less because the current circulating in the primary is less. Since the secondary diodes switch to reverse polarity before the current they carry is reset, reverse recovery losses are high, which increases electromagnetic dissipation. The frequency range is wide when the converter operates in this region, but the switching frequency becomes very high in the no-load condition. This mode is preferred in applications where the gain is low, that is, low output voltage is required. Such as LCD TV applications, laptop adapter applications. Simplified waveforms where the operating frequency is above the resonant frequency are given in Fig. 33.

In each switching period, when the switching frequency is below the resonant frequency, half-cycles are completed and the next semiconductor is switched while the freewheeling operation is in progress. Freewheeling starts after the current on the series resonance inductance and the parallel resonance inductance (magnetic inductance) are equalized, while there is no energy transfer to the secondary of the transformer. The resonant current circulates in the primary. Therefore, transmission losses are high in LLC MOSFETs. There is no reverse recovery loss in the secondary diodes. When the converter operates in this region, it has a narrow frequency range according to the load change, even in the no-load state the switching frequency is limited by the resonant frequency. This mode is preferred in applications where the gain is high, that is, high output voltage is required. Like Plasma TV apps. Simplified waveforms where the operating frequency is below the resonant frequency are given in Fig. 33.

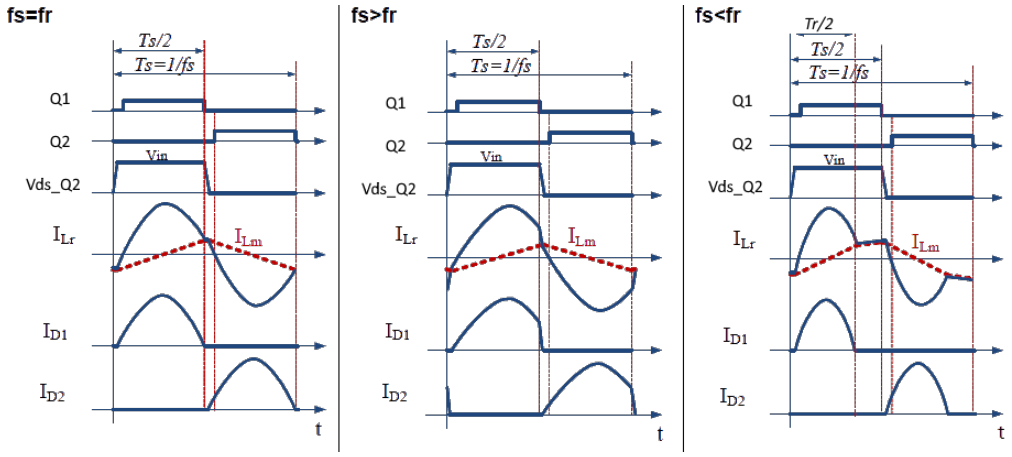

Figure 33 LLC circuit modes of operation [14]

3.2.2.4 LLC Equivalent Circuit Parameters

Fig. 34a shows the equivalent circuit of the LLC resonant converter. In the circuit, the load resistance in the secondary of the transformer is different from that reflected to the primary. The load in the transformer primary can be calculated using the load current and the load voltage. $|I_{ac}|$ equals half the current through the load if we model the transformer's primary as a current source, as shown in Fig. 34b. The resonant current is calculated in eq. (4) using the first harmonic approximation,

$$I_{ac} = \frac{\pi I_0}{2} \sin wt \tag{4}$$

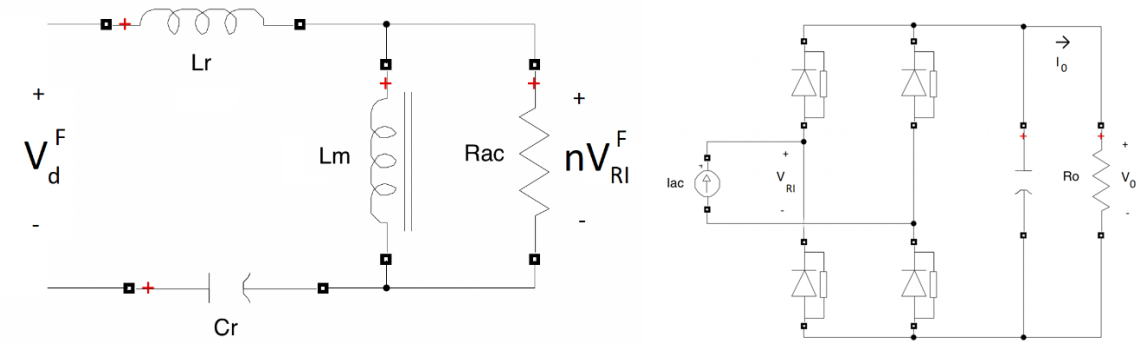

(a) LLC half-bridge (b) Derivation of load resistance

Figure 34 Equivalent circuits

If the output voltage of the secondary rectifier block on the equivalent circuit is V_0, the reflection of the output voltage on the secondary winding of the transformer will be equal to itself in the positive cycle and in the reverse polarity in the negative cycle, given in eq. (5).

$$\begin{aligned} V_{RI} &= +V_0 \text{ if } \sin wt > 0 \\ V_{RI} &= -V_0 \text{ if } \sin wt < 0 \end{aligned} \tag{5}$$

The fundamental component in the secondary winding of the transformer is given in eq. (6) using Fourier transform,

$$V_{RI}^F = \frac{4V_0}{\pi} \sin wt \tag{6}$$

The reflection of the load resistance to the primary is given in eq. (7), calculated using eq. (4) and eq. (6) (assume turn ratio = n = N_p/N_S)

$$R_{ac} = n^2 \frac{V_{RI}^F}{I_{ac}} = n^2 \frac{8}{\pi^2} \frac{V_0}{I_0} = \frac{8n^2}{\pi^2} R_0 \tag{7}$$

The input voltage of the resonance block (V_d) can be written in eq. (8) according to the switching sequences since the output voltage of the power factor corrector circuit is V_{in}.

$$V_d = +V_{\text{in}} \text{ if } MOSFET_1 \text{ is ON}$$
$$V_d = 0 \text{ if } MOSFET_2 \text{ is ON} \tag{8}$$

In Fig. 34a, the ratio of the converter's output and input voltage gives the voltage gain in the converter, M, as given in eq. (9).

$$M = \frac{V_{RO}^F}{V_d^F} = \frac{n \times V_{RI}^F}{V_d^F} = \frac{\frac{4n \times V_0}{\pi} \sin(\omega t)}{\frac{4}{\pi}\frac{V_{in}}{2} \sin(\omega t)} = \frac{2n \times V_0}{V_{\text{in}}} = \\ = \left| \frac{\left(\frac{\omega}{\omega_0}\right)^2 (m-1)}{\left(\frac{\omega^2}{\omega_p^2} - 1\right) + j\frac{\omega}{\omega_0}\left(\frac{\omega^2}{\omega_0^2} - 1\right)(m-1)Q} \right| \tag{9}$$

There are two different resonance points in the LLC circuit. The first point is determined by the leakage inductance of the transformer L_r and the resonance capacitor C_r, given in eq. (10). When LLC works at this frequency, voltage gain M is equal to 1. The resonance tank has the best and most optimized efficiency at this point. Therefore, the transformer winding ratio is designed so that the converter operates at rated input and output voltages at this point.

$$w_0 = \frac{1}{\sqrt{L_r C_r}} \tag{10}$$

The second point is determined by the primary inductance of the transformer which is the sum of the magnetic and leakage inductance, ($L_p = L_m + L_r$), and the resonant capacitor, C_r, given in eq. (11).

$$w_p = \frac{1}{\sqrt{L_p C_r}} \tag{11}$$

In Eq. (12), m is the ratio of the transformer's total primary inductance to the transformer's leakage inductance. If the converter operation will be in a limited frequency band where the load does not change much and it will operate at higher gain points than the first resonance point, the value of m should be chosen as large. A lower value of m will reduce the magnetizing current that circulates in the primary

of the transformer and does not contribute to energy transfer, resulting in increased efficiency.

$$m = \frac{Lp}{L_r} \tag{12}$$

How much the voltage gain will be affected when the converter's working frequency changes is represented by the quality factor, Q, as given in eq. (13).

$$Q = \sqrt{\frac{L_r}{C_r}} \frac{1}{R_{ac}} \tag{13}$$

Resonance frequencies, converter gain, and inductance ratio parameters are important as they determine the operating mode and operating region of the converter. Transformer winding turns, and resonance block elements will be selected to form these parameters.

3.3 Dual Transformer LLC Resonant Converter Design Parameters

At the beginning of the design, the first step is to determine the transformer turn ratio, series resonance inductance, resonance capacitance value and the ratio of the magnetic inductance to the leakage inductance. The input parameters we use in transformer design are given in the table 2.

Table 2 Transformer design parameters

Input voltage	$380 - 420$ V
Input capacitor	329μF
Output voltage	150V
Hold-up time	60ms
Output power	145 W
Input power	145W/0.95=152.63W

In the use of multiple transformers, the primary and secondary winding ratios of the transformer are determined using eq. (14). In the formula, N is the ratio of the

primary and secondary turns of the transformer, V_{in} is the output voltage of the PFC block, V_{LED} is the voltage of the LEDs connected in parallel at the backlight output, and N_T indicates the number of transformers used.

$$N = \frac{N_p}{N_s} = \frac{V_{in}}{2.N_T.V_{LED}} = 0.6667 \tag{14}$$

The magnetic inductance of the transformer should be chosen to keep the magnetic current low and to perform ZVS at all designed frequencies. as explained in the LLC switching period to accomplish ZVS, switching MOSFET's C_{OSS} is deceived into discharging its energy into the load, resulting in zero V_{DS} prior to the application of the next gate signal.

The formula of the magnetic current flowing in the primary winding of the transformer is given in eq. (15) and the transformer magnetic inductance is given in eq. (16).

$$I_{MPk} = \frac{2.C_{OSS}.V_{IN\_MAX}}{T_{DT}} = 0.65A \tag{15}$$

$$L_{MP\_MAX} \leq \left(\frac{\frac{V_{IN\_MAX}}{2}}{(2 \times I_{MPk}) \times N_T} \right) \left(\left(\frac{1}{(f_O) \times 2} \right) - T_{DT} \right) = 363\mu\text{H} \tag{16}$$

C_{OSS} is the average output capacitance value of the MOSFETs to be used in the switching block. T_{DT} is dead time set as 500nS by the controller, it is the time without switching between the gate signals of the high side and low side MOSFETs and f_O represents the resonant frequency that is planned to be switched.

The gain (M) is calculated in the equations below for its minimum and maximum values. In eq. (17), L_m represents magnetic inductance, and L_{lkp} represents leakage inductance.

$$
\begin{aligned}
\mathrm{M^{min}} &= \frac{\mathrm{V_{RO}}}{\frac{\mathrm{V_{in}}^{\max}}{2}} = \frac{\mathrm{L_m} + \mathrm{n}^2\,\mathrm{L_{lks}}}{\mathrm{L_m}} = \frac{\mathrm{L_m} + \mathrm{L_{lkp}}}{\mathrm{L_m}} = 1.38 \\
\mathrm{M^{max}} &= \frac{\mathrm{V_{in}}^{\max}}{\mathrm{V_{in}}^{\min}}\mathrm{M^{min}} = 1.52 \\
m &= \frac{L_m}{L_{lkp}} = 2.58
\end{aligned}
\tag{17}
$$

Using eq. (7) R_{ac} is calculated as 150Ω and using eq. (13), Q is calculated as 0.35. In Fig. 35 two gain graphs are given when the voltage gain is 3 and 5 for six different Q values. Q has a direct impact on the voltage gain between f_0 and f_p. As the Q increases, higher voltage gain is achieved at a lower bandwidth. In addition, the voltage stress on the resonance capacitance can be controlled by limiting the Q value.

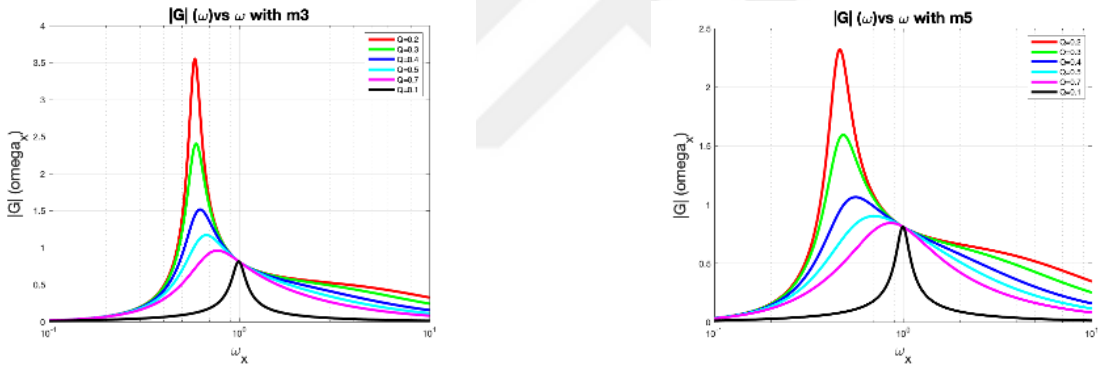

(a) m=3 (b) m=5

Figure 35 Resonant converter gain graph when m=3 and m=5

The minimum number of turns wound in the transformer primary is calculated as 38Ts in eq. 18, Al value of EFD50 core is taken as 83.89 mm^2.

$$
\mathrm{N_p^{min}} = \frac{\mathrm{n}\,(\mathrm{V_o} + \mathrm{V_F})}{2\mathrm{f_s^{min}}\Delta\mathrm{B}\mathrm{A_e}} = 38Ts \tag{18}
$$

If the operating frequency is selected as 100kHz, after iterations, the magnetic and leakage inductance values of the transformers were determined as, $L_{m1} = 175\mu$H, $L_{m2} = 183\mu$H, $L_{lk1} = 75\mu$H, $L_{lk2} = 64\mu$H. The resonant capacitance was chosen as

24nF. Turn ratios of the transformer are selected as 48 turns to 44 turns. 48 turns are obtained by connecting the primary windings of two transformers in series. Using eq. (10) f_0 is calculated as 87.13kHz and using eq. (11), f_p is calculated as 46.082kHz.

Texas Instruments UCC25710 is selected as LLC half-bridge resonant IC in the backlight block. IC provides ease of driving the LEDs from the output of the PFC block over the transformer and has specialized LED protections for under-voltage, and over-voltage situations. Also, UCC25710 has two-level current and thermal protection features. UCC25710 operates with a fixed dead time of 500 ns. The functional block diagram is given in Fig. 67 in the Appendix A.

IC starts to switch 10ms after the voltage on the VCC pin exceeds the minimum VCC_{ON} level, 9.3V, and the capacitance connected to the soft-start pin starts to charge. Meanwhile, the dim pin and under-voltage protection are not active to allow the output capacities to be sufficiently charged. When the current compensation pin is equal to the soft-start pin voltage, the controller continues to operate with all its protections active and dimmable. The timing diagram of the first energizing moment of the IC is given in Fig. 36.

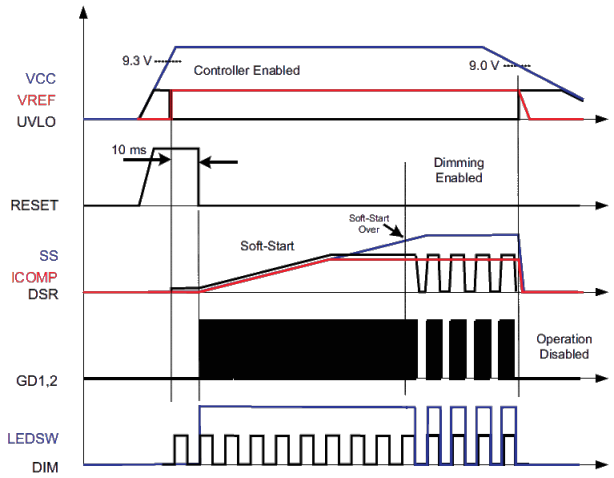

Figure 36 Start-up timing diagram [15]

The switching frequency is controlled by a voltage-controlled oscillator, the feedback is taken over the current sense resistors of the channel return MOSFET. The voltage generated on the current sense resistors is compared with the internal reference voltage. Also, if there is dimming in the system, the switching signal is synchronous with the dim signal.

The minimum frequency allowed to operate without operating the transformer into the capacitive region, adjusted from the 20th pin of the IC, is 85kHz given in eq. 19,

$$\mathrm{R_{MIN}} = \frac{0.15}{49.2\mathrm{pF} \times \mathrm{F_{SW(min)}}} = 85kHz \tag{19}$$

In addition, the maximum switching frequency at which the IC can operate is calculated as approximately 200kHz in the equation eq. 20. Limiting the maximum frequency the IC allows to switch is important to ensure that the semiconductors operate in the safe range. The low Q value of the transformer allows us to reach high gains, while it is disadvantageous in terms of frequency modulation as the frequency will change depending on the load. If the operating frequency is not limited, it may rise so high that we do not want to run the converter because of the switching losses.

$$\begin{aligned} \mathrm{R_{MAX}} &= \frac{0.0664}{49.2\mathrm{pF} \times \mathrm{F_{SW}}(\text{ Delta })} = 200kHz \\ \mathrm{F}_{SW}(\text{ Delta }) &= F_{SW(\max)} - F_{SW(\min)} = 112kHz \end{aligned} \tag{20}$$

Eight strings connected in parallel are driven using two transformers in the backlight circuit, given in Fig. 37. 1,2,3 and 4th strings are fed from $transformer_1$, and 5,6,7, and 8th strings are fed from $transformer_2$. The reason of the primary windings of the transformers are connected in series is to minimize the current deviation between the LED strings. Ideally, when the primary windings are connected in series, the same current will flow through the resonance tank. If the turn ratios between the primary and the secondary in transformers and the voltages of the LEDs are equal,

therefore the secondary currents will be equal. But when multiple transformers drive parallel-connected LED strings, the difference in transformer leakage inductance and LED string voltage tolerances creates a backlight current imbalance problem and causes reliability issues.

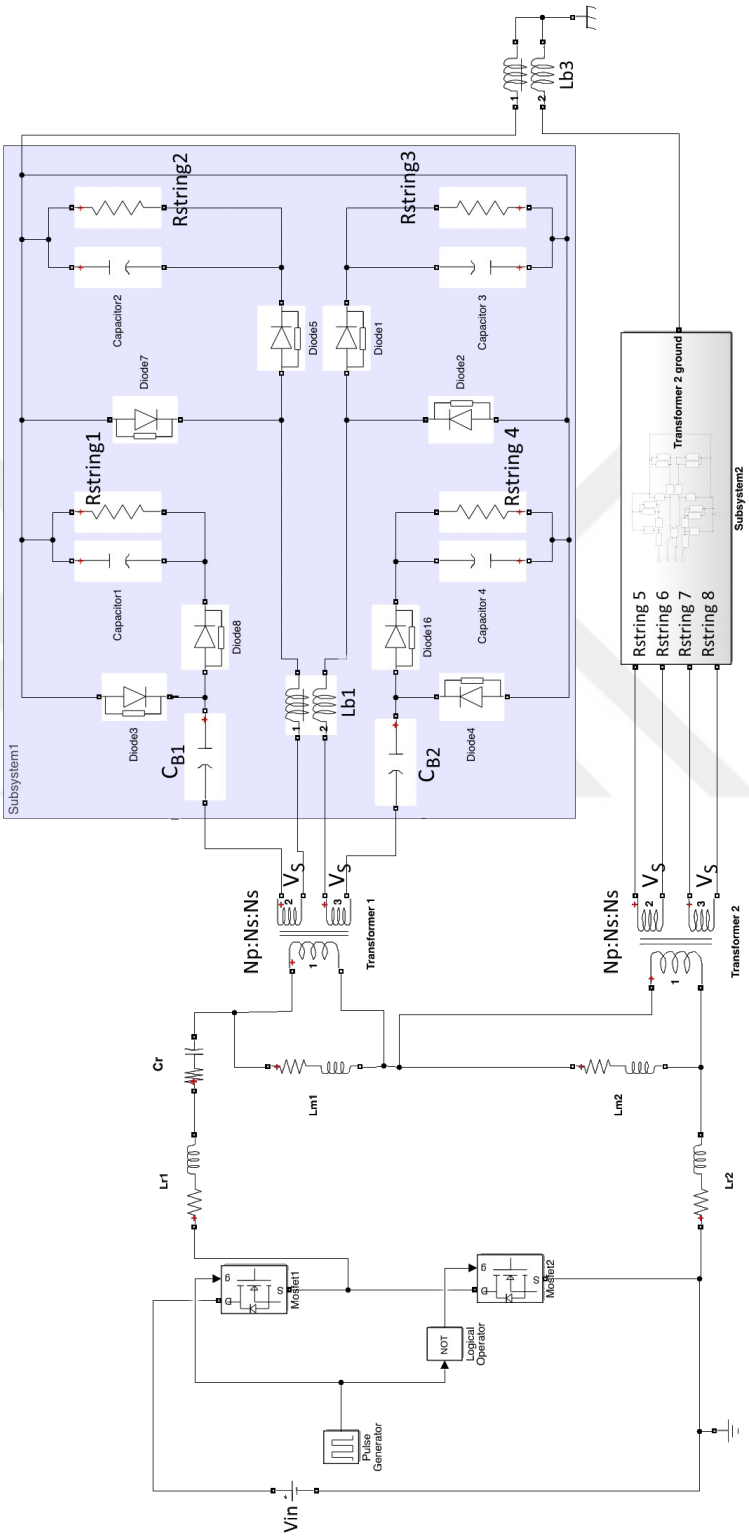

Figure 37 Proposed circuit diagram in Simulink

3.4 Current Balancing Circuit Design

Three current balancing transformers and four DC blocking capacitors are used to minimize the backlight current mismatch in parallel connected LED strings. The imbalance between the LED string currents is minimized in two stages, within the transformers, and between the transformers. One current-balancing inductor (L_B) and two DC-blocking capacitors (C_B) are used to balance the currents within the transformer. Inside the transformers, both of them have two output windings on their secondary, and the voltage formed in each secondary winding is rectified with a full-bridge diode rectifier. However, the output of the full-bridge rectifier is separated into two to feed two separate LED loads. If we look at an output winding, one LED string is fed in the positive cycle and the other LED string is fed in the negative cycle. The current mismatch between the positive and the negative cycles is minimized using a (C_B) capacitor.

In the circuit, strings 1 and 2 in the secondary of the transformer are connected to receive energy in the positive and negative cycles of the same winding. This is also valid for strings 3-4, strings 5-6, and strings 7-8.

In the case of high-side MOSFET, Q_1 is conducting, while the resonant current is in a positive cycle, the current difference between the main branch current and the magnetic inductance will be reflected to the secondary of the transformer in proportion to the number of turns. If the number of turns is the same, the same current flows through the two outputs on the secondary, given in eq. (21). Currents passing through parallel strings in positive sequence and conducting diodes are marked in Fig. 38.

$$i_{sec1} = i_{sec2} = i_{sec3} = i_{sec4} = n < i_{resonant} - i_{LM1,2} > \tag{21}$$

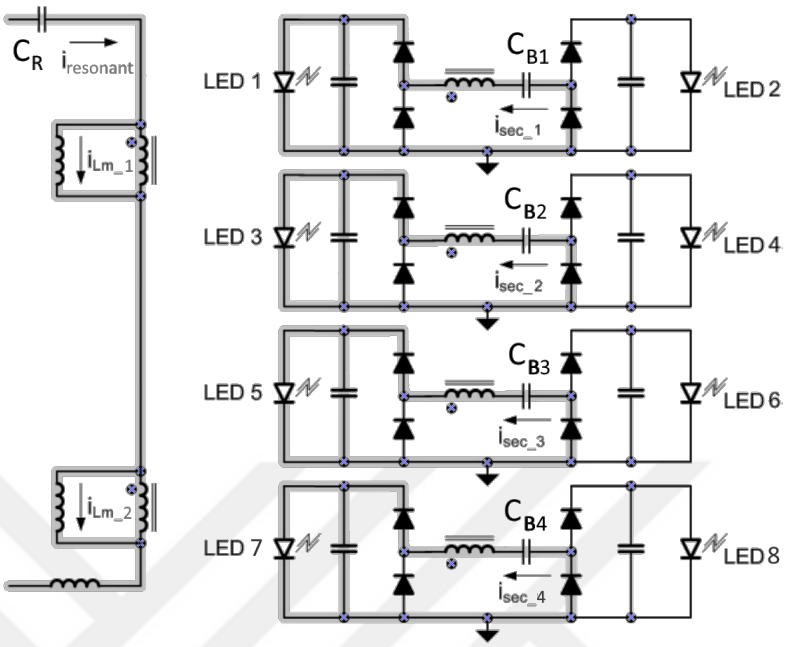

Figure 38 Capacitor balancing in positive cycle

In low side MOSFET, Q_2 is conducting, when the resonant current is in a negative cycle, the current difference between the main branch current and the magnetic inductance will be reflected to the secondary of the transformer in proportion to the number of turns. If the number of turns is the same, the same current flows through the two outputs on the secondary. Currents passing through parallel strings in positive sequence and conducting diodes are marked in Fig. 39. Since the balancing capacitor C_B is connected in series with the secondary windings, it is used to compensate for any imbalance that may occur between positive and negative cycles.

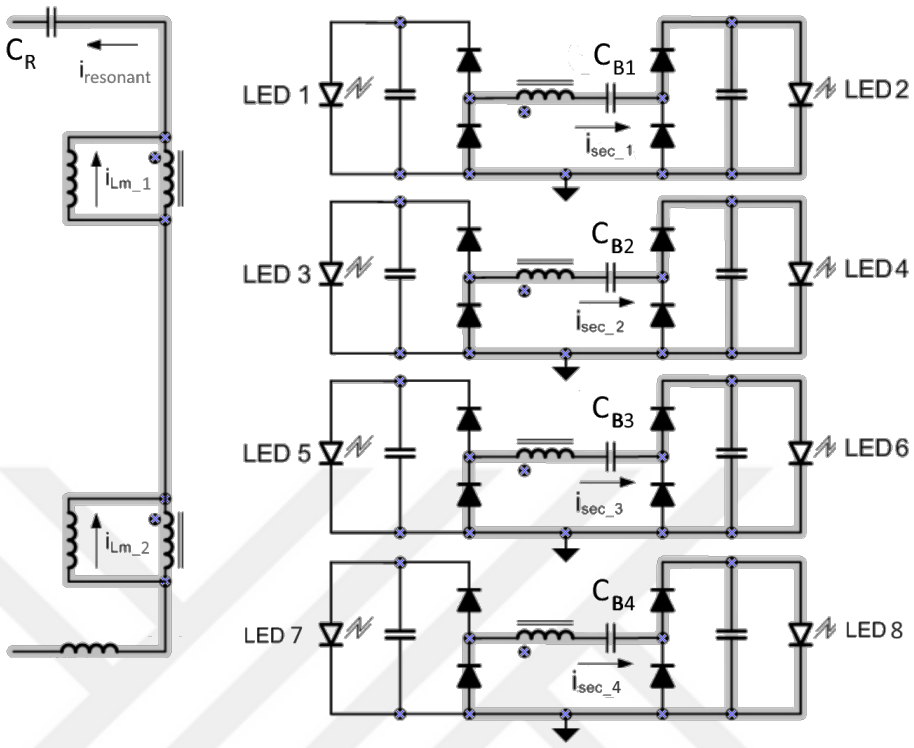

Figure 39 Capacitor balancing in negative cycle

In the first transformer, C_{B1} minimizes the current mismatch between $Load_1$ and $Load_2$, while C_{B2} minimizes the current mismatch between $Load_3$ and $Load_4$. The current balancing inductor, L_{B1} is used to minimize the current imbalance between the two outputs of the first transformer, as illustrated in Fig. 40 and Fig. 41.

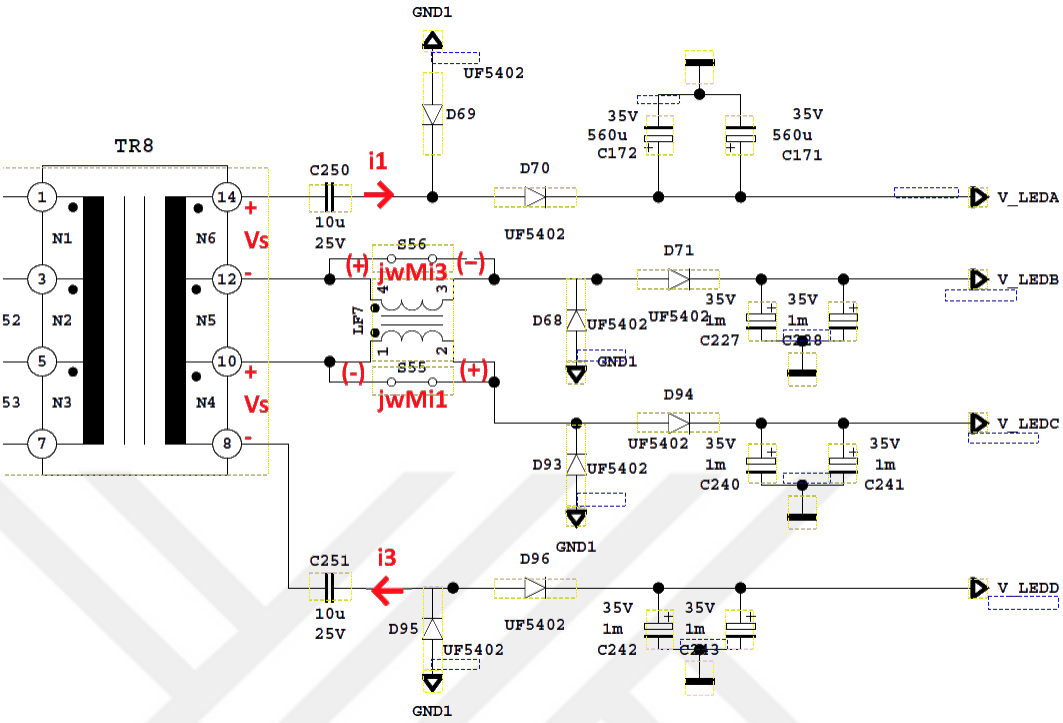

Figure 40 Current balancing between $string_1$ and $string_3$ in $transformer_1$

Eq. (22) gives the AC load resistance calculation using the first harmonic approximation [40] for the LED load.

$$R_{\text{String 1}} = \frac{8}{\pi^2} R_{\text{Led 1}} \tag{22}$$

In the first transformer, current flows through the first and third strings in the positive half cycle. In Fig. 40, to write the currents in the frequency domain, winding voltages must be known. The string voltages are the same because they have equal turns. The currents are expressed in eq. (23) by taking mutual inductance into account.

$$\begin{aligned} V_s &= (\ \text{Rstring}_{\ 1} + jwL_{b1})\, i_1 - jwMi_3 \\ V_s &= (\ \text{Rstring}_{\ 3} + jwL_{b1})\, i_3 - jwMi_1 \end{aligned} \tag{23}$$

If the leakage inductance inside the current balancing inductor is not taken into

account, the equations can be rewritten as in eq. (24). (Assumption, $M = L_B$).

$$\begin{aligned} V_s &= (\ \text{Rstring}_{\ 1} + jwL_{b1})\, i_1 - jwL_{b1} i_3 \\ V_s &= (\ \text{Rstring}_{\ 3} + jwL_{b1})\, i_3 - jwL_{b1} i_1 \end{aligned} \tag{24}$$

Eq. (24) states that the current mismatch flowing through the two outputs in the positive half-cycle will be minimized when $|\ \text{Rstring}_{\ 1} - \ \text{Rstring}_{\ 3}\ | \ll wL_b$. In the first transformer, current flows through the second and fourth strings in the negative half cycle. In Fig. 41, string currents can be written as in eq. (25) by adding the mutual inductance.

$$\begin{aligned} V_s &= (\ \text{Rstring}_{\ 2} + jwL_{b1})\, i_2 - jwMi_4 \\ V_s &= (\ \text{Rstring}_{\ 2} + jwL_{b1})\, i_2 - jwMi_4 \end{aligned} \tag{25}$$

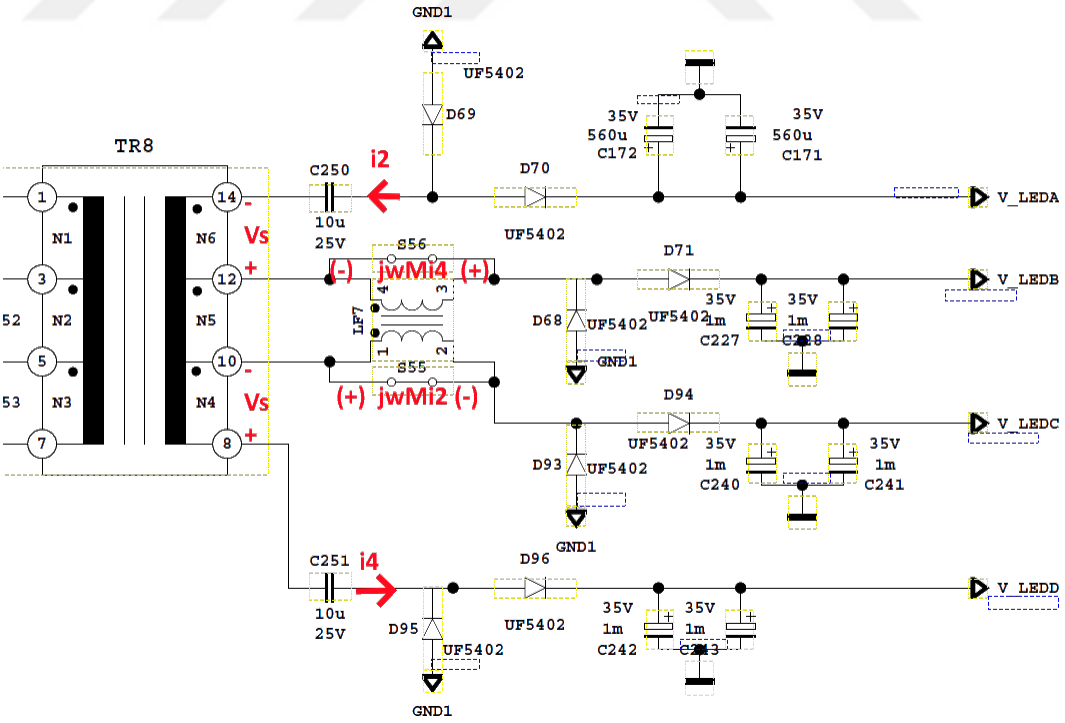

Figure 41 Current balancing between $string_2$ and $string_2$ in $transformer_1$

If the leakage inductance inside the current balancing inductor is not considered,

the current mismatch flowing through the two outputs will be minimized in the negative half-cycle when | Rstring $_2$− Rstring $_4$ |≪ wL_b. This section describes how to minimize the current mismatch inside the first transformer without adding string voltage into the equations. Within the second transformer, the current imbalance between loads 5, 6, 7, and 8 is minimized using DC blocking capacitors $C_{B3,4}$, and current balancing inductor L_{B2}. Balancing on L_{B2} will be between the fifth and seventh strings in the positive half cycle, and the sixth and eighth strings in the negative half cycle.

Current balancing between the transformers is done with a third current balancing inductor. L_{B3} is connected to the ground return of the rectifier diodes and minimizes the current imbalance between the transformers. Hence provides equal distribution of load currents between two transformers as demonstrated in Fig. 42. On L_{B3}, in the positive half-cycle, the current balancing is done between the first and third strings fed from the first transformer and the fifth and seventh strings fed from the second transformer. In this case, the equivalent resistance of the first transformer is equal to the equivalent resistance of the first and third strings connected in parallel. In the negative half-cycle, the current balancing is done between the second and fourth strings fed from the first transformer and the sixth and eighth strings fed from the second transformer.

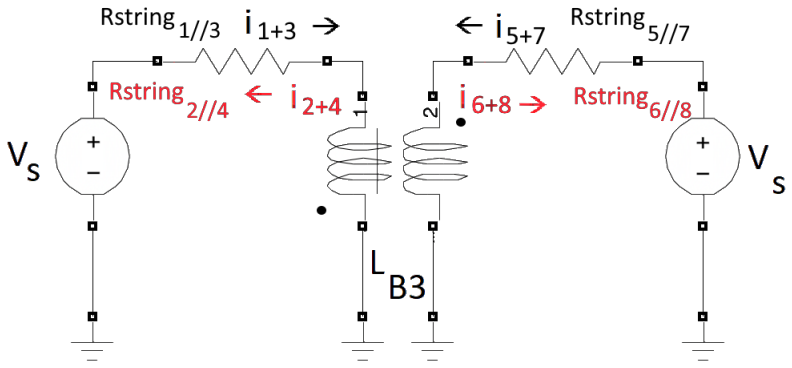

Figure 42 Equivalent circuit of the proposed circuit for current balancing between $transformer_1$ and $transformer_2$

The graphical result while determining the ground return balancing inductor value is given in Fig. 43. When eq. (24) is rewritten, the effect of the resistance differences created by the LED strings on current matching can be calculated. The balancing inductance values to minimize the imbalance in the current were decided by using eq. (26). R_{eqTR1} and R_{eqTR2} represent the equivalent load resistance of the parallel LED strings connected to the transformers' secondary.

$$\frac{i_{TR1}}{i_{TR2}} = \frac{R_{\mathrm{eqTR1}} + 2j\omega L_{b3}}{R_{\mathrm{eqTR1}} + 2j\omega L_{b3}} \tag{26}$$

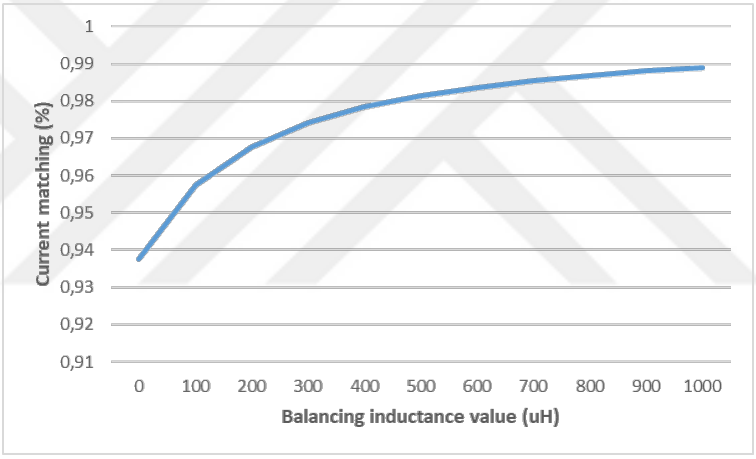

Figure 43 Balancing inductance calculation

In the circuit diagram, the current balancing capacitor for transformer no.8 is C_{250} and C_{251}, and the current balancing coil is LF_7. The current balancing capacitor for transformer no. 9 is C_{252} and C_{253}, and the current balancing coil is LF_8. The current balancing between the backlight transformers is LF_9, which is used in the ground returns of the rectifier diodes, as shown in Fig. 29.

The contribution of this method is to balance the backlight current independent of the voltage tolerance in LED strings and the leakage inductance tolerance in transformers. Because when multiple transformers drive parallel-connected LED strings, the difference in transformer leakage inductance and LED string voltage tolerances

creates a backlight current imbalance problem and causes reliability issues.

3.5 Secondary Rectifier Block

The square wave obtained by switching the MOSFETs in the primary of the transformer is reflected to the secondary winding in proportion to the number of turns of the transformer and this voltage is rectified in the rectification block of the power supply, thus DC voltage is obtained. The waveforms of the current and voltages passing over the diodes in a full wave rectifier structure are given in Fig. 32.

In the circuit diagram given in Fig. 29, a full bridge rectifier is used. However, the output of the full bridge rectifier is divided into two as explained in the capacitor balancing part, one of the parallel strings is fed in the positive cycle and the other of the parallel strings is fed in the negative cycle. 16 ultra-fast diodes with 3A, 400V rating are used for 8 parallel LED loads. The reason for using ultra fast diode is that when operating above the LLC resonant frequency, reverse polarity occurs without resetting the current on the diode, so it is necessary to use a diode with a fast reverse recovery time. The other criteria to be considered when choosing a diode are the current flowing through it and the voltage level it will block in case of reverse polarity.

A full wave rectifier could also be selected instead of a full bridge rectifier. In this case, the number of diodes to be used would be halved, but the voltage stress that the diodes would withstand in case of reverse polarity doubled. When we use the system as a full bridge since the diodes are connected in series, the same current passes over it and the conduction losses increase, in this case, low Vf diodes can be preferred if the blocking voltage is the limiting factor in the design. The copper losses that will occur in the transformer are twice as high in the full wave rectifier. The reason why synchronous MOSFET is not preferred in the rectification block is that the number of synchronous driver ICs operating at high voltage in the drain pin is less, and the

total cost of suitable drivers with low R_{dson} mosfets is higher than the diode.

3.6 Overall Power Supply Circuit

In this section, the circuit designed in dual transformer LLC resonance topology for 145W backlighting is explained in blocks. In addition, the current balancing circuit in 8 parallel strings in the backlight is explained in two stages. The overall circuit diagram is given in Fig. 44.

The input voltage from the AC socket is filtered to prevent electromagnetic radiation. Then, the voltage obtained after rectifying the voltage in the rectification block and correcting the power factor in the PFC block is transferred to the DC-DC block. In the first part, the types of electromagnetic emission and the components on the circuit diagram are used to suppress which emission is given. In addition, current limiting elements are used between the filter elements and the rectifier block on the circuit. NTC or PTC can be preferred for current limiting according to the application and the environmental conditions in which the application is used. NTC is used in this circuit. The designer is free on the topology to be selected in the PFC block. In this PSU, interleaved PFC structure is used in boost topology. The reason why the boost converter is preferred is that the inductance current at the input is continuous and it is easy to ensure that this continuous current follows the bridge rectifier output voltage. In the PFC block, which we have to use in TV cards over 80W as a standard, a PFC controller should be selected according to the application. In applications where standby power consumption is limited, the controller must have burst mode.

In the DC-DC block, on the other hand, the DC voltage level at the PFC output is converted to the backlight voltage with the LLC resonant topology. The output voltage can be higher or lower than the input voltage, in this application the output voltage is lower. The proposed circuit diagram in the dual transformer LLC structure

is given in Fig. 29. Since reliability problems will be experienced with a single transformer and the output power cannot be met with a slim core size, dual transformer structure is used. In the design parameters section, transformer inductance and turn ratio calculations are given. The simulation results of the gain graph taken while determining the transformer winding ratios are given. The side components of the selected LLC controller have been calculated. Current balancing is done in two stages in 8 parallel LED strings in dual transformer structure. Current balancing inside the transformer is done with one current transformer and two DC-blocking capacitors. Current balancing between the transformers is done with a current transformer added to the ground return of the transformers. The selection of current balancing elements and their mathematical calculations are also included in this section.

In the secondary rectification block, the voltage created on the secondary windings of the transformer is rectified at the output of the LLC resonance topology. Half-wave or full-wave rectifier can be used in this block. In this application, the full bridge rectifier is used by dividing its output into two as positive and negative cycles. For this reason, current imbalance occurs between parallel strings fed from a single winding in the same transformer.

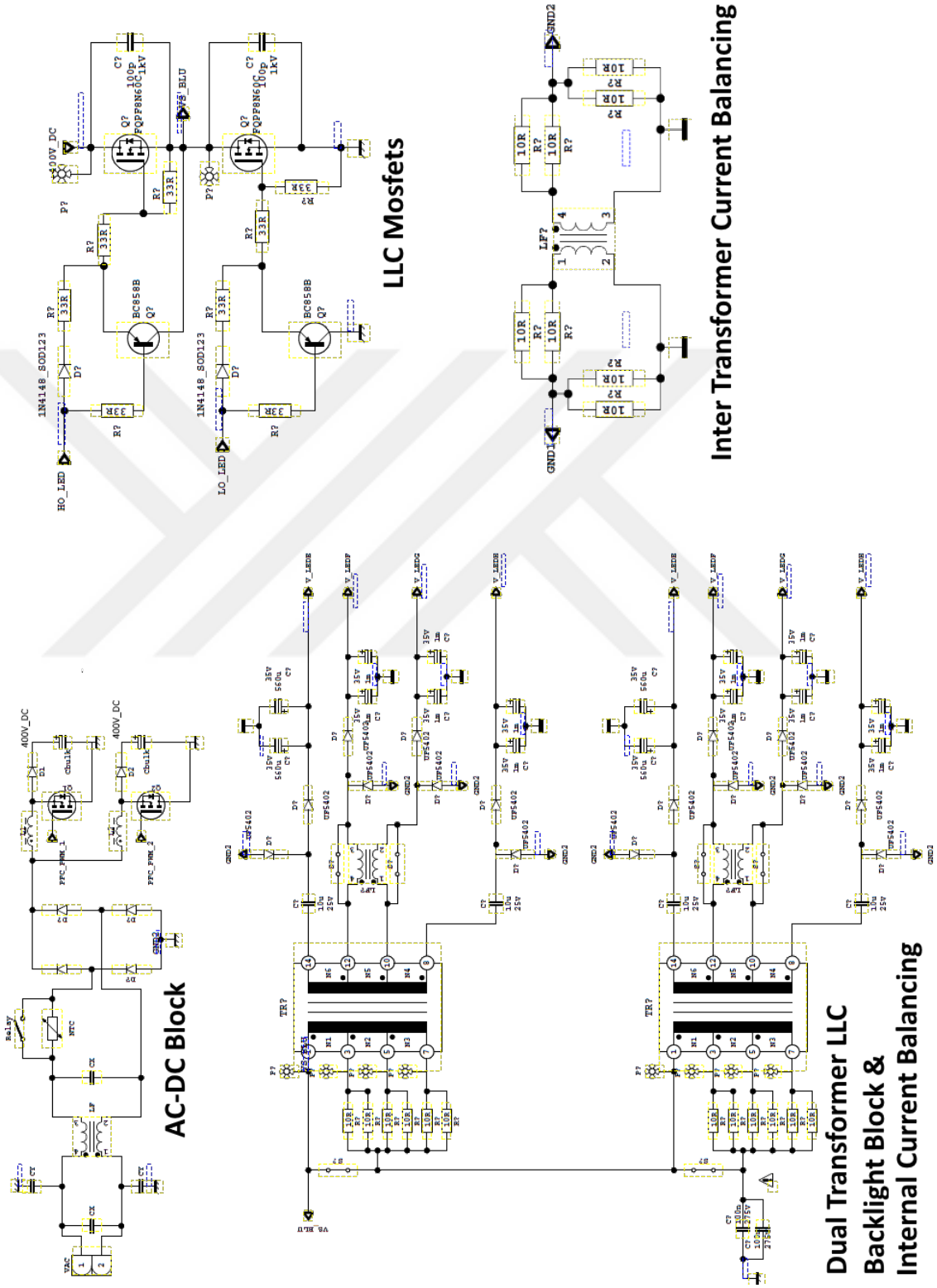

Figure 44 Overall power supply circuit diagram

CHAPTER IV

SIMULATION RESULTS

4.1 Dual Transformer LLC Backlight Simulation

The design parameters used in the simulation and hardware implementation phase are given in table 3. MATLAB Simulink was used to create the simulations.

Table 3 Backlight block design parameters

Input voltage	$380 - 420$ V
Number of LED	8 string x 50 LED
LED current of each string	$I_{LED} = 120$ mA
Operation frequency	f $= 110 - 120$kHz
Rectifier diodes	16
Output capacitor	66μF
Output power	145 W
Transformer 1 primary inductance	$L_{p1} = 247\mu$H
Transformer 1 leakage inductance	$L_{r1} = 64\mu$H
Transformer 2 primary inductance	$L_{p2} = 250\mu$H
Transformer 2 leakage inductance	$L_{r2} = 75\mu$H
Resonant capacitor	$C_r = 24$nF
DC blocking capacitor	$C_B = 1n$F
Internal balancing inductor	$L_{B1,2} = 2x700\mu$H
Ground balancing inductor	$L_{B3} = 2x700\mu$H

As seen in Fig. 45, in the circuit used in the simulation, two transformers whose primary windings are connected in series are feeding two LED strings connected in parallel. Strings 1,2,3, and 4 are modeled with a single load resistor and are fed from $transformer_1$. Strings 5, 6, 7, and 8 are modeled with a single load resistor and are fed from $transformer_2$. In order to minimize the current mismatch between transformers, the current balancing inductor, L_{B3}, is connected to the ground return of the transformers. Because the current in the positive and negative sequences

flowing in the secondary of the transformer is equal in the linear transformer block in Simulink, C_B was not used.

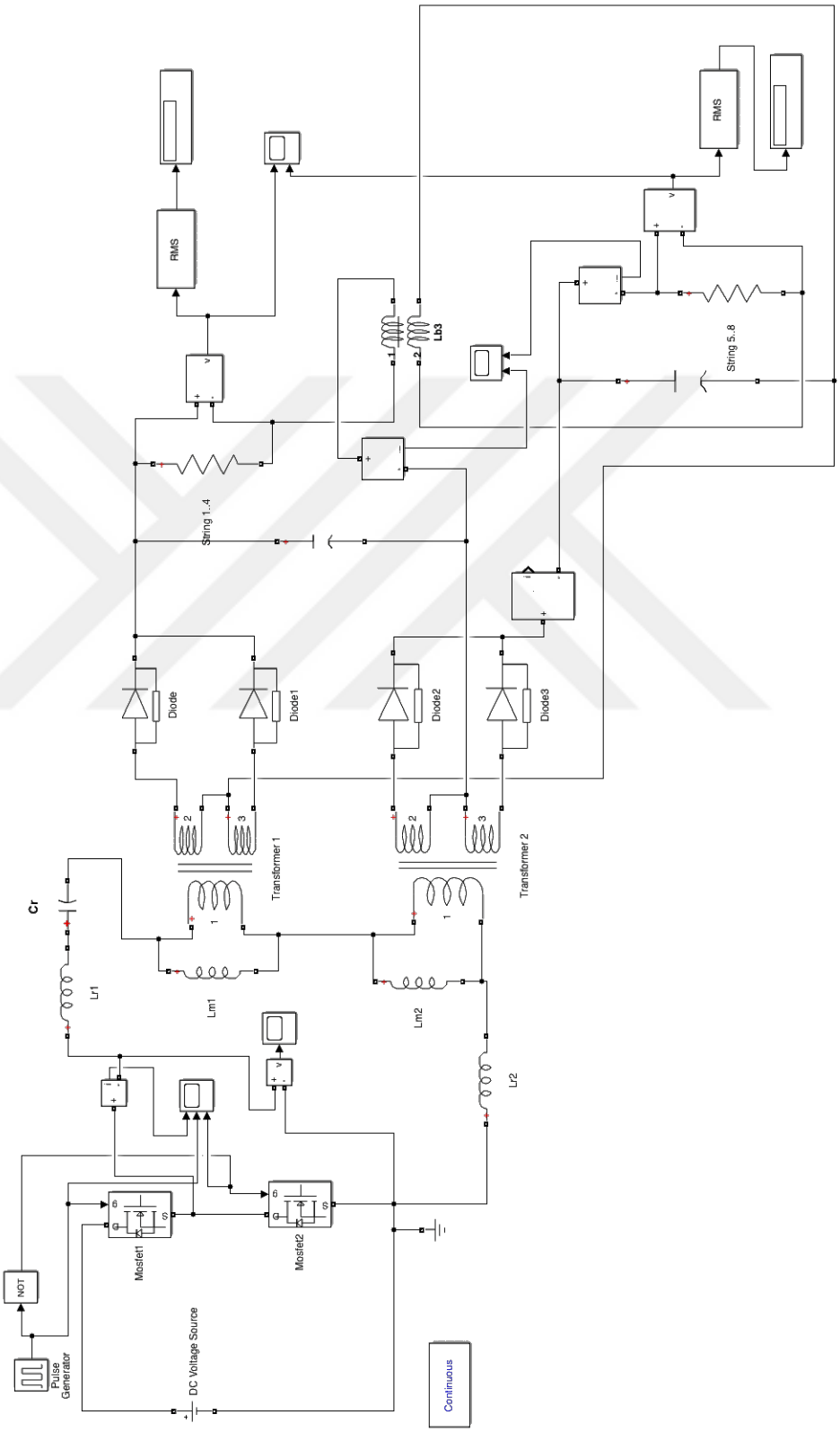

Figure 45 Simplified version of proposed circuit

Fig. 46 shows the resonant current measured from the primary, and the gate signals of high-side and low-side MOSFETs operated with 50% duty cycles. The simulation is done over the resonant frequency, at f=120kHz. When the switching frequency is greater than the resonant frequency, then the resonant current is not sinusoidal.

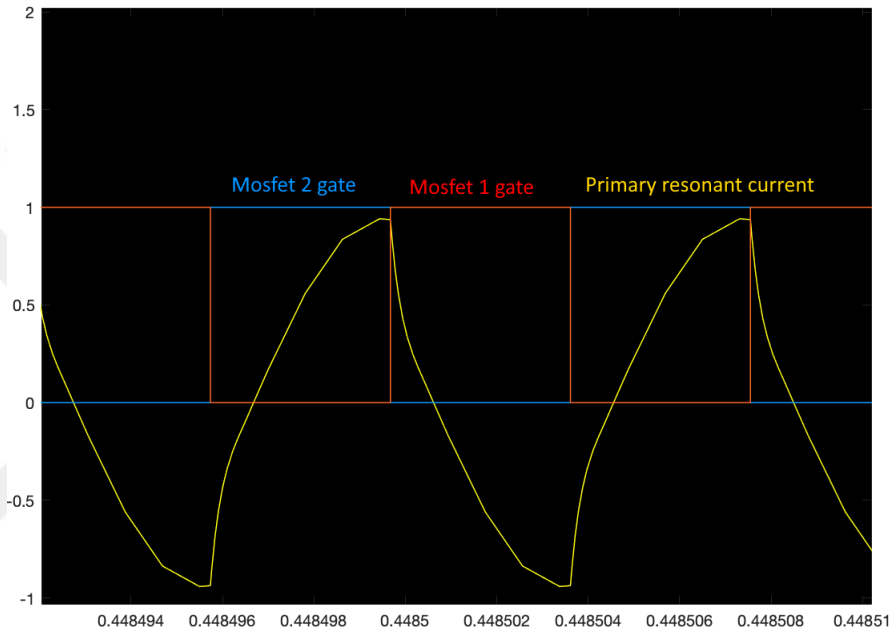

Figure 46 Primary resonant current and gate signals

Channel 1 (Yellow): Primary magnetizing current
Channel 2 (Red): Gate signal of $MOSFET_2$
Channel 3 (Blue): Gate signal of $MOSFET_1$

When determining the simulation parameters, if the LED loads are selected the same, it is seen that the currents in the parallel LED strings are the same. LED currents are both 390mA and string voltages are 140V, as shown in Fig. 47.a and 47.b.

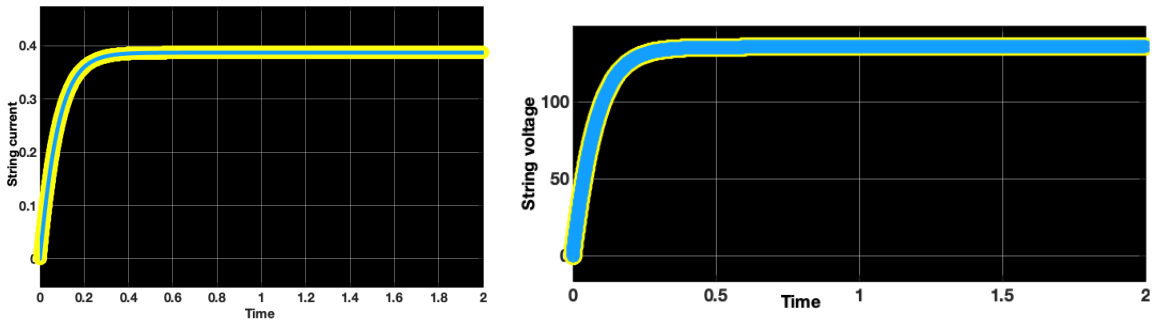

(a) Backlight currents (b) String voltages

Figure 47 Simulation results when string voltages are equal

(a) (b)

Channel 1 (Yellow): String current 1..4 Channel 1 (Yellow): String voltage 1..4

Channel 2 (Blue): String current 5..8 Channel 2 (Blue): String voltage 5..8

Before current balancing, when the strings are adjusted to 120V and 140V, it is seen that the LED currents are 440 mA and 390mA. String voltages and currents are shown in Fig. 48.a and 48.b.

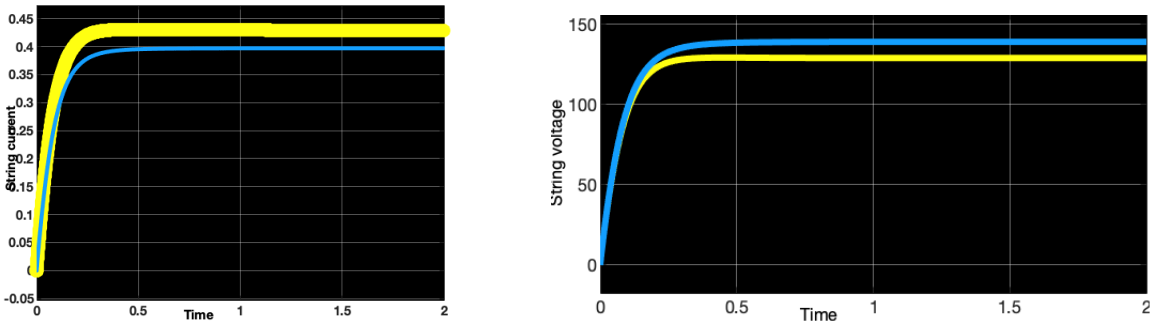

(a) Backlight currents (b) String voltages

Figure 48 Simulation results when string voltages are not equal before balancing

(a) (b)

Channel 1 (Yellow): String current 1..4 Channel 1 (Yellow): String voltage 1..4

Channel 2 (Blue): String current 5..8 Channel 2 (Blue): String voltage 5..8

Although the strings are adjusted to 120V and 140V, it is seen that the LED

currents are both 390 mA. String voltages and currents are shown in Fig. 49.a and Fig. 49.b. Although the LED loads are different, the currents are the same because of the current transformer L_{b3}. The leakage inductance of L_{b3} has not been taken into account during the simulations.

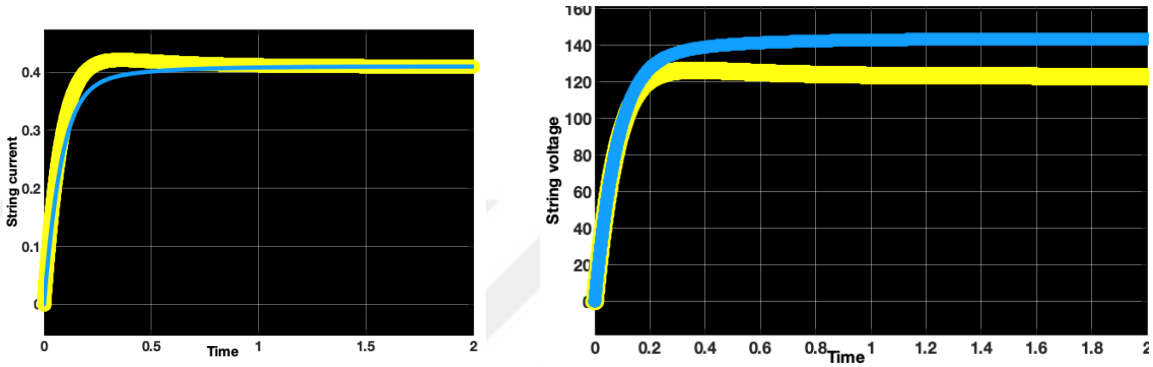

(a) Backlight currents (b) String voltages

Figure 49 Simulation results when string voltages are not equal with balancing

(a)	(b)
Channel 1 (Yellow): String current 1..4	Channel 1 (Yellow): String voltage 1..4
Channel 2 (Blue): String current 5..8	Channel 2 (Blue): String voltage 5..8

When the simulation results are examined, it is seen that the LED string currents are exactly the same, although there is a 20V difference between the string voltages. It is because the leakage inductance is not taken into account in the simulations and the simulation is done in a lossless transformer. Since leakage inductance is unavoidable in the current balancing inductor during the application phase, there is a current mismatch between the LED currents.

CHAPTER V

EXPERIMENTAL RESULTS

5.1 Dual Transformer LLC Backlight Block Results

The Tektronix DPO 7104C oscilloscope, Hioki 3332 power meter, and Fluke E54 thermal camera were used to get the measurements. Fig. 50 shows the measuring setup in the laboratory.

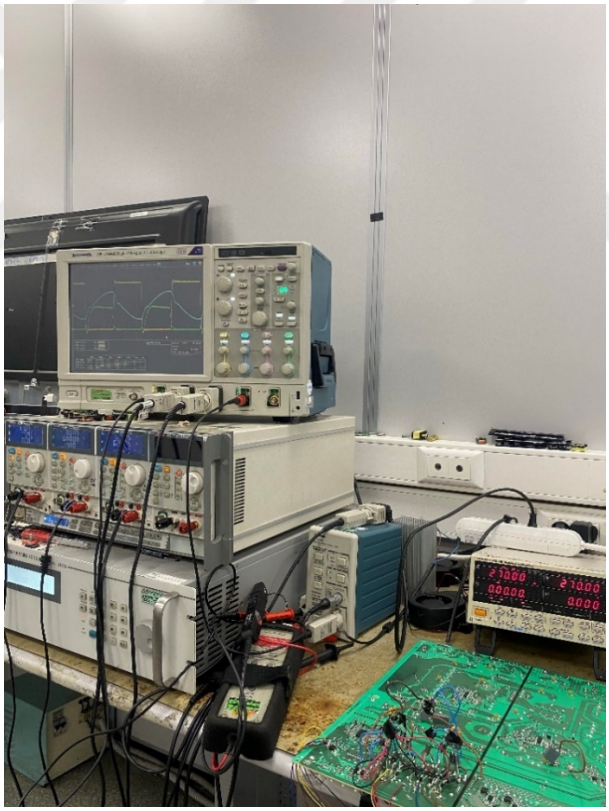

Figure 50 Measurement setup

Measurements were started by driving four parallel strings in LLC half bridge topology from two transformers with primary connected in series, the circuit diagram is given in Fig. 51. In the first step, LED currents were measured in strings where

the string voltages were the same. In the next step, LED current measurements were repeated by changing the string voltages by 5%. The first measurements were obtained when none of the compensation elements to minimize current imbalance were not connected to the circuit. The error rate between the strings connected to a single transformer was measured as 6.08%. The current imbalance between transformers was measured as 1%. Results are given in the first column in table 4.

When the string voltages were not equal, the error rate between the strings connected to a single transformer was measured as 23% in the case before current balancing. In this case, the current imbalance between transformers was measured below 1%. Results are given in the second column in table 4.

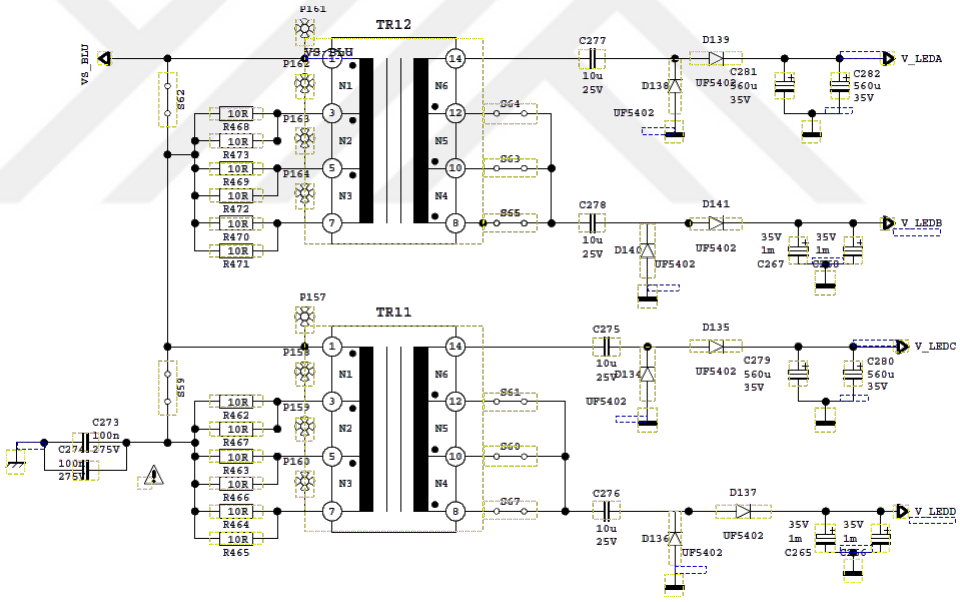

Figure 51 Circuit diagram of four parallel LED strings driven from two transformers in LLC

Since the current imbalance is caused by the imbalance occurring in the positive and negative switching periods, balancing capacitors (C_{B1}, C_{B2}) were added to the circuit. In case the string voltages are not equal, the error rate between the strings connected to a single transformer was measured as 1.27%. In this case, the current imbalance between transformers was measured as 1%. For this reason, although we

used the current balancing element (L_{B3}) between transformers in the simulation on MATLAB, it was not used at this stage. Balancing inductors (L_{B1}, L_{B2}) were also not used at this stage since two strings were connected to a transformer. Results are given in the third column in table 4.

Table 4 Backlight current measurements in four parallel LED strings

LED current / String no.	String voltages are equal	String voltages are not equal	With internal balancing circuit
String 1	261.9mA	256.2 mA	241.5 mA
String 2	239.1 mA (5.88% error)	233 mA	242.2 mA (1.19% error)
String 3	236mA	303.2 mA (23% error)	236.3 mA (1.27% error)
String 4	266 mA (6.08% error)	192.5 mA (21.81% error)	238.4 mA

Fig. 52 shows the LED string currents in $string_2$ and $string_4$. Current measurements were made when the voltage of one of the parallel strings decreased by 5%. The IC is supplied with 12V.

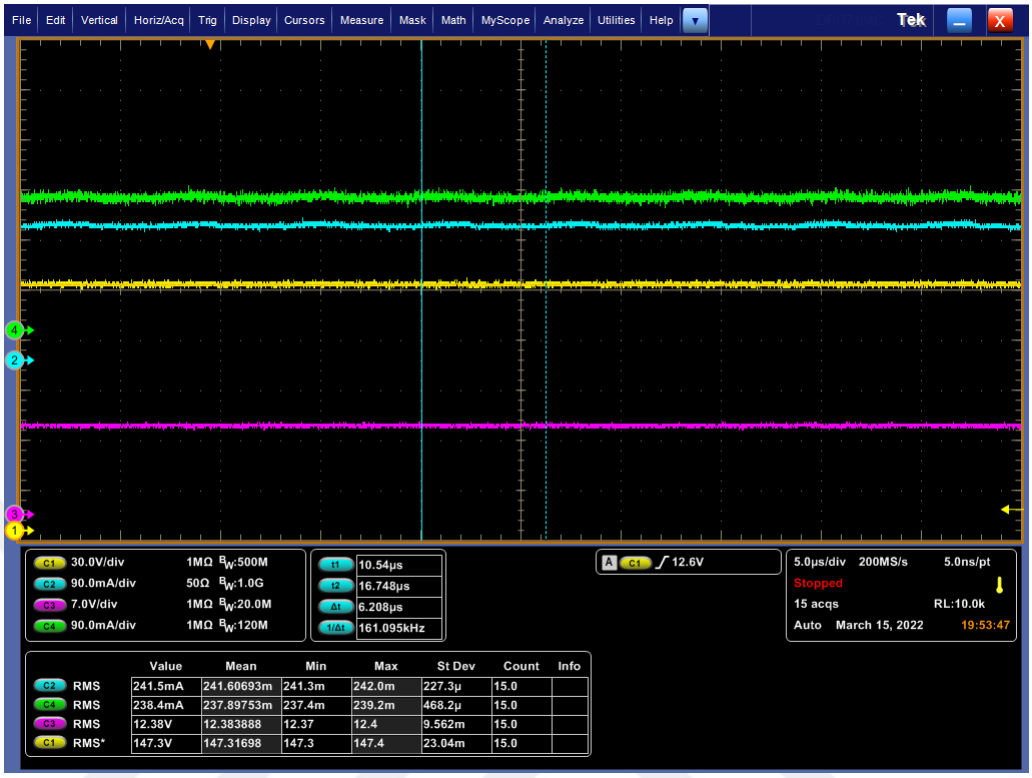

Figure 52 Backlight current and voltage measurements in four parallel LED strings

Channel 1 (Yellow): $String_1$'s voltage
Channel 2 (Blue): $String_1$'s current
Channel 3 (Purple): Supply pin voltage
Channel 4 (Green): $String_4$'s current

In Fig. 53, the current measured in the number two led string, the resonant current flowing from the primary, and the gate signal measurement of the high side MOSFET are given. When the high side MOSFET ($MOSFET_1$) gate signal is high, stored energy on C_r and L_s is used to power the load. MOSFET works with 500ns fixed dead time and 50% duty cycle. As seen from the waveform of the resonant current flowing from the primary, the system operates in the over-resonance region, the next semiconductor is switched before the half-cycles are completed.

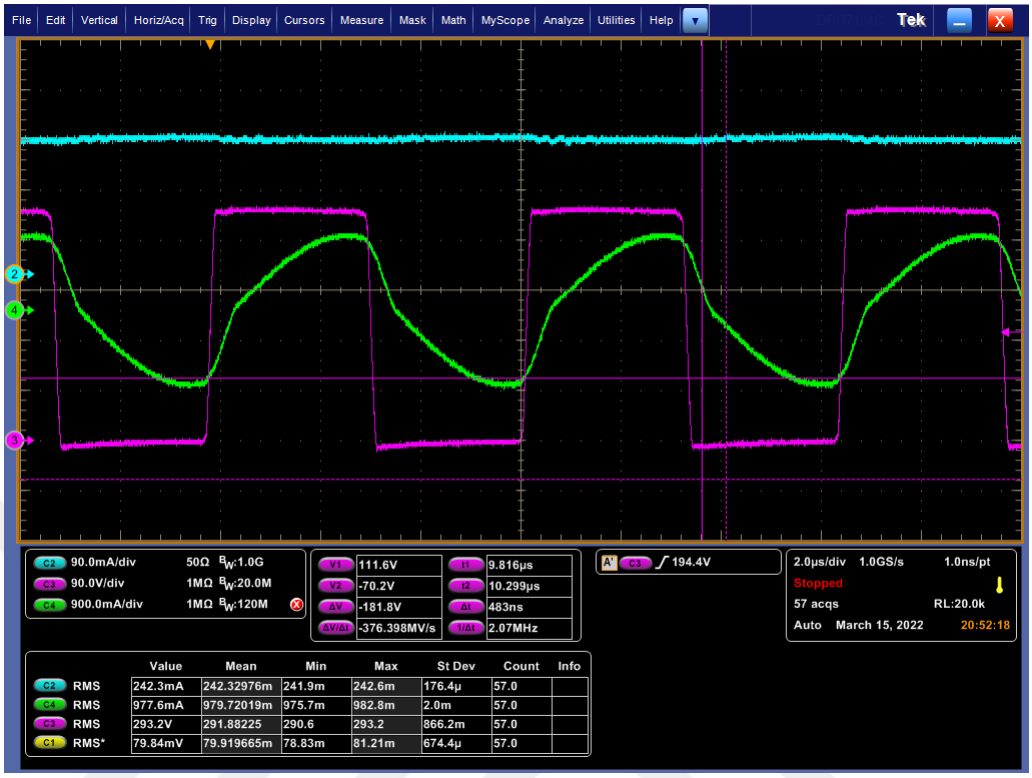

Figure 53 $String_2$ LED current, primary resonant current and gate signal of $MOSFET_1$

Channel 2 (Blue): LED $string_2$'s current
Channel 3 (Purple): Gate signal of $MOSFET_1$
Channel 4 (Green): Primary resonant current

In case the string voltages are different from each other, 300Hz PWM dim is given while current balancing capacitors are connected to the system. Measurements taken at 80%, 50%, 20% and 11% dim condition, given in Table 5.

Table 5 Backlight current measurements in four parallel LED strings under PWM dim

LED current / String no.	%80 dim	%50 dim	%20 dim	%11 dim
String 2	188.4 mA	117.2 mA	47.5 mA	25.44 mA
String 3	196.4 mA	121.95 mA	48.39 mA	27.11 mA

The maximum current deviation between strings measured 3.17% in the 11% dim condition. When the dim signal is given to the system, the primary MOSFETs keep switching for a while after the PWM falls to zero, this is achieved by limiting the switching frequency change. In this way, the closed-loop compensation of the system increases, which is especially important when the dim levels are low. The dimming slew rate is adjusted according to the capacitor to be connected to the DSR pin on IC, given in eq. (27). Fig. 54 shows a 50μS delay from the falling edge of the dim signal.

$$C_{DSR} = \frac{44\mu\text{A} * T_{SLEW}}{V_{ICOMP} - 0.9V} \tag{27}$$

Figure 54 Dimming slew rate adjustment for current compensation

Channel 1 (Yellow): $String_2$'s voltage
Channel 2 (Blue): $String_1$'s current
Channel 3 (Purple): DSR pin voltage
Channel 4 (Green): $String_2$'s current

Measurements were continued by driving eight parallel strings in LLC half-bridge topology from two transformers with primary connected in series.

The oscilloscope screen displays the main branch resonant current passing through the primary of the transformer, the signals on the drain port, and the gate port of the $MOSFET_1$. As seen in Fig. 55, the drain voltage of the high side MOSFET is 400V, which is the max PFC output, and the gate voltage is 12V. Also, the moment when the MOSFET is switched under zero voltage is marked on the waveform.

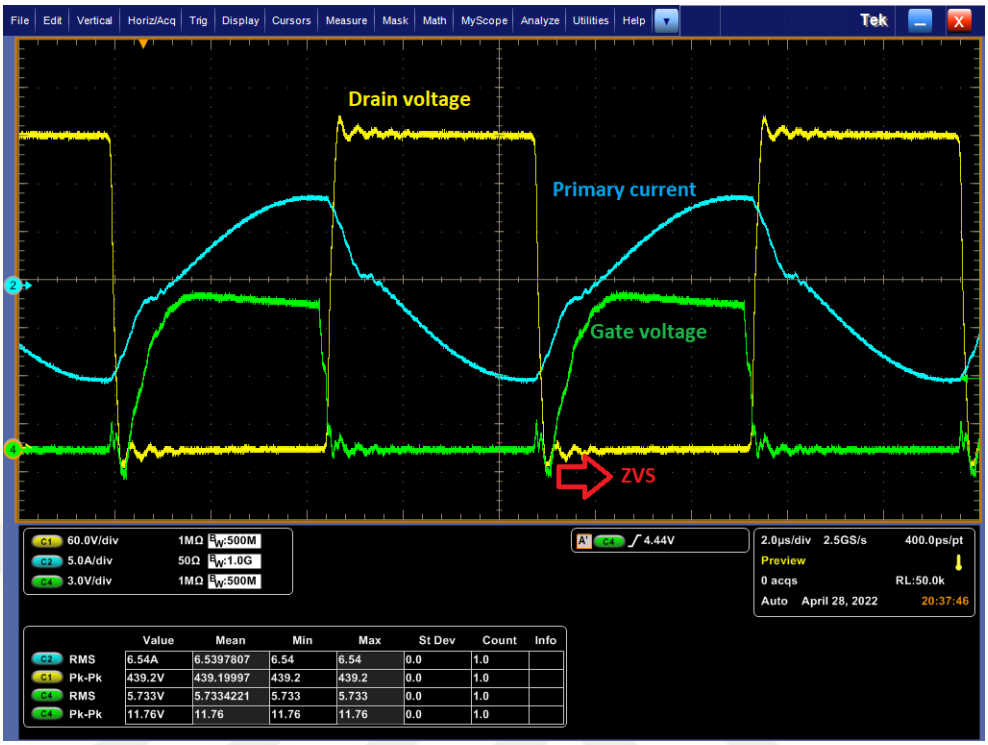

Figure 55 Resonant current on the primary side, high side MOSFET's gate, and drain voltage

Channel 1 (Yellow): Drain voltage of $MOSFET_1$
Channel 2 (Blue): Primary resonant current
Channel 3 (Green): Gate signal of $MOSFET_1$

From the resonant current waveform, it is seen that the converter operates at 110kHz and above the resonance frequency mode. When the LLC converter operates in this mode, the resonant current is less compared to other operating frequency modes. Hence the primary MOSFETs' conduction losses are less because the switching period is interrupted by the start of the next period. Therefore, reverse recovery losses occur in the rectifying diodes located in the secondary of the transformer, and in this application, Schottky diodes are preferred to increase efficiency and decrease EMI caused by reverse recovery. Also, it can be seen that the waveform is the same as the result in the simulation. The reason for working over the resonant frequency is that the current balancing between the strings is better in this region.

In the first step, LED currents were measured in strings where the string voltages were the same. In the next step, LED current measurements were repeated by changing the string voltages by 10%. The first measurements were obtained when none of the compensation elements to minimize current imbalance were not connected to the circuit. Results are given in the first column in table 6. Fig. 57a shows the LED string currents in the first transformer and Fig. 57b shows the LED string currents in the second transformer.

In the second stage, in order to minimize the current imbalance within the transformers themselves balancing components were connected to the circuit and LED current measurements were obtained. Since the current imbalance is caused by the imbalance occurring in the positive and negative switching periods, balancing capacitors $C_{B1,2}$ were added to the first transformer and $C_{B3,4}$ were added to the second transformer. When four parallel strings are driven from a single transformer, (L_{B1}) has been added to balance between $string_{1-2}$ and $string_{3-4}$, and (L_{B2}) has been added to provide balancing between $string_{5-6}$ and $string_{7-8}$. Results are given in second column in table 6. LED string currents can be seen in Fig. 58a and Fig. 58b.

In the third stage, the third current balancing inductor L_{B3} was added to the ground return of the transformers, and connected to the circuit in order to minimize the current imbalance between the two transformers. TABLE II shows measurements obtained when string voltages are equal. Results are given in the third column in table 6. LED string currents can be seen in Fig. 59a and Fig. 59b. The implementation image of the current balancing components at the last step is given in Fig. 56.

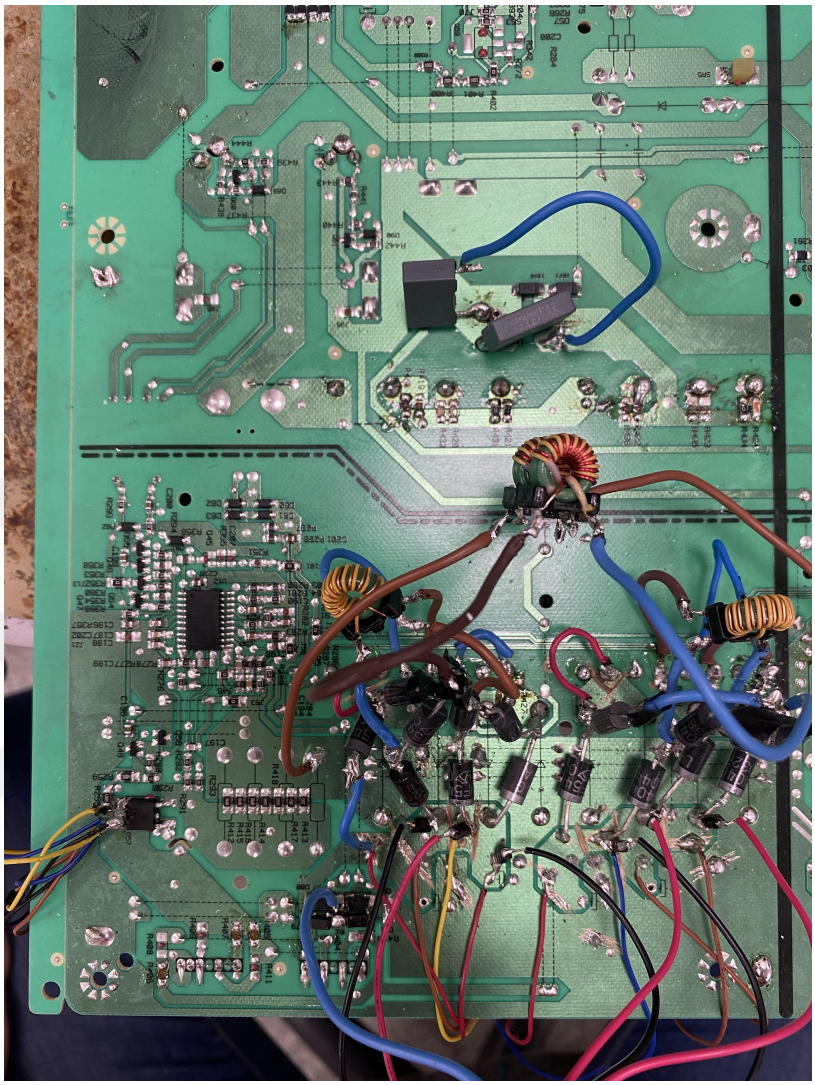

Figure 56 Implementation of the circuit with all current balancing components

Measurements taken when string voltages are equal and none of the compensation elements to minimize current imbalance were not connected to the circuit are given in table 6. The current error was 11.25% between $strings_{7-8}$. When two current balancing inductors and four DC balancing capacitors ($L_{B1,2}$ and C_B) were connected to the circuit, the current error is reduced to 6.76%. In the last step, when the third current balancing inductor L_{B3} was added to the ground return of the transformers the current error is measured as 2.59% between $strings_{1-2}$.

Table 6 Backlight current measurements in eight parallel LED strings when string voltages are the same

LED current / String no.	without balancing	with internal balancing circuit	with two transformer balancing circuit
String 1	131 mA (9.46% error)	129 mA (6.76% error)	121.3 mA
String 2	122.8 mA	124.7 mA	121.4 mA (2.59% error)
String 3	125.7 mA	121 mA	119.6 mA
String 4	110.6 mA	120.6 mA	118.8 mA
String 5	124.3 mA	119.4 mA	115.7 mA (2.22% error)
String 6	112 mA	115.7 mA (4.25% error)	117.5 mA
String 7	124.8 mA	118.1 mA	116.2 mA
String 8	106.2 mA (11.25% error)	118.2 mA	116.2 mA

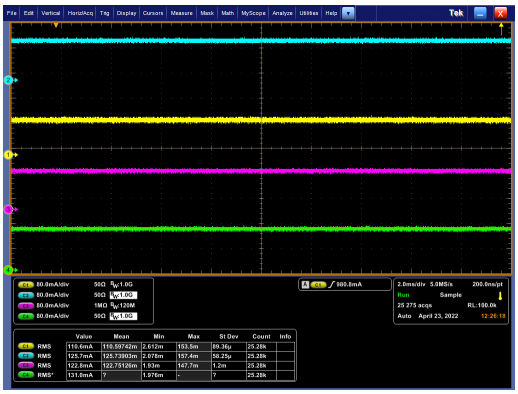

(a) String no 1..4

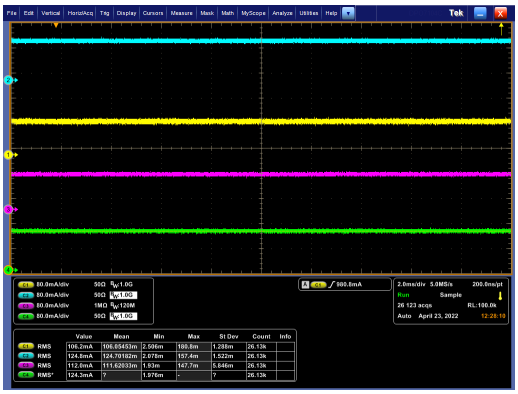

(b) String no 5..8

Figure 57 Current measurements when string voltages are equal, without balancing circuit

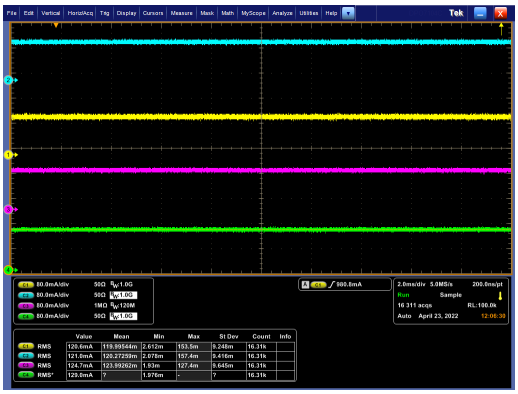

(a) String no 1..4

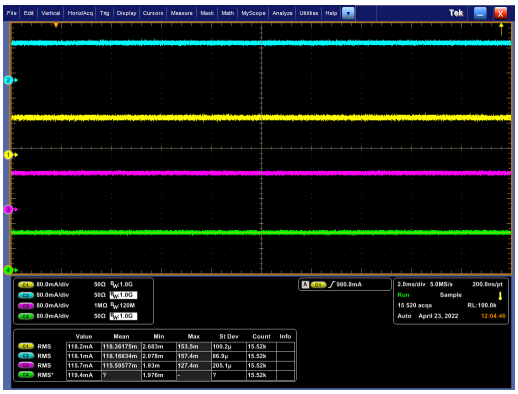

(b) String no 5..8

Figure 58 Current measurements when string voltages are equal, with internal balancing circuit

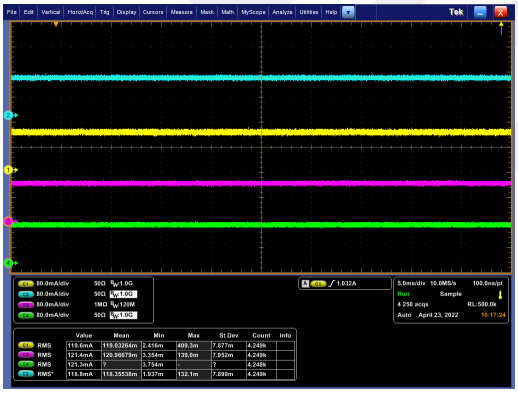

(a) String no 1..4

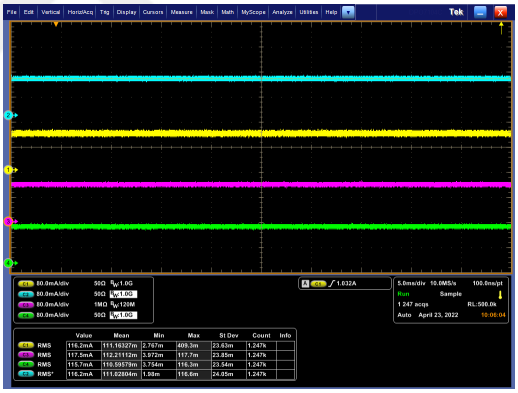

(b) String no 5..8

Figure 59 Current measurements when string voltages are equal, with two transformer balancing circuit

(a)	(b)
Channel 1 (Yellow): $String_4$'s current	Channel 1 (Yellow): $String_8$'s current
Channel 2 (Blue): $String_3$'s current	Channel 2 (Blue): $String_7$'s current
Channel 3 (Purple): $String_2$'s current	Channel 3 (Purple): $String_6$'s current
Channel 4 (Green): $String_1$'s current	Channel 4 (Green): $String_5$'s current

Measurements taken when the voltages of the LEDs are different are given in table 7. The first measurements were obtained when none of the compensation elements

to minimize current imbalance were not connected to the circuit. Results are given in the first column in table 7. Fig. 60a shows the LED string currents in the first transformer and Fig. 60b shows the led string currents in the second transformer.

In the second stage, in order to minimize the current imbalance within the transformers themselves, two current balancing inductors ($L_{B1,2}$) and four DC balancing capacitors (C_B) were connected to the circuit and LED current measurements were obtained. Results are given in second column in table 7. LED string currents can be seen in Fig. 61a and Fig. 61b.

In the third and last stage, the third current balancing inductor L_{B3} was connected to the ground return of the transformers in order to minimize the current imbalance between the two transformers. Results are given in third column in table 7. LED string currents can be seen in Fig. 62a and Fig. 62b.

Table 7 Backlight current measurements in eight parallel LED strings when string voltages are different

LED current / String no.	without balancing	with internal balancing circuit	with two transformer balancing circuit
String 1	127.8 mA	119.4 mA	109 mA (9.99% error)
String 2	79.08 mA	116.8 mA	109.5 mA
String 3	123.1 mA	131.7 mA (8.79% error)	128.3 mA
String 4 (3 LEDs are short circuit)	162.6 mA	128.7 mA	128.9 mA
String 5	117 mA	106.8 mA (11.77% error)	129.2 mA (6.68% error)
String 6	50.9 mA (57.58% error)	109.2 mA	128.3 mA
String 7	117.6 mA	130.7 mA	119 mA
String 8 (5 LEDs are short circuit)	182 mA (51.65% error)	125.1 mA	116.6 mA

When the voltages of the LEDs are different and none of the compensation elements to minimize current imbalance were not connected to the circuit the current

error was measured as 57.58% between $strings_{5-6}$. When two current balancing inductors and four DC balancing capacitors ($L_{B1,2}$ and C_B) were connected to the circuit the maximum error rate is reduced to 11.77%. In the last step, when the third current balancing inductor L_{B3} was added to the ground return of the transformers the current error is measured as 9.99% between $strings_{1-2}$. Bifilar windings are utilized in circuit components such as transformers and current balancing inductors.

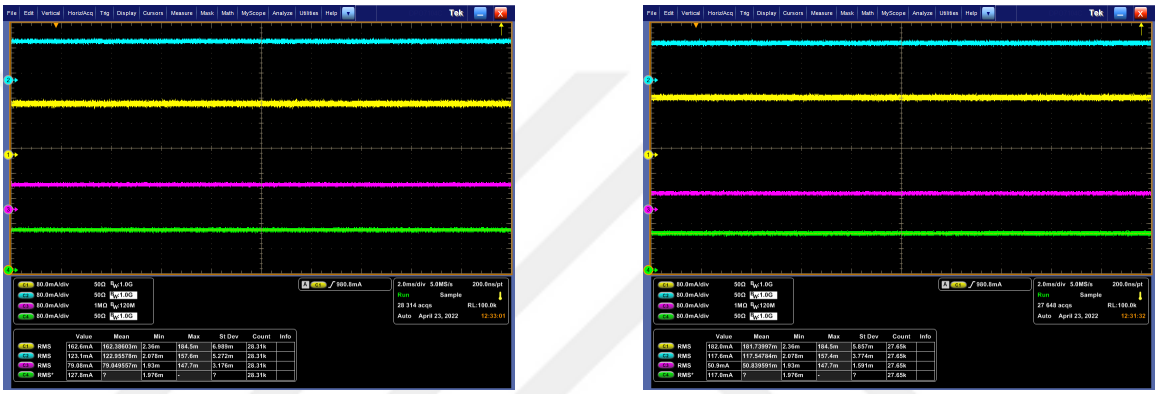

(a) String no 1..4 (b) String no 5..8

Figure 60 Current measurements when string voltages are not equal, without balancing circuit

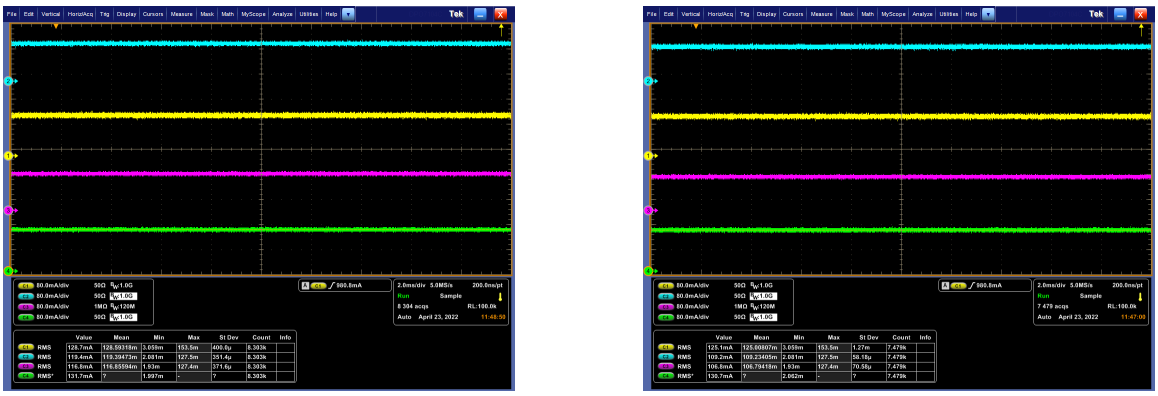

(a) String no 1..4 (b) String no 5..8

Figure 61 Current measurements when string voltages are not equal, with internal balancing circuit

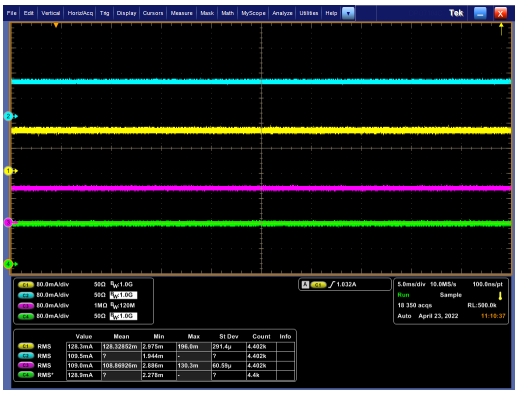

(a) String no 1..4

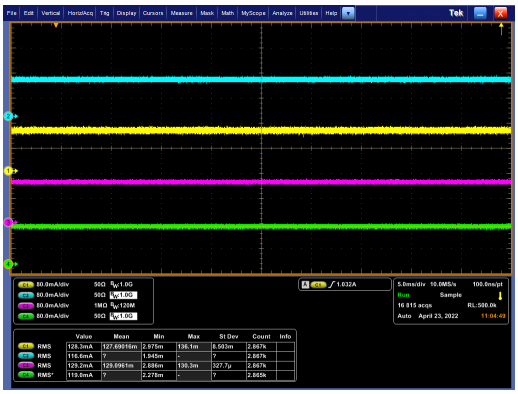

(b) String no 5..8

Figure 62 Current measurements when string voltages are equal, with two transformer balancing circuit

(a)	(b)
Channel 1 (Yellow): $String_4$'s current	Channel 1 (Yellow): $String_8$'s current
Channel 2 (Blue): $String_3$'s current	Channel 2 (Blue): $String_7$'s current
Channel 3 (Purple): $String_2$'s current	Channel 3 (Purple): $String_6$'s current
Channel 4 (Green): $String_1$'s current	Channel 4 (Green): $String_5$'s current

In case the string voltages are different from each other, 300Hz PWM dim is given while current balancing components are connected to the system. Measurement is taken at 50% dim condition for eight strings, given in table 8. The maximum current deviation between strings is 3.41% in 50% dim. LED string currents can be seen in Fig. 63a and Fig. 63b.

Table 8 Backlight current measurements in eight parallel LED strings when string voltages are different under dim (with balancing circuit)

LED current / String no.	100% dim	50% dim
String 1	109 mA	54.18 mA
String 2	109.5 mA	55.13 mA
String 3	128.3 mA	53.71 mA
String 4 (3 LEDs are short circuit)	128.9 mA	56.03 mA
String 5	129.2 mA	53.46 mA (2.15% error)
String 6	128.3 mA	53.81 mA
String 7	119 mA	54.33 mA
String 8 (5 LEDs are short circuit)	116.6 mA	56.51 mA (3.41% error)

(a) String no 1..4

(b) String no 5..8

Figure 63 Eight string current measurements when string voltages are not equal with all current balancing components under 50% dim

(a)

Channel 1 (Yellow): $String_1$'s current

Channel 2 (Blue): $String_2$'s current

Channel 3 (Purple): $String_3$'s current

Channel 4 (Green): $String_4$'s current

(b)

Channel 1 (Yellow): $String_5$'s current

Channel 2 (Blue): $String_6$'s current

Channel 3 (Purple): $String_7$'s current

Channel 4 (Green): $String_8$'s current

When the dim signal is given to the system, the primary MOSFETs keep switching

for a while after the PWM falls to zero, this is achieved by limiting the switching frequency change. In this way, the closed-loop compensation of the system increases, which is especially important when the dim levels are low. In Fig. 64, primary current and transformer 1's output LED current are seen under 50% dimming. The switching in the primary is synchronous with an adjustable delay time to the PWM signal.

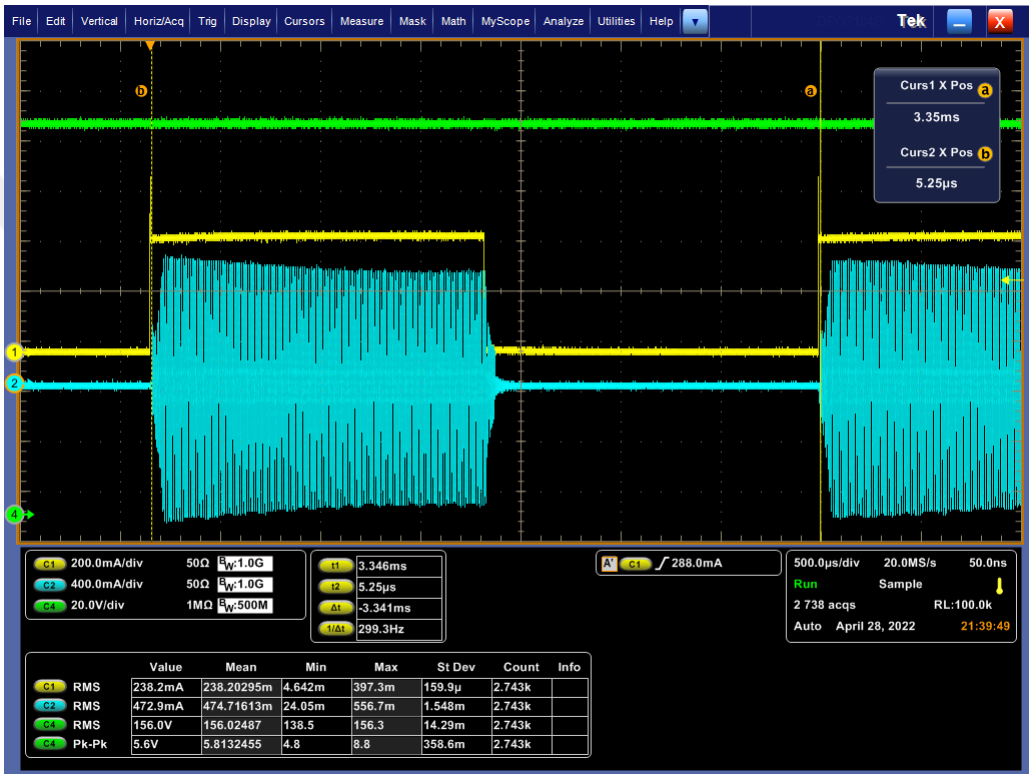

Figure 64 Primary resonant current under 50% dim

Channel 1 (Yellow): $Transformer_1$ output LED current under 50% dim
Channel 2 (Blue): Primary resonant current under 50% dim
Channel 4 (Green): $String_1$'s voltage

5.1.1 Thermal Results

When the voltages of the LEDs are different and none of the compensation elements to minimize current imbalance were not connected to the circuit, the maximum error rate is measured as 57.58% between $strings_{5-6}$. In this case, the back cover was removed and measurements are given in table 9. The difference in temperature between the

LED strings was recorded at room temperature as 31.8°C, as shown in Fig. 65. Higher currents drawn from the low-voltage strings form hot spots on the back cover and cause the product to have a shorter lifespan.

Table 9 Backlight current and thermal measurements in eight parallel LED strings when string voltages are different (without balancing circuit)

String no.	LED current without balancing	Measured Temperature
String 1	127.8 mA	46.8°C
String 2	79.08 mA	41°C
String 3	123.1 mA	44.2°C
String 4 (3 LEDs are short circuit)	162.6 mA	52.3 °C
String 5	117 mA	43.3 °C
String 6	50.9 mA (57.58% error)	38.1 °C
String 7	117.6 mA	44.1 °C
String 8 (5 LEDs are short circuit)	182 mA (51.65% error)	69.9 °C

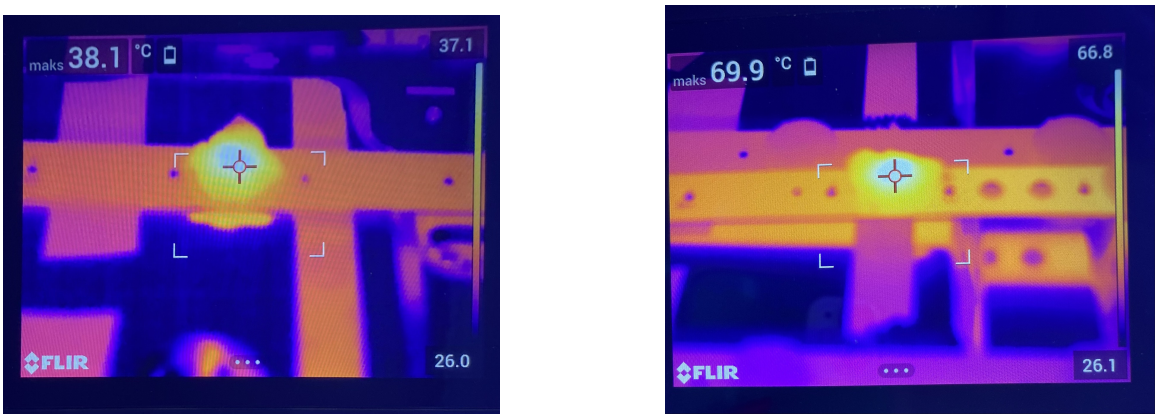

(a) String no 6

(b) String no 8

Figure 65 Thermal measurements when string voltages are not equal, without balancing circuit

5.1.2 Efficiency Comparison

Efficiency measurement was made while transferring the same backlight power at variable input voltages with the conventional method and the proposed method, the results are given in Fig. 66. With the proposed method, 0.9288% efficiency was measured in the backlight block at 145W output at 230V input voltage. For the same backlight power with a conventional method (boost converter at the LLC output), 0.8722% efficiency was measured. This 5.6% gain in efficiency will significantly reduce the thermal stress on the components at 145W output power.

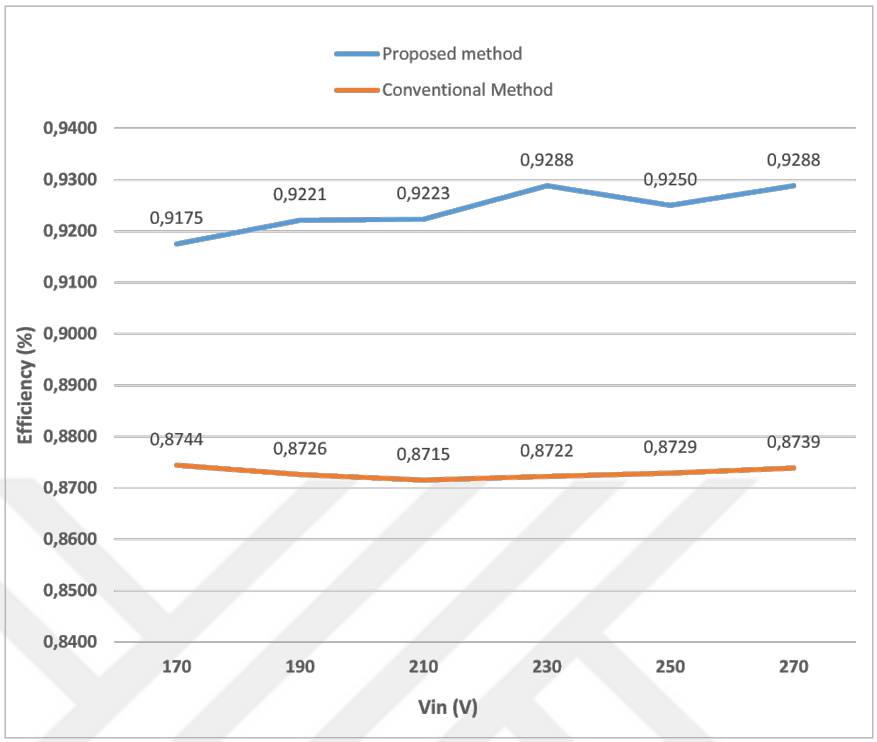

Figure 66 Efficiency comparison

5.1.3 Cost Comparison

Table 10 compares the main components used in the previously used method, that is, when a boost converter cascaded to the half-bridge resonant converter output with the elements to be used in the proposed method, that is, LEDs are driven directly from the transformer using the two transformer half-bridge resonant converter to feed the same amount of backlight power. In terms of cost, the prices are almost three times lower as compared to the conventional solution. Besides the cost advantage, not using the second DC-DC converter to supply the backlight will decrease the form factor of the PSU.

Table 10 Cost analysis

Conventional Method	**Number of components**	**Proposed Method**	**Number of components**
LLC HB IC	1	LLC HB IC (UCC25710)	1
LLC MOSFET (600V, TO220 package)	2	LLC MOSFET (600V, TO220 package)	2
LLC transformer (EFD40)	2	LLC transformer (EFD40)	2
Synchronous controller	2	Pulse transformer (EFD15)	1
Synchronous mosfet	2	Secondary side rectifier diode (DO201 package)	16
Boost converter IC	2	LED channel MOSFET (Dpak)	1
Boost converter MOSFET (Dpak)	6	Balancing inductor	3
Boost converter inductor (EFD22 core)	2	Balancing capacitor	4
Boost converter diode (SMA package)	4		
Additional 2-layer PCB	1		

CHAPTER VI

FUTURE WORK

In this study, the switching semiconductor material is Si. The reason for the preference is the cost of the material and the frequency range (maximum 350kHz) supported by the controller used is suitable for working with Si. Today, however, the demand for gallium nitride (GaN) and silicon carbide (SiC) semiconductors is increasing due to their use in electric vehicles and onboard chargers. This will ensure that the material becomes widespread, suitable controllers take their place in the market, and the price of the material decreases. The necessity for change in the semiconductor material is, that Si has its limitations such as voltage blocking capability, operation temperature, switching frequency, etc. which makes it unfavorable in today's high voltage high-efficiency solutions. However, wide bandgap (WBG) power devices offer high voltage blocking capability, smaller size, more reliable operation, high-temperature operation, and high switching frequencies. Hence WBG devices can be the next-generation devices for general semiconductor use in energy-efficient systems. Increasing the operating frequency in the system will bring a reduction in transformer size and the balancing elements. This will enable a more efficient PSU design in a smaller space.

CHAPTER VII

CONCLUSION

The goal of this study is to reduce the current imbalance when the cascade-connected structure cannot be used in the backlight block due to the space limitations in slim designs. Delivering the increasing backlight power demand in slim designs is possible with small form factor designs. When multiple transformers drive parallel-connected LED strings, the difference in transformer leakage inductance and LED string voltage tolerances creates a backlight current imbalance. The current mismatch between LED strings is seen on the customer side as an unevenly distributed backlight. The imbalance between the LED string currents is minimized in two stages, within the transformers, and between the transformers.

This study presents the simulation and application of the current balancing circuit designed for use in the LLC half-bridge resonant topology, in which eight parallel-connected LED strings are fed from two transformer outputs. Three current balancing transformers and four DC blocking capacitors are used to minimize the backlight current mismatch in parallel connected LED strings.

In the case of driving four parallel strings in the LLC half-bridge topology from two transformers when the string voltages are equal and the current balancing elements are not connected, the error rate between the strings was measured as 6.08%. The current imbalance between transformers was measured as 1%. When the string voltages were not equal, the error rate between the strings was measured as 23% before the current balancing. Using balancing capacitors, this LED current difference is reduced to 1.27%. When the string voltages were different, current measurements were taken at different dim levels of the system. The current deviation between strings is 3.17% in

11% dim. The current deviation on the LED strings is studied under two variables, these are the change in the LED voltage and the change in the leakage inductance of the transformer. The voltage difference between the LED strings varies due to the manufacturer and these LEDs are used randomly in mass production. The leakage inductance value, on the other hand, is given with an 8% tolerance in transformer specs.

In the case of driving eight parallel strings in the LLC half-bridge topology from two transformers, current balancing measurements were taken in two stages in order to measure the necessity of current balancing between transformers. In the first step, only the elements that balance the currents for each transformer are added to the circuit and then, the current-balancing elements between the transformers are included in the system.

When string voltages are equal and none of the compensation elements to minimize current imbalance were not connected to the circuit the current error was 11.25%. When two current balancing inductors and four DC balancing capacitors ($L_{B1,2}$ and C_B) were connected to the circuit, the current error is reduced to 6.76%. In the last step, when the third current balancing inductor L_{B3} was added to the ground return of the transformers the current error is measured as 2.59% between $strings_{1-2}$.

When the voltages of the LEDs are different and any of the compensation elements to minimize current imbalance were not connected to the circuit the current error was measured as 57.58%. When $L_{B1,2}$ and C_B were connected to the circuit the maximum error rate is reduced to 11.77%. If the balancing inductor L_{B3} was added to the ground return of the transformers the current error is measured as 9.99% between $strings_{1-2}$. Bifilar windings are utilized in circuit components such as transformers and current balancing inductors. When the string voltages were different, under 50% dim, the maximum current deviation between strings is measured as 3.41%.

On the other hand, the current balancing circuit proposed in this study improves

system reliableness in the event of system failures. When the voltages of the LEDs are different and the current error is measured as 57.58%, the back cover was removed, and the difference in temperature between the LED strings was recorded at room temperature as 31.8°C. Because higher currents are drawn from the low-voltage strings and form hot spots on the back cover. Hot spots cause the product to have a shorter lifespan.

The second advantage is, two boost converter circuits whose outputs are connected in parallel are removed from the system. With the current balancing elements added instead, the space gain on the power supply is 20cm x 16cm. Reduced board size is important because back cover designs are getting slimmer.

Other advantages of driving the system with this topology are cost, EMI, and efficiency. In terms of cost, the prices are almost three times lower when a half-bridge resonant converter is used to feed the same amount of backlight power. Although a DC-DC converter stage was removed during the backlight driving step, in practice, two switching blocks were removed from the system. This will reduce the electromagnetic emission of the system. When the backlight was driven directly from the transformer, 0.9288% efficiency was achieved at 230Vac. An efficiency increase of 5.6% significantly reduces thermal stress on components at 145W output power.

When the simulation results are examined, it is seen that the LED string currents are exactly the same, although there is a 20V difference between the string voltages. It is because the simulations are done in a lossless transformer and the leakage inductance is not taken into account. Since the leakage inductance is unavoidable in the current balancing inductor during the application phase, there is a current mismatch between the LED currents.

In the paper [4], a single-stage led driver was presented, and six parallel strings were driven from three transformers and balanced using three DC blocking capacitors at 120W backlight power. In our study, it was seen that using a balancing capacitor

was sufficient when four strings were driven from two transformers in parallel. But when more than two strings were driven from a transformer output, the balancing capacitor was not sufficient enough to balance LED currents. In addition, capacitor-balanced systems will provide current balancing as long as ($1/wC_B \gg R_{LED}$) equality is maintained, the detailed analysis was done in [5].

In the paper [17], to improve reliability in a standard backlight converter, the current imbalance between strings was minimized using the current mirror circuit and two opamps. Besides the advantage of driving single-stage LEDs, due to the significant losses on transistors, this approach is not applicable to high-power circuits. In addition, as the number of strings increases, high current gain transistors should be used to increase accuracy.

In the paper [6], a current transformer was used to balance the AC LED loads. The distinction in this approach is that instead of an additional balancing coil, the current balancing transformer is wounded on the transformer's outer legs. In order not to induce any voltage from the main transformer when the extra coil was wound on the transformer, each of the windings must be divided into two and wound in the opposite direction to each other. This application was not preferred due to the possibility of carrying the switching noise from the primary to the secondary, the possibility of creating parasitic capacitance on the transformer, and the difficulty of winding the transformer.

The disadvantage of the proposed method is that the total LED current flowing through all the strings will pass through the inter-transformer current balancing coil. So this coil will be larger than the internal balancing coils. Component selection should be made accordingly.

The contribution of this method is to balance the backlight currents independent of the voltage tolerance in LED strings and the leakage inductance tolerance in transformers. Because when multiple transformers drive parallel-connected LED strings,

the difference in transformer leakage inductance and LED string voltage tolerances creates a backlight current imbalance problem and causes reliability issues. In the application phase, an interleaved PFC was used at the input of the circuit, and a full bridge diode rectifier was used in the secondary rectification block.

APPENDIX A

APPENDIX

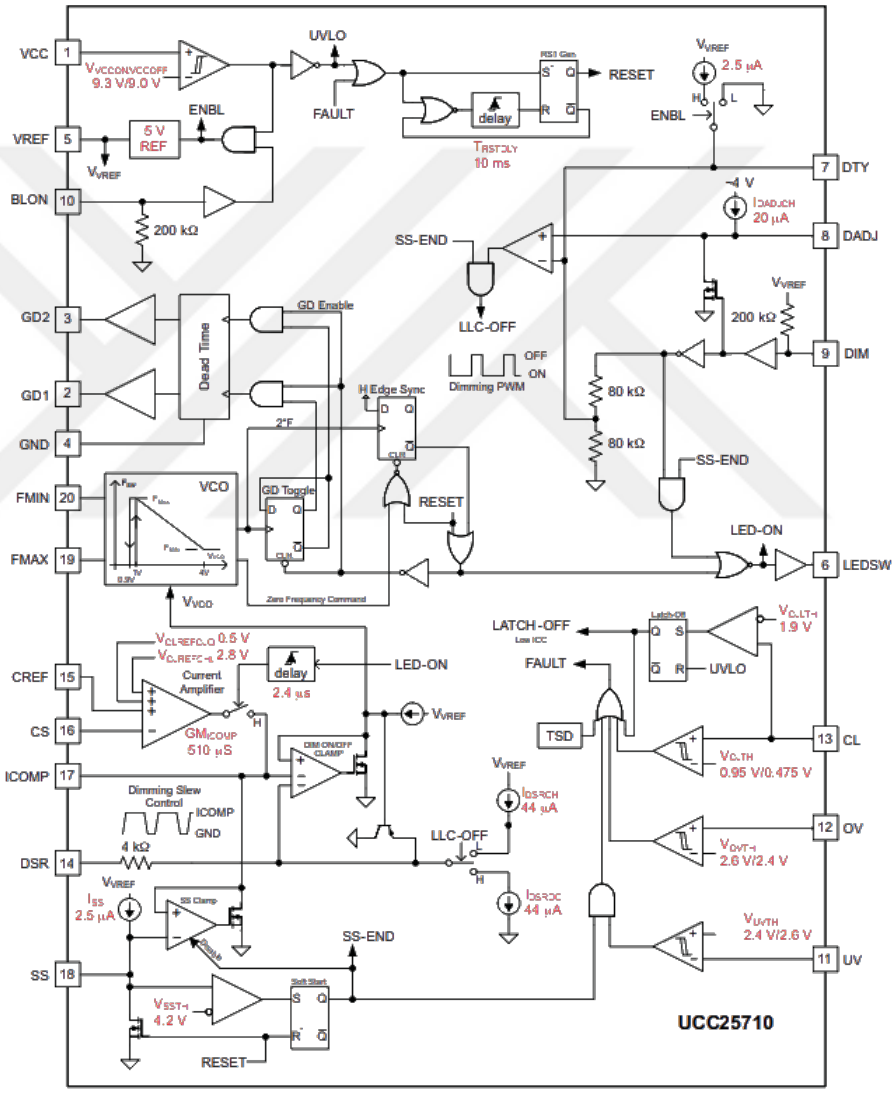

Figure 67 UCC25710 functional block diagram [15]

REFERENCES

[1] L. Rozenblat, *Switching power supply design: A concise practical handbook*. Lulu com, 2021.

[2] S. Baddela and D. Zinger, "Parallel connected leds operated at high to improve current sharing," in *Conference Record of the IEEE Industry Applications Conference, 2004. 39th IAS Annual Meeting.*, vol. 3, pp. 1677–1681 vol.3, 2004.

[3] C. C.-G. Kim, K.-C. Lee, and B. H. Cho, "Uniform current distribution in driving cold cathode fluorescent lamps (ccfl) in parallel," in *IEEE 36th Power Electronics Specialists Conference*, pp. 1087–1093, 2005.

[4] S.-H. Lee, S.-H. Cho, C.-W. Roh, S.-S. Hong, and S.-K. Han, "A new cost-effective current-balancing multi-channel led driver for a large screen lcd back-light units," *The Transactions of the Korean Institute of Power Electronics*, vol. 15, 07 2010.

[5] K. H. Loo, Y. M. Lai, and C. K. Tse, "Design and analysis of *lcc* resonant network for quasi-lossless current balancing in multistring ac-led array," *IEEE Transactions on Power Electronics*, vol. 28, no. 2, pp. 1047–1059, 2013.

[6] B.-G. Kang, Y. Choi, and S.-K. Chung, "High frequency ac-led driving for street light," in *9th International Conference on Power Electronics and ECCE Asia (ICPE-ECCE Asia)*, pp. 1246–1251, 2015.

[7] Y. Liu, "High Efficiency Optimization of LLC Resonant Converter for Wide Load Range," p. 119, 2007.

[8] Rohm, "Understanding mosfet characteristics." https://www.rohm.com/electronics-basics/transistors/understanding-mosfet-characteristics, (accessed February 20, 2022).

[9] B. Agrawal, M. Preindl, B. Bilgin, and A. Emadi, "Estimating switching losses for sic mosfets with non-flat miller plateau region," in *IEEE Applied Power Electronics Conference and Exposition (APEC)*, pp. 2664–2670, 2017.

[10] M. H. Rashid, *"Power Electronics Handbook"*. Elsevier, 2017.

[11] C.-T. Tsai and J.-C. Su, "A Soft-Switching SEPIC with Multi-Output Sources," *Electronics*, vol. 6, p. 35, May 2017.

[12] R. Steigerwald, "A comparison of half-bridge resonant converter topologies," *IEEE Transactions on Power Electronics*, vol. 3, no. 2, pp. 174–182, 1988.

[13] A. Pawellek, C. Oeder, J. Stahl, and T. Duerbaum, "The resonant llc vs. lcc converter - comparing two optimized prototypes," in *IEEE Energy Conversion Congress and Exposition*, pp. 2229–2235, 2011.

[14] ST, "AN2644: An introduction to llc resonant half-bridge converter," tech. rep., 2008.

[15] T. Instruments, "UCC25710 LLC half-bridge controller for multi-string led lighting," tech. rep., 2016.

[16] C. Chang and G. Bruning, "Voltage-fed half-bridge resonant converter for multiple lamp independent operation," in *Conference Record of the IEEE Industry Applications Conference. 36th IAS Annual Meeting (Cat. No.01CH37248)*, vol. 1, pp. 218–222 vol.1, 2001.

[17] C.-L. Chiu and K.-H. Chen, "A high accuracy current-balanced control technique for led backlight," in *IEEE Power Electronics Specialists Conference*, pp. 4202–4206, 2008.

[18] P. R. Surkanti, D. Mehrotra, M. Gangineni, and P. M. Furth, "Multi-string led driver with accurate current matching and dynamic cancellation of forward voltage mismatch," in *IEEE 60th International Midwest Symposium on Circuits and Systems (MWSCAS)*, pp. 229–232, 2017.

[19] "Museum displays inventions of edison, zworykin, other "firsts" in the communications field," *Electrical Engineering*, vol. 79, no. 1, pp. 115–115, 1960.

[20] B. D. Inglis and G. D. Couples, "John logie baird and the secret in the box: The undiscovered story behind the world's first public demonstration of television [scanning our past]," *Proceedings of the IEEE*, vol. 108, no. 8, pp. 1371–1382, 2020.

[21] R. C. Webb, *"Tele-Visionaries: The People Behind the Invention of Television"*. 2005.

[22] P. Goldmark, J. Dyer, E. Piore, and J. Hollywood, "Color television-part 1," *Proceedings of the IRE*, vol. 30, no. 4, pp. 162–182, 1942.

[23] R. Dressler, "The pdf chromatron-a single or multi-gun tri-color cathode-ray tube," *Proceedings of the IRE*, vol. 41, no. 7, pp. 851–858, 1953.

[24] F. Tian, X. Wu, and J. Liu, "Research and realization of innovative led illumination system for dlp projector," in *International Conference on Audio, Language and Image Processing*, pp. 194–199, 2008.

[25] H. Kawamoto, "The history of liquid-crystal displays," *Proceedings of the IEEE*, vol. 90, no. 4, pp. 460–500, 2002.

[26] M.-H. Kim, S.-H. Chae, and J.-S. Kim, "A burn-in potential region detection method for the oled panel displays," in *IEEE International Symposium on Multimedia (ISM)*, pp. 182–183, 2018.

[27] H. Chen, J. He, and S.-T. Wu, "Recent advances on quantum-dot-enhanced liquid-crystal displays," *IEEE Journal of Selected Topics in Quantum Electronics*, vol. 23, no. 5, pp. 1–11, 2017.

[28] Z. Bouhamri and E. Virey, "Oled, miniled, microled and qned: The battle for the next generation of televisions," in *28th International Workshop on Active-Matrix Flatpanel Displays and Devices (AM-FPD)*, pp. 25–28, 2021.

[29] ST, "170w high input voltage two switch flyback based on l6565 and 1500v k5 mosfets," tech. rep., 2020.

[30] D. Murthy-Bellur and M. Kazimierczuk, "Two-switch flyback pwm dc-dc converter in continuous-conduction mode," *International Journal of Circuit Theory and Applications*, vol. 39, 11 2011.

[31] V. Wuti, A. Luangpol, K. Tattiwong, A. Sopin, P. Sirisuk, and C. Bunlaksananusorn, "Performance comparison between a two-switch and rcd clamp forward converters," in *5th International Conference on Engineering, Applied Sciences and Technology (ICEAST)*, pp. 1–4, 2019.

[32] J. B. Lee, J. I. Baek, H. S. Youn, C. O. Yeon, C. Y. Lim, and G. W. Moon, "A high efficiency half-bridge llc converter with simple hold-up compensation circuit," in *9th International Conference on Power Electronics and ECCE Asia (ICPE-ECCE Asia)*, pp. 227–232, 2015.

[33] Rohm, "Calculation of power loss (synchronous)," tech. rep., 2016.

[34] T. Halder, "Hard and soft switching geometries for operations of the mosfet used for the smps," in *Devices for Integrated Circuit (DevIC)*, pp. 1–6, 2021.

[35] E. P. N. Mohan, R. Ayyanar, ""soft-switching in dc-dc converters: Principles, practical topologies, design techniques, latest developments"," in *IEEE Applied Power Electronics Conference and Exposition (APEC)*, 2002.

[36] B. Akin and I. Aksoy, "Active snubber components optimization for zvt-zct soft switched pfc converter," in *International Conference on Consumer Electronics, Communications and Networks (CECNet)*, pp. 4711–4714, 2011.

[37] R. L. Steigerwald, "High-frequency resonant transistor dc-dc converters," *IEEE Transactions on Industrial Electronics*, vol. IE-31, no. 2, pp. 181–191, 1984.

[38] M. E. Tulu and D. Yildirim, "Induction cooker design with quasi resonant topology using jitter drive method," in *12th International Conference on Environment and Electrical Engineering*, pp. 1–6, 2013.

[39] A. Eshraghi, S. Sariri, V. Schwarzer, and R. Ghorbani, "Islanding detection and over voltage mitigation using wireless sensor networks and electric vehicle charging stations," 06 2016.

[40] T. Duerbaum, "First harmonic approximation including design constraints," in *INTELEC - Twentieth International Telecommunications Energy Conference (Cat. No.98CH36263)*, pp. 321–328, 1998.

VITA

Melisa Ersoy graduated from Izmir Karsıyaka Anatolian High School in 2014. Later, she received her B.Sc. degree in electrical and electronics engineering from Dokuz Eylul University in 2019. She started her M.Sc. degree at Ozyegin University in 2020. She has been working as a system design engineer at the TV Power Electronics Design team in Vestel Electronics since February 2019. Her research interests are mainly DC-DC converters. Currently, she works with flyback and LLC topologies. Her near future goal is to design PSU using SiC and GaN.

A conference paper related to the thesis topic is published at UPEC 2022 with the title of "Current Balancing Circuit Design for Parallel LED Strings in QDOT High Bright TV with Dual Transformer LLC Resonant Topology" at 30th August-2nd September 2022.